Reviews in Mineralogy & Geochemistry
Vol. 89 pp. 453-507, 2023
Copyright © Mineralogical Society of America

Lunar Mare Basaltic Volcanism: Volcanic Features and Emplacement Processes

James W. Head[1], Lionel Wilson[2], Harald Hiesinger[3], Carolyn van der Bogert[3], Yuan Chen[4], James L. Dickson[5], Lisa R. Gaddis[6], Junichi Haruyama[7], Erica R. Jawin[8], Lauren M. Jozwiak[9], Chunlai Li[4], Jianzhong Liu[10], Tomokatsu Morota[11], Debra H. Needham[12], Lillian R. Ostrach[13], Carle M. Pieters[1], Tabb C. Prissel[14], Yuqi Qian[15], Le Qiao[16], Malcolm R. Rutherford[1], David R. Scott[1], Jennifer L. Whitten[17], Long Xiao[15], Feng Zhang[18], Ouyang Ziyuan[4]

[1]Department of Earth, Environmental and Planetary Sciences, Brown University, Providence, RI 02912, USA
[2]Lancaster Environment Centre, Lancaster University, Lancaster, LA1 4YQ, UK
[3]Institut für Planetologie, Westfälische Wilhelms-Universität, Wilhelm-Klemm-Str. 10, 48149 Münster, Germany
[4]Key Laboratory for Lunar and Deep Space Exploration, National Astronomical Observatories, Chinese Academy of Sciences, 20A Datun Road, Chaoyang District, Beijing 100101, China
[5]Division of Geological and Planetary Science, California Institute of Technology, 1200 E California Blvd, MC 150–21. Pasadena, CA, 91125, USA
[6]Lunar and Planetary Institute, 3600 Bay Area Boulevard, Houston, Texas 77058, USA
[7]Institute of Space and Astronautical Science, JAXA, Japan (3–1-1 Yoshinodai, Chuo-ku, Sagamihara, Kanagawa 252–5210, Japan)
[8]Smithsonian Institution National Museum of Natural History, Department of Mineral Sciences, PO Box 37012, Washington, DC 20013–7012, USA
[9]Johns Hopkins Applied Physics Laboratory, 11100 Johns Hopkins Rd, Laurel, MD 20723, USA
[10]Center for Lunar and Planetary Sciences, Institute of Geochemistry, Chinese Academy of Sciences, Guiyang 550081, China
[11]Department of Earth and Planetary Science, University of Tokyo, Bunkyō-ku, Tokyo, Japan
[12]National Aeronautics and Space Administration Headquarters, Washington, D.C. 20546, USA
[13]US Geological Survey Astrogeology Science Center, 2255 N. Gemini Drive, Flagstaff, AZ USA
[14]Astromaterials Research and Exploration Science Division NASA Johnson Space Center, Houston, TX 77058 USA
[15]Planetary Science Institute, China University of Geosciences, Wuhan, 430074, China
[16]Institute of Space Science, Shandong University, Weihai, 264209, China
[17]Department of Earth and Environmental Sciences, Tulane University, New Orleans, LA 70118 USA
[18]National Space Science Center, No. 1 Nanertiao, Zhongguancun, Haidian District, Beijing, China

1529-6466/23/0089-0011$10.00 (print)
1943-2666/23/0089-0011$10.00 (online)
http://dx.doi.org/10.2138/rmg.2023.89.11

1. INTRODUCTION AND BACKGROUND

Volcanism is a fundamental process in the geological evolution of the Moon, providing clues to the composition and structure of the mantle, the location and duration of interior melting, the nature of convection and lunar thermal evolution. Progress in understanding volcanism has been remarkable in the short 60-year span of the Space Age. Before Sputnik 1 in 1957, the lunar farside was unknown, the origin of the dark lunar maria was debated (sedimentary or volcanic), and significant controversy surrounded the question of how the multitude of craters on the surface formed. Was the Moon formed hot or cold, was the lunar surface young or old, were the craters of impact or volcanic origin? A lunar farside deficient in the darker maria was revealed by Luna 3 in 1959 (Lipsky 1965a,b). The Ranger, Lunar Orbiter, Surveyor, Luna and Zond missions significantly augmented pre-Sputnik telescopic observations and began to reveal the diversity of lunar geologic landforms. Return of lunar soil and rock samples from the lunar surface by Apollo (11–12, 14–17) (Compton 1989) and Luna (16, 20, 24) missions (Harvey 2007a,b; Huntress and Marov 2011) changed the debates overnight (Hinners 1971; Taylor 1975). The lunar rocks were igneous and extremely ancient, all from the first half of Solar System history; the oldest, highland anorthosites, were overlain by relatively younger, but still extremely old, extrusive basalts forming the maria.

In the five decades following Sputnik, detailed radiometric dating, and descriptions of samples and landforms, led to more integrated studies of fundamental processes that form and shape planetary landscapes and interiors. Early studies used geological, petrological, and remote sensing data to define and characterize deposits and features associated with lunar volcanism (e.g., Hinners 1971; Wilhelms and McCauley 1971; Head 1976), and to model the generation, ascent and eruption of lunar magma (e.g., Wilson and Head 1981). Remote sensing data were used to define and characterize volcanic geological units (e.g., McCord et al. 1972a,b, 1976, 1979; Head et al. 1978; Pieters 1978), to link these units to Apollo/Luna (Wilhelms 1987; Heiken et al. 1991; Hiesinger and Head 2006), and to assess the role of volcanism in lunar thermal history (e.g., Solomon and Head 1980; Kirk and Stevenson 1989). Also explored were the implications of lunar volcanism for other planetary bodies (BVSP 1981; Taylor 1983). The advent of Galileo and Clementine remote sensing data permitted more extensive definition and characterization of units, and impact crater size–frequency distribution (CSFD) analyses provided an important assessment of the chronology of emplacement (e.g., Hiesinger et al. 2002, 2003; Wagner et al. 2002). Improved spatial/spectral resolution and coverage permitted further documentation of lunar volcanic features and deposits (e.g., Greeley et al. 1993; Weitz et al. 1998; Weitz and Head 1999; Heather et al. 2003) and assessment of the implications for generation, ascent and eruption of magma (e.g., Head and Wilson 1992; Wilson and Head 2003a).

A plateau was reached in 2006 near the end of these five decades with the synthesis and publication of *New Views of the Moon* (Jolliff et al. 2006), a compendium of the geology, remote sensing), petrology, chronology and thermal evolution of the Moon. The role of volcanism, however, was treated separately in each chapter and there was no individual chapter dedicated to lunar mare volcanism. In the years since 2006, a flood of new data has been obtained and continue to be acquired for the Moon. Missions such as Lunar Reconnaissance Orbiter (LRO), Chandrayaan 1–2, SELENE-Kaguya, Chang'e 1–5, LADEE, LCROSS and GRAIL have provided views of the Moon and its environment in unprecedented detail. Much of this new information has significant implications for the characterization and understanding of lunar volcanism. From these missions, extremely high resolution image data have revealed the characteristics and distribution of volcanic features and structures (sinuous rilles, cones, domes, flow fronts, vents, pits, etc.) (e.g., Head and Wilson 2017), discovered the wide distribution of a host of fascinating enigmatic features (e.g., Irregular Mare Patches (IMPs), Braden et al. 2014; Ring Moat Dome Structures (RMDS), Zhang et al. 2017) and permitted improved and more extensive chronology from CSFD analyses (e.g., Morota et al. 2008, 2009, 2011a,b; Hiesinger et al. 2011). Spectral data have revealed the mineralogy of volcanic features (e.g., Staid et

al. 1996, 2011; Whitten et al. 2011; Jawin et al. 2015; Trang et al. 2017; Weitz et al. 2017), and gravity data have provided new insight into the thickness and physical properties of the low-density lunar anorthositic crust that mantle-derived melts must transect (e.g., Wieczorek et al. 2013, Zuber et al. 2013), as well as the nature of shallow crustal anomalies associated with impact basins (e.g., Neumann et al. 2015; Wang et al. 2016) and craters (e.g., Li et al. 2014; Jozwiak et al. 2015a,b, 2017; Soderblom et al. 2015; Evans et al. 2016, 2018; Zhang et al. 2018; Lu et al. 2019). New data have brought new approaches to the geologic mapping of the Moon (e.g., Gaddis et al. 2004; Ouyang and Liu 2014; Liu et al. 2016; Han et al. 2019).

These new data have permitted a host of analyses in the last decade that have changed our view of lunar volcanism and the processes of magma generation, ascent and eruption. We now have an improved understanding of the global distribution and characteristics of an array of volcanic features: IMPs, interpreted as very recent volcanism (Braden et al. 2014); floor-fractured craters, evidence for shallow intrusions and eruptions (Jozwiak et al. 2012, 2015a,b); sinuous rilles, indicators of thermal erosion by turbulent lava flows (Carr 1974; Hurwitz et al. 2013); shield volcanoes, formed by low volume-flux eruptions (Spudis et al. 2013); pyroclastic deposits, indicators of magma volatile contents (Gaddis et al. 2003; Li and Milliken 2017; Morgan et al. 2021); cryptomaria, keys to early lunar volcanism (Whitten and Head 2015a,b); and cones, domes and flows in volcanic complexes (Bugiolacchi and Guest 2008; Campbell et al. 2009; Besse et al. 2011; Lawrence et al. 2013; Stopar et al. 2014; Chen et al. 2019a,b). New data have provided an improved chronology for lunar volcanic deposits on the lunar nearside and farside (e.g., Harayuma et al. 2009b; Morota et al. 2009, 2009b, 2011b; Hiesinger et al. 2011; Whitten et al. 2011; Paskert et al. 2015) adding temporal constraints to lunar geological and thermal evolution. Building on the individual contributions in *New Views of the Moon* (2006), the observational, experimental, analytical and modelling basis for the analysis of lunar volcanism has increased substantially, so that the synergistic integration of these data has been possible (Head and Wilson 2017; Wilson and Head 2017a). We are now in an era that represents a transition from predominantly descriptive lunar field volcanology, to a more holistic, multi-disciplinary physical volcanology-based approach to the generation, ascent and eruption of magma. The goal of this chapter is to summarize that synergism and the progress achieved in understanding this important process, and to outline currently unresolved questions as a basis for future exploration strategies (e.g., Jawin et al. 2019; Head and Wilson 2022) (EA-11-17,18).

Thus, *New Views of the Moon 2* provides a unique opportunity to synthesize recent important developments in our understanding of lunar mare volcanism and its relation to and implications for lunar petrology, crustal and internal structure and the chronology and thermal evolution of the Moon. Equally importantly is to identify the set of outstanding questions and research that will help improve our understanding in the coming decades. In the future exploration of the Moon, where do we need to go and what do we need to do to address these most critical questions? How can our current knowledge and questions inform the design of new instruments and spacecraft and the architecture of new lunar exploration strategies? What are the roles for robotic orbiters, landers, rovers, and sample return missions? What are the roles for human exploration and human-robotic partnerships?

2. VOLCANISM AS A PROCESS IN THE EVOLUTION OF PLANETARY BODIES

Mapping and assessment of the nature and distribution of volcanic activity on any planetary body is critical in order to fully understand the nature of its interior and its thermal and tectonic evolution. How does a planet lose internally generated heat (crustal spreading, conduction, advective cooling through volcanism)? How does the atmosphere and water inventory form and evolve (cometary accretion, internal outgassing)? How does this vary with time and what are the sources and sinks of these volatiles? Volcanic eruption styles change with composition,

volatile content, crustal structure, thermal structure, substrate density, atmospheric density and gravity. How can we use the nature of planetary volcanic processes to assess these variables?

Individual volcanic features on the Earth (Fig. 1a) have always been viewed as providing insight into the modes of eruption (e.g., effusive, explosive), the composition of the magma (e.g., long lava flows, steep-sided domes), the rates of eruption (e.g., limited flows, flood basalts), the styles of lava cooling (e.g., resulting in pahoehoe and 'a'a morphologies), the gas content of the magma (e.g., hawaiian, plinian) and the medium into which the magma is intruded and erupted (e.g., subaerial, shallow groundwater phreatomagmatic, submarine). Furthermore, the nature and morphological manifestations of volcanic edifices (e.g., shield volcanoes, stratovolcanoes), and the distribution and configuration of volcanic features (e.g., Hawaiian-Emperor Seamount Chain, Large Igneous Provinces, Mid-Ocean Ridges) have served to provide insight into modes of mantle convection and lithospheric dynamics. It was only natural, then, that the analysis of lunar volcanism began historically with the documentation of features that could be interpreted to be of volcanic origin, an assessment of their areal and temporal distribution, and their comparison to similar volcanic features on Earth to analyze the processes of lunar magma generation, ascent and eruption.

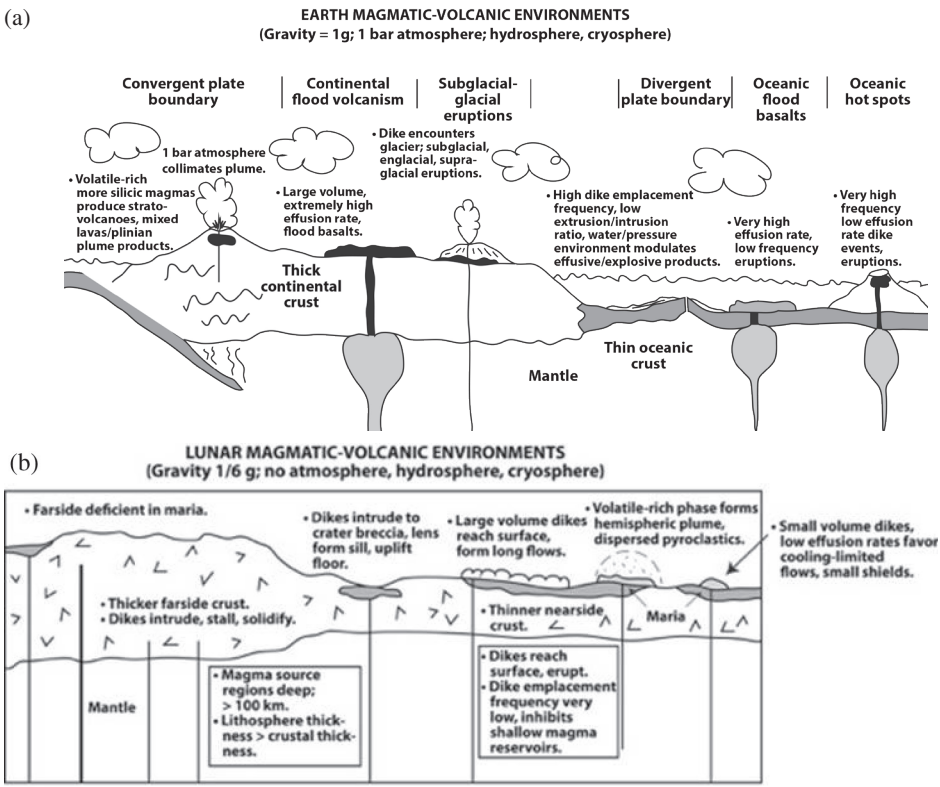


Figure 1. Planetary environmental factors influencing the ascent and eruption of magma on the Earth and Moon. **a)** Earth magmatic (plutonic/volcanic) environments, modulated by gravity, mantle composition and convection, plate tectonics, crustal composition and thickness, and surface environment (atmosphere, cryosphere and hydrosphere). **b)** Lunar magmatic (plutonic/volcanic) environments, modulated by low gravity, mantle composition and convection, depth of melting, lack of plate tectonics, temporally thickening lithosphere, density, composition and thickness of crust, presence of impact craters and basins, and surface environment (lack of an atmosphere, cryosphere and hydrosphere).

On the Earth, the global plate tectonic environment largely dictates the location and rates of volcanic activity, with intrusive and extrusive basaltic volcanism at divergent plate boundaries contributing ~20 km^3 of magma per year to the crust, and convergent plate boundaries being the focus of subduction, melting and remobilization of crustal material to produce more evolved magmas and stratovolcanoes (Lockwood and Hazlett 2017). On longer time-scales, mantle convection at various scales produces hot spots, large shield volcanoes, and in extreme cases, large igneous provinces (LIPS) (Ernst 2014). A map of volcanic landforms and deposits on Earth reflects this intimate interaction of plate tectonics and volcanic processes back into the discernible past. Hot spot traces and LIPS provide clues to mantle convection patterns. Samples, both xenoliths and partial melts, provide insights into mantle compositions and partial melting processes. Geological evidence provides insight into earlier history, but the dynamic nature of plate tectonics has largely destroyed the record of the first half of Earth history. We have a first-order idea of the role of volcanism in these environments in relatively recent Earth history, but little knowledge of the role of plate tectonics and volcanism in Earth's formative years; the nature of komatiites suggests that the mantle at these times was much hotter and the degree of partial melting much higher (e.g., Arndt 2003), but the initial cause and time of onset of plate tectonics is debated.

A paradigm for the role of volcanism in the history of terrestrial planet evolution has been provided by Taylor (1989), who described three crustal types: *primary crust*, derived from large-scale melting by accretional and heavy impact bombardment energy (the lunar anorthositic crust), transitioning to *secondary crust*, the product of partial melting of the mantle (manifested in seafloor spreading on Earth, and hot spots and vertical crustal accretion on various terrestrial planets), and *tertiary crust*, derived from reworking of primary and secondary crust (e.g., continental crust on Earth). How do the other terrestrial planetary bodies, the Moon in particular, provide insight into the early history of secondary crust formation and evolution, and how might they provide insight into the onset of plate tectonics on Earth and its transition to its current regime?

Of critical importance in interpreting the volcanic geological record of other planetary bodies are broad environmental factors: how do planetary variables (size, density, gravity, thermal and crustal structure, presence/absence of a hydrosphere and atmosphere) influence the resulting landforms. Most of our knowledge concerning the generation, ascent and eruption of magma derives from our knowledge of Earth and eruptions in its environment (Fig. 1a). The corresponding processes on the Moon (Fig. 1b) must be significantly influenced by the different thermal structure, one-sixth Earth gravity, and lack of an atmosphere. Basic observations need to be made and models accounting for these differences need to be constructed and tested (e.g., Wilson and Head 1981) in order to properly interpret the lunar volcanic record.

In summary, the Moon offers a laboratory for the study of secondary crust, a common mantle-derived crustal type seen on Mercury, Venus, Earth and Mars (Taylor 1989). Accessibility to exploration provides the opportunity to ask a series of fundamental questions: What is the total volume of secondary crust and how does this compare with other planets? What is the intrusion/extrusion ratio? Is there a specific onset to secondary crustal formation or is it transitional from primary crustal formation? How does the presence of large impact basins influence the formation and evolution of secondary crust? What is the onset, duration and rate of lunar secondary crustal formation? Is there active volcanism today? What is the array of volcanic landforms and what does it mean? How do landforms relate to eruption conditions? What accounts for the diversity of volcanic unit mineralogies? Are there temporal trends in composition? What do mare landforms and deposits tell us about the presence and abundance of magmatic volatiles? Did the Moon ever have an atmosphere? If so, what was its composition, pressure and duration? Is volcanism the source of volatiles thought to be sequestered at the poles? Do we see surface evidence of plumes and hot spots? Why are major Hawaii-like shield volcanoes absent on the Moon? How does secondary crust differ between the Moon and Earth given the different physical and environmental characteristic of the two

bodies? How can we use the characteristics of lunar secondary crustal formation to gain insight into the same processes on Mars, Mercury and Venus?

To address these questions, we describe the nature and characterization of lunar volcanism (Figs. 2, 3), beginning with the distribution and setting, and then summarizing recent progress in understanding the generation ascent and eruption of basaltic magma on the Moon, and how these principles and findings help us to interpret the nature and relationships of the disparate deposits, landforms and features observed.

3. DISTRIBUTION AND SETTING OF LUNAR MARE VOLCANISM

In contrast to the Earth's dynamic lithosphere (plate tectonics), crust (seafloor spreading and continental drift) and mantle (plumes, hot spots and large igneous provinces) (Fig. 1a), the setting for lunar volcanism is relatively static (Fig. 1b). The lunar primary anorthositic crust formed a global low-density layer that served as a platform for volcanic eruptions following its solidification. The lack of plate tectonics on the Moon (a one-plate planet), and the rapidly thickening lithosphere and deeper magma source regions, meant that magma rising from the mantle in plumes and dikes had to overcome both rheological traps (the base of the lithosphere) and density traps (the base of the crust) in order to erupt to the surface (Fig. 4). This general setting of chemical and rheological layering of the Moon was disrupted from time to time by the formation of huge multi-ringed impact basins which thinned the crust in the basin interior, thickened it on the basin rim, created seas of impact melt in the basin interior (Vaughan et al. 2013; Vaughan and Head 2014), and raised deep isotherms to the surface during basin collapse. Another dimension to the setting of lunar volcanism is the distribution of radioactive elements that might be important in magma generation in the mantle and of the thermal gradients and thicknesses of the shallower crust and lithosphere. A primary example of this is the presence of the Procellarum-KREEP Terrane (PKT) (Jolliff et al. 2000), a major compositional province on the northwest lunar nearside. Did the PKT influence and prolong the generation, ascent and eruption of magma in this region? We now use this general framework to address some specific questions where recent progress enables a deeper understanding of the role and importance of lunar basaltic volcanism.

What is the areal distribution, thickness and volume of lunar volcanic deposits of secondary crustal origin (Fig. 3), and what does this tell us about the state and nature of mantle source regions, the flux of magma, and the thermal evolution of the Moon? To successfully address these questions, we require the following information:

1. *What is the range of types of volcanic deposits observed on the Moon?* The stark albedo contrast between the anorthositic highlands and the lunar mare deposits, and their prominence on the nearside, mark mare basaltic volcanism as the dominant type of extrusive lunar volcanism. Much lower in abundance and different in surface morphology and composition are the collection of features and deposits known as "red spots" (due to the downturn in their UV spectra) or "silicic volcanism" (due to their mineralogy and common expression as steep-sided domes and cones). Prior to Apollo, the Cayley Formation, an upland smooth plains unit (Fig. 3g), lying stratigraphically between the cratered highland crust and the maria, was thought to represent extrusive volcanism of a composition different (less mafic) from that of the maria (e.g., Trask and McCauley 1972). Exploration of the Cayley in the Descartes region by the Apollo 16 mission revealed that the Cayley plains were formed by ponded impact basin ejecta (e.g., Muehlberger et al. 1972; Young et al. 1972; Oberbeck 1975), further focusing attention on the lunar maria as the major type of extrusive basaltic volcanism (e.g., Taylor 1975; Head 1976).

The lunar highlands sample collection provided another perspective on volcanism. In addition to the results from landings on the maria (Apollo 11, 12, 15, 17 and Luna 16, 24), fragments in lunar breccias interpreted to be igneous rocks showed evidence for various non-mare types of magmatic rocks (Fig. 2a), including KREEP basalts, high-

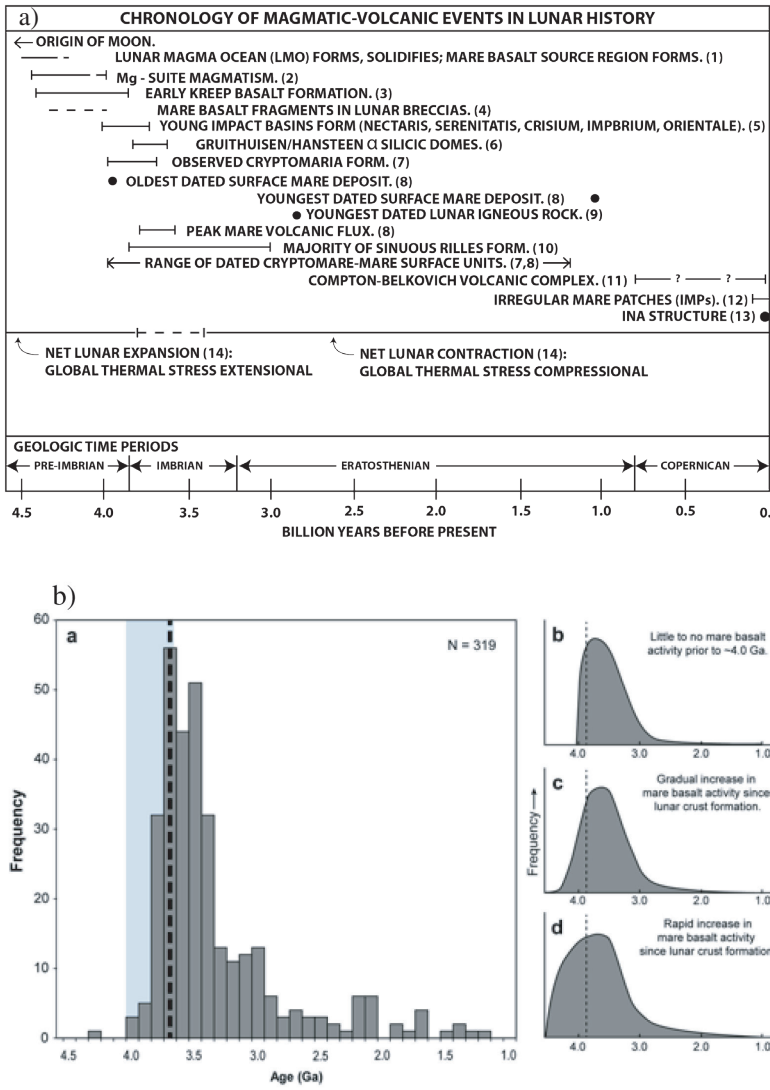


Figure 2. Lunar secondary crust chronology and recent flux estimates. **a)** Chronology of key magmatic-volcanic events in lunar history. (1) Elkins-Tanton et al. (2011); (2) Shearer et al. (2015); (3) Nyquist and Shih (1992); (4) Shearer et al. (2006), Sokol et al. (2008), Curran et al. (2019), Snape et al. (2018, 2019), Terada et al. 2007); (5) Stöffler et al. (2006); (6) Wagner et al. (2002, 2010); (7) Whitten and Head (2015a,b); (8) Hiesinger et al. (2011), Stadermann et al. (2018); (9) Borg et al. (2004); (10) Hurwitz et al. (2013); (11) Jolliff et al. (2011); (12) Braden et al. (2014); (13) Schultz et al. (2006); (14) Solomon and Head (1980). Recent radiometric dates from Chang'e 5 Oceanus Procellarum samples are ~2 Ga. (Che et al. 2021; Li et al. 2021) (From Head and Wilson 2017). **b)** (a) Histogram of mare surface deposit model ages as of ~2011 (**dark gray bars**) (derived from CSFD from Hiesinger et al. 2011; Whitten et al. 2011; *N* = total sample in histogram). Exposed mare basalt emplacement appears to start abruptly at ~3.8 Ga and slowly decrease over the next 2.5 Gy. Most mare basalts appear to have erupted during peak volcanic activity at ~3.7 Ga (the mode of this mare basalt age distribution; **vertical dashed black line**). These data give an average mare basalt age of ~3.3 Ga. The **vertical blue band** illustrates the range of returned sample isotopic ages inferred for impact basins (Stöffler et al. 2006). (b)–(d) illustrate the uncertain options for the onset and early flux of mare basalt eruptions (**dashed vertical line** = 3.9 Ga). (From Whitten and Head 2015a).

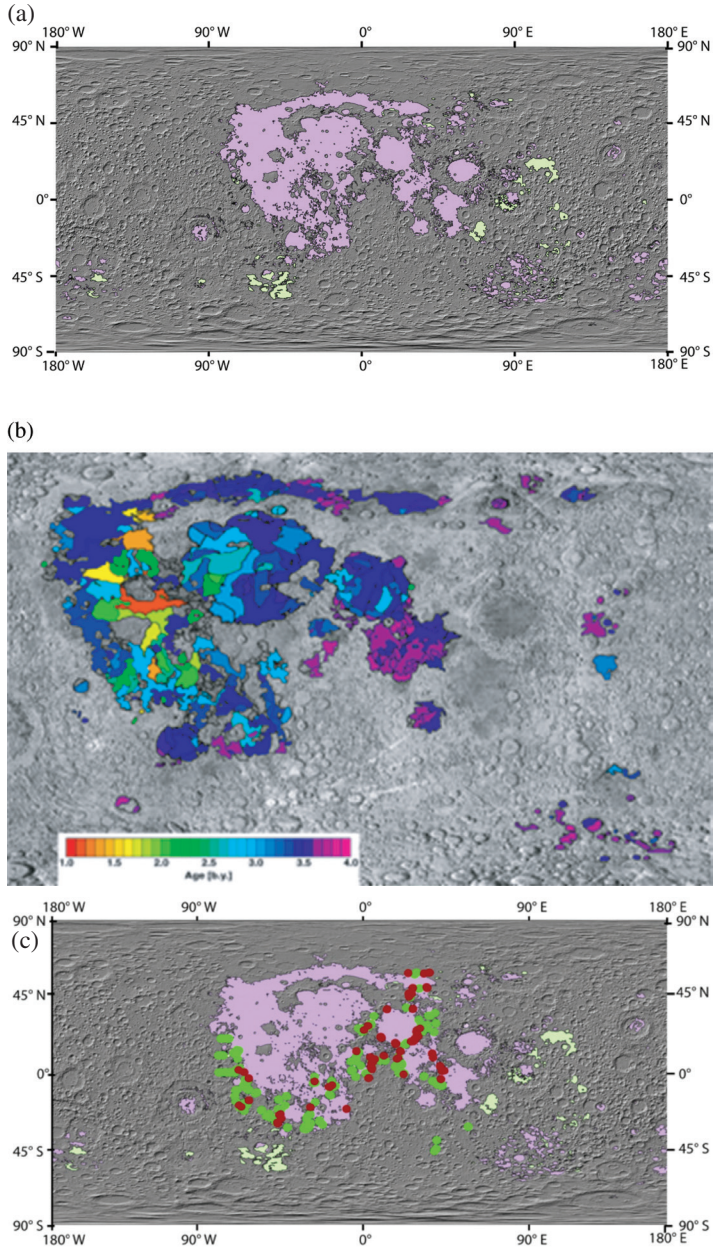


Figure 3. Global distribution of features and units. Basemap for a), c), d), f) and g) is LOLA hillshade, equidistant cylindrical projection. a), c), d) from Head and Wilson 2017. **a)** Mare and cryptomaria. Global map showing the distribution of lunar mare basalts (**purple**) and cryptomaria (**light green**) (Cryptomaria distribution data from Whitten and Head 2015a,b). **b)** Areal distribution of lunar mare basalt units dated by CSFD methods (modified from Hiesinger et al. 2011; for recent updates see Morota et al. 2015; Hiesinger et al. 2023, this volume, and Fig. 11–12). **c)** Global distribution of linear and arcuate rilles interpreted as graben (**red dots** show rilles with evidence for associated volcanic features; green dots show rilles with no evidence). (Data from Petrycki and Wilson 1999a,b, and Petrycki et al. 2004). Lunar mare basalt distribution shown in **purple** and cryptomaria in **light green** (Data from Whitten and Head 2015a,b).

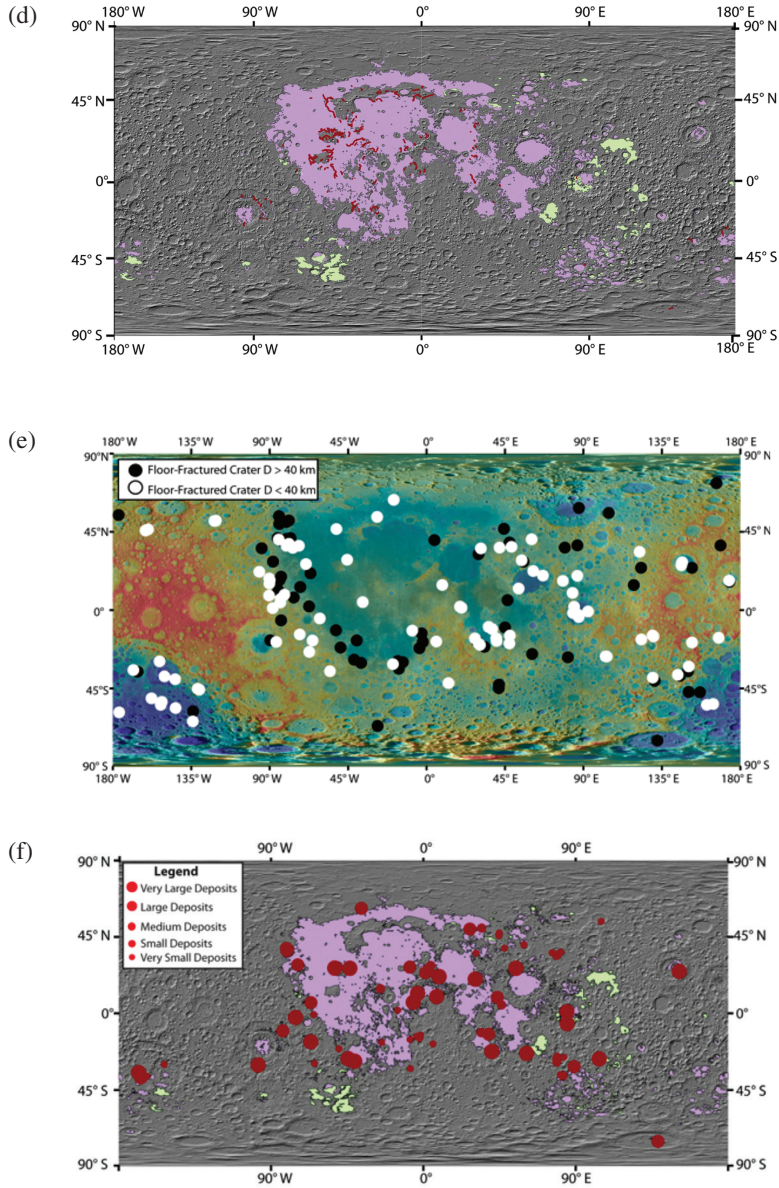


Figure 3 (cont'd). Global distribution of features and units. Basemap for a), c), d), f) and g) is LOLA hill-shade, equidistant cylindrical projection. a), c), d) from Head and Wilson 2017. **d)** Global distribution of lunar sinuous rilles (data from Hurwitz et al. 2013). Lunar mare basalt distribution shown in purple and cryptomaria in light green (data from Whitten and Head 2015a,b). **e)** Global distribution of lunar floor-fractured craters (FFCs) (Jozwiak et al. 2012). On the basis of crater floor shape and structure, FFCs >40 km diameter (**black dots**) are interpreted to be sills; those <40 km (**white dots**) are interpreted to be laccoliths (data from Jozwiak et al. 2015b); see EA-11–3-4). (Data from Jozwiak et al. 2015b.) **f)** Global distribution of lunar pyroclastic occurrences (**red dots**; dot size, small to large, reflects relative size of deposit). The distribution of mare basalts (**purple**) and cryptomaria (**light green**) is also shown (data fromWhitten and Head 2015a,b). (Data from Gaddis et al. 2003.)

(g)

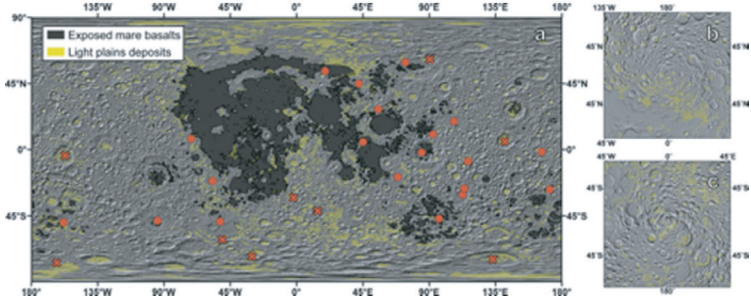


Figure 3 (cont'd). Global distribution of features and units. Basemap for a), c), d), f) and g) is LOLA hillshade, equidistant cylindrical projection. a), c), d) from Head and Wilson 2017. **g)** Cryptomare (**red symbols**) and light plains (**yellow**) (Whitten and Head 2015a,b). Detected cryptomaria (**red circles**), regions of proposed cryptomaria (**red x marks**) that do not have basaltic mineralogies (or a high concentration of dark-halo craters). See Whitten and Head (2015a,b) for references for the light plains units included. (Data from Whitten and Head, 2015a,b).

aluminum basalts, Mg-suite rocks, etc. Were any of these rock types ever emplaced as extrusive deposits on the lunar surface? Do these KREEP/aluminous basaltic fragments represent more extensive early volcanic deposits that have been obscured by the intense bombardment history? Do they represent fragments of impact melt deposits? Some, such as the Mg-suite, have been traditionally interpreted as plutonic in nature (e.g., Shearer et al. 2015), and thus are not expected to have been extruded to the surface, but recent work (Prissel et al. 2016) has shown that these magmas are likely to have had the capability to erupt to the surface. Are such extrusive deposits, too, lost in the vertically and laterally homogenized megaregolith? Future remote sensing and sample return missions need to address these important questions. It is clear, though, that the primary type of extrusive lunar volcanic deposits are the mare basalts, and with the unresolved questions mentioned above, we proceed with a primary focus on these.

2. *When did mare volcanism begin?* Samples returned from Apollo 11 revealed a very ancient age for mare basalts, ~3.7 Ga, but fragments of mare basalts in highland breccias and meteorites suggested that the onset was earlier (Fig. 2a). In addition, the presence of dark-halo craters in light plains (punching through the light plains and excavating buried mare deposits) suggested that the record of extrusive mare deposits was not limited to those plains with a strong albedo contrast to the highlands. Thus began the search for "cryptomaria" (Schultz and Spudis 1979, 1983; Head and Wilson 1992), near-surface mare deposits that are obscured by the emplacement of ejecta from nearby craters and basins. This search, aided by high spatial and spectral resolution remote sensing data (e.g., Whitten and Head 2015a,b), confirmed the presence of extensive deposits of cryptomaria (Fig. 3a), expanded the known area of mare volcanism by 1.8%, and revealed that their mineralogy was similar to later mare basalts exposed in the same areas. Whitten and Head (2015a,b) also showed that mare volcanism is likely to have commenced sometime during the era of large impact basin formation (Figs. 2, 3a). Sori et al. (2016) undertook a search for cryptomare deposits using GRAIL data (Zuber et al. 2013) and concluded that huge volumes, comparable to the total volume of mare basalts, might exist. Remaining uncertainty about the beginning of lunar mare volcanism is the actual time of onset (Fig. 2), its relationship to the lunar magma ocean and its density stratification aftermath (e.g., Hess and Parmentier 1995; Mallik et al. 2019), and distinguishing buried mare deposits in the crust from Mg-suite intrusions (e.g., Sori et al. 2016) and similarly obscured extrusions (e.g., Prissel et al. 2016).

3. *When did volcanism end?* The youngest radiometrically-dated lunar magmatic rock yet known is from meteorite NWA 773, a KREEP-rich olivine cumulate dated at ~2.865 Ga (Borg et al. 2004), while the youngest radiometrically-dated mare basalt was from Apollo 12 at 3.1 Ga (Nyquist et al. 1979) (Fig. 2a) until the recent Chang'e 5 mission returned ~2.0 Ga

basalt samples (Che et al. 2021; Li et al. 2021) from Oceanus Procellarum (Qian et al. 2018; 2021a,b). Stratigraphic evidence, together with ages from size–frequency distributions (CSFD) of craters superposed on flow units, suggest a youngest age of ~1.0 Ga from a unit south of Aristarchus Plateau (e.g., Stadermann et al. 2018) (Fig. 2b, 3b). Optical immaturity and morphologic freshness led Schultz et al. (2006) to propose that recent outgassing activity occurred within the last 10 million years at Ina, a small shield volcano summit depression. Braden et al. (2014) used high resolution image and topography data from LRO to document the presence of a group of very unusual features associated with the lunar maria and termed "Irregular Mare Patches" (IMPs). The largest of these, Ina, Sosigenes and Cauchy 5, were dated using superposed craters and were all found to be less than 100 Ma in age! The occurrence of several dozen smaller IMP features in the lunar maria led Braden et al. (2014) to conclude that mare volcanic activity extended to the very recent geologic past, within the last 100 Ma, and that lunar thermal evolution models needed to be extensively adjusted accordingly. While the age interpretation is not without controversy (see Qiao et al. 2021a), the presence of IMPs and their young CSFD ages raise significant questions about the duration of lunar mare volcanism. Furthermore, the documentation of the widespread occurrence of Ring Moat Dome Structures (RMDS), a populations of several hundred-meter-wide low mounds surrounded by moats, and first seen in Lunar Orbiter images (Schulz and Greeley 1976), has been interpreted as possibly representing relatively recent mare volcanism (Zhang et al. 2017, 2020; Basilevsky et al. 2019) due to their topographic crispness and embayment relationships with craters superposed on the underlying mare units. Thus, these interpretations of very young volcanism (Fig. 2a), while the subject of current debate (Zhang et al. 2020), present significant research challenges to the traditional views of the waning stages of lunar thermal evolution and the nature and duration of mare volcanic magma generation, ascent and eruption.

4. *What is the areal distribution and coverage of volcanic deposits?* Our historical view of the Moon has been dominated by the abundance of nearside dark mare plains, a perception disrupted by the discovery by Luna 3 in 1959 that there was a distinct paucity of maria on the farside. Proper equal-area projection of the nearside also showed that the nearside limbs were deficient in maria, further reducing the earlier apparent widespread nearside nature of their distribution. Currently, low-albedo lunar mare deposits cover ~16.3% of the Moon; recent assessments of the distribution of cryptomaria have increased this area to 18.1% (Whitten and Head 2015b) (Fig. 3a), and suggestions have been made that GRAIL data may reveal even more buried maria (e.g., Evans et al. 2016; Gong et al. 2016; Sori et al. 2016). In addition to the dramatic nearside-farside discrepancy in mare basalt deposit distribution, areas that are covered by maria are concentrated in young impact basins (e.g., Imbrium, Serenitatis, Crisium), older degraded basins (e.g., Tranquillitatis and Fecunditatis), and the floors of large impact craters. Mare deposits on the farside are much less areally abundant, do not significantly flood large impact basins, and even the mare deposits in the largest farside basin (South Pole–Aitken) tend to occur on the floors of superposed ancient craters (Fig. 3a), although much of the basin floor may be occupied by cryptomere obscured by Orientale ejecta (Whitten and Head 2015). It is still not clear whether the nearside-farside asymmetry in mare basalt distribution could be due primarily to differences in crustal thickness (e.g., Wilson and Head 2017a), or instead represents fundamental differences in the nature of nearside-farside crust and mantle properties (e.g., asymmetric distribution of heat producing elements; Wieczorek and Phillips 2000; Wieczorek et al. 2001; Parmentier et al. 2002; Laneuville et al. 2013).

5. *What is the regional and average thickness of mare volcanic deposits?* Derivation of total volumes requires thickness data in addition to areas. Estimates of basaltic fill thickness have employed a wide variety of techniques. Quantitative embayment relationships with impact craters (height of the rim crest of a pre-mare flooded crater) (e.g., DeHon 1976) and spectral analysis of superposed craters (the smallest crater that excavates submare material)

(e.g., Thomson et al. 2009; Weider et al. 2010) are useful techniques for local determinations. These can be supplemented and complemented by models of landscape flooding (e.g., Whitten and Head 2013), radar sounding data (e.g., Phillips et al. 1973), seismic data, gravity data and models (e.g., Wieczorek et al. 2006), as well as interpretations of the underlying topography of large basins (Head 1982). Virtually all of these techniques have been employed to derive both local and regional mare basalt thickness estimates. The relatively small number of data points (e.g., superposed craters with non-mare ejecta and appropriately flooded craters) and the lack of detailed and widespread geophysical seismic and sounding data, point to the need for improved measurements for mare basalt thicknesses. One of the greatest uncertainties is the thickness of mare fill in impact basin interiors, which could range up to 5–10 km, depending on the thermal structure at the time of basin formation, and thus the initial depth of the basin, as well as its relaxation, subsequent loading and subsidence. High-resolution global GRAIL gravity data offer the promise of helping to constrain these thickest parts of the lunar maria. Using GRAIL gravity data, Gong et al. (2016) employed a localized multitaper spherical-harmonic analysis to calculate an effective density spectrum to yield an estimate of crustal density average as a function of spherical harmonic degree. Comparing this observed effective density spectrum with one generated from a theoretical model, Gong et al. (2016) estimated the total thickness of basalts on the nearside to be 0.74 km, twice as large as previous estimates by DeHon (1979) for northern Oceanus Procellarum. Further analyses of GRAIL data (e.g., Evans et al. 2016) utilized the presence of more than 100 quasi-circular gravity anomalies in the maria interpreted to be buried impact craters and concluded that the average nearside mare thickness was at least 1.5 km and that local lenses could be up to 7 km thick. On the basis of the differences in approach and total estimates, the average and local thicknesses of mare basalts remain to be accurately determined, and are a key topic for future exploration. More detailed local studies with GRAIL data will contribute significantly to improving the estimate of mare basalt thicknesses (e.g., Kiefer 2013; Evans et al. 2016, 2018; Gong et al. 2016; Deutsch et al. 2019; Head et al. 2020), and thus total volumes.

6. *What is the total volume of mare basalt?* Using the area of the Moon covered by mare basalts, and estimates of their thicknesses, the total volume of mare basalts has been estimated to be ~1×10^7 km^3 (e.g., Head and Wilson 1992), less than 1% of the total volume of the lunar crust (Head 1976). In a study of features detected in GRAIL data and interpreted to be impact craters buried by mare volcanism, Evans et al. (2016) estimated the total volume of nearside mare basalts to lie between 1.1 and 3×10^7 km^3. Uncertainties in the total volume of mare basalts derive from three sources: 1) estimates of the ranges and average thickness of the surface mare volcanic record described above; 2) the volume of cryptomaria that might exist in the near-surface (Whitten and Head 2015a,b) and deeper subsurface (Sori et al. 2016); and 3) the percentage of mare basalts that are plutonic and might exist as dikes, sills and other intrusions (e.g., Andrews-Hanna et al. 2018), complementing the numbers for extrusive volumes. Several factors influence the volume of the plutonic component of mare basalt volcanism. First, the low density of the lunar anorthositic crust, as well as the great depth of mare basalt source regions in the mantle (Figs. 1b, 4), both disfavor plutonic activity associated with mare volcanism other than the dikes that delivered the extrusive volcanic magma to the surface (except under certain circumstances, such as floor-fractured craters; e.g., Jozwiak et al. 2017; Wilson and Head 2018c). Furthermore, the great depth of mare basalt source regions, the rapid ascent of magma to the surface, and the relatively low frequency of diking events, have been called upon as an explanation for the general lack of shallow magma reservoirs, large shield volcanoes and calderas on the Moon (Head and Wilson 1991). Although such dikes may have been tens to over a hundred meters wide (Wilson and Head 2017a), relaxation of elastic forces holding the dike open in the waning stages of the eruptions will have tended to reduce their widths to significantly smaller values before their solidification (e.g., Wilson and Head 2018d). Head and Wilson (1992) estimated that the lunar crust might consist of up to ~37% dikes by volume. An important area for future research is the refinement of these intrusive estimates and an

assessment of the implication of the presence of dikes for models of lunar crustal density structure and thickness. In summary, the estimated total volume of extrusive lunar mare basalt volcanism is currently estimated to be on the order of ~1–3 × 10^7 km^3.

7. *What is the mare basalt flux?* Armed with these data, what can we say about the flux (volume as a function of time) of lunar volcanism, and implications for the state and nature of mantle source regions and the thermal evolution of the Moon? On the basis of the areal distribution of mare deposits and the CSFD age distribution of these deposits, the sign and shape of the flux curve is clear: mare volcanism was much more abundant in early lunar history than in later times (Fig. 2b). The quantitative definition of this flux curve is less clear. Each succeeding lava flow unit can serve to partly or wholly bury earlier units, a process exacerbated by the pronounced vertical topography of impact craters and basins. Plots of the frequency distributions of dated mare units are helpful (Fig. 2b), but again, the total volume (and often ages) of earlier units are currently unknown. If the total volume of mare basalt extruded to the surface is of the order 10^7 km^3, how much is extruded as a function of time? Mapping and CSFD dates from exposed mare basalt units (Hiesinger et al. 2011; Morota et al. 2015) show that the flux decreased significantly over the extended period of mare basalt volcanism (Fig. 2b). To a first order, the volcanic flux is trivial, and at its peak flux in the Imbrian period, was ~10^{-2} km^3/a, comparable to fluxes from individual volcano sources on Earth, such as Vesuvius and Kilauea (Head and Wilson 1992). Needham and Kring (2017) recently calculated the flux of mare basalts in an attempt to estimate the flux of volatiles at the lunar surface, and to assess whether the rate was sufficiently high to form and retain a lunar atmosphere. On the basis of their analysis of the volumes and dates of lunar mare basalt eruptions, assumptions about the buried structure of mare-filled lunar impact basins, and volatile release patterns of erupted magmas, they concluded that during an interpreted peak volcanic flux at ~3.5 Ga (~5.5 × 10^6 km^3; ~10,000 kg/s), volatile release could have formed a maximum lunar surface atmospheric pressure of ~1 kPa and that the atmosphere could have taken as much as ~70 million years to fully dissipate. Head et al. (2020) revised these volume/flux estimates downward, and outlined areas of future investigation and exploration needed to improve volume and flux estimates.

Recent acquisition of high resolution image data from LRO and Kaguya have permitted the dating of small mare units and a more representative set of farside mare units (Morota et al. 2009, 2011b, 2015; Hiesinger et al. 2011; see summary in Hiesinger et al. 2023, this volume). This enables the comparison of the nearside, limbs and farside, and correlations with crustal thickness (Morota et al. 2015). For example, Whitten et al. (2011) found that the range of ages of volcanic units associated with the Orientale basin on the western limb (intermediate thickness crust between the thin nearside and the thick farside) was comparable to the age range of nearside lunar maria, but that the abundances and volumes of volcanic deposits were much lower. A similar situation exists on the lunar farside (e.g., Morota et al. 2015; Paskert et al. 2015, 2018): mare volcanic unit ages range from ~3.8 to 1.5 Ga, but occur in much lower abundances Hiesinger et al. 2023, this volume). This has been interpreted to imply that both nearside and farside mare basalt mantle sources were active throughout the mare volcanism era, but that less magma was being generated on the farside, or less reached the surface on the farside, or both (Fig. 1b). These observations and results have important implications for mantle source regions and the thermal evolution of the Moon. Despite the uncertainty of the earlier part of the magma flux curve (Fig. 2b), the general trends are clear (Whitten and Head 2015a,b; Hiesinger et al. 2023, this volume). Mare volcanism peaked between 3.8 and 3.4 Ga, declined rapidly to a low plateau between 3.3 and 3.0 Ga, and then was very low (averaging less than 3–4 units per 100 My for the next 1.8 Gy); no major units are found in the last ~1.0 Ga, but local young activity associated with RMDSs and IMPs has not been ruled out.

We now summarize the broad progress in the understanding of the relationship between lunar mare volcanism and its mantle source regions, and how this informs us about the nature of magma generation, ascent and eruption and emplacement mechanisms.

4. WHAT HAVE WE LEARNED ABOUT PROCESSES OF BASALTIC MAGMA GENERATION, ASCENT AND ERUPTION?

In order to fully understand the implications of surface volcanic deposit morphologies, observations and interpretations must be placed in the context of a model for the generation, ascent and eruption of magma, a model that can be tested and refined by observations. Following the early recognition and cataloguing of a wide variety of lunar volcanic features and deposits, Wilson and Head (1981) sought to apply terrestrial models to the Moon, but not finding a suitable end-to-end model for the Earth, developed a terrestrial model and then applied it to the Moon. Subsequently, significant advances in the understanding of lunar crustal density and thickness, magma physical properties, density and volatile content, lunar thermal gradients and thermal evolution, as well as diapiric processes, melt generation processes, and dike emplacement theory (summarized in other NVM-2 chapters), all led toward a convergence of information that could be applied to increasingly detailed models of lunar magma ascent and eruption (e.g., Wilson and Head 1981, 2003a,b, 2017a,b, 2018c,d; Head and Wilson 1992, 2017). Results from the long and productive period of field volcanological observations could now be combined with data from the broader perspectives of lunar science to generate a physical volcanological view of lunar volcanism (Fig. 4). From these considerations, we now highlight some of the most important themes that have emerged.

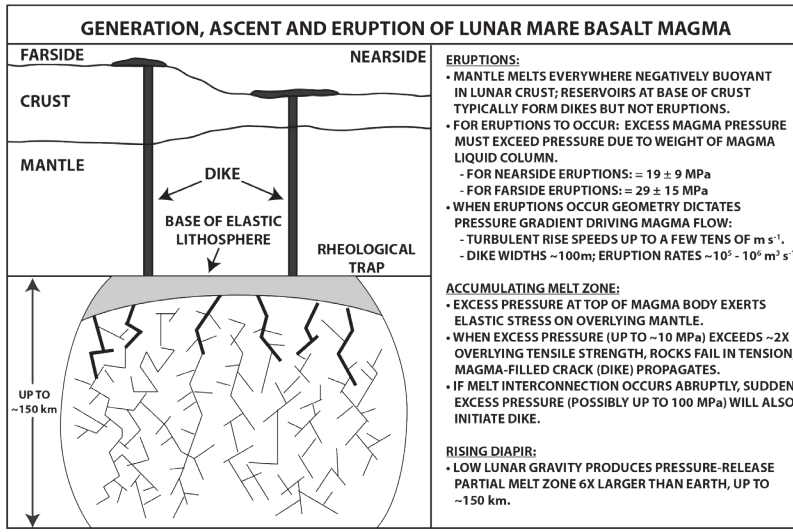
4.1. Magma buoyancy

Most recently, Wilson and Head (2017a) have modeled the principles of ascent and eruption of lunar mare basalt magmas with new data on 1) crustal thickness and density (GRAIL), 2) magma properties, and 3) surface topography, morphology and structure (LRO). For example, GRAIL recently measured the broad spatial variation of the bulk density structure of the crust of the Moon (Wieczorek et al. 2013), finding a mean crustal density of ~2550 $kg{\cdot}m^{-3}$. Using the range of liquidus densities of mare basalts (2775 to 3025 $kg{\cdot}m^{-3}$) and lunar picritic magmas (2825 to 3150 $kg{\cdot}m^{-3}$), the average magma density was modeled as ~2950 ± 200 $kg{\cdot}m^{-3}$ (Wilson and Head 2017a). These results show that essentially all basaltic magmas were negatively buoyant everywhere within the lunar crust (Fig. 4a–b).

4.2. Magma positive excess pressures

Due to the presence of lava on the surface, positive excess pressures must have been present in melts at or below the crust-mantle interface in order for them to erupt. The excess pressure source is clear from the following principles for melt in any region experiencing partial melting, or in any region containing accumulated melt (Fig. 4). The melt will behave as though an excess pressure is present at the top of the melt column if 1) the melt is positively buoyant relative to the host rocks and 2) the melt forms a continuously interconnected network. This means that in partial melt regions, at least a few percent melting must have taken place. Evidence from lunar petrology suggests that mare basalts and picritic glasses may have been derived from polybaric melting of source rocks in regions that extended vertically for at least a few tens of km (e.g., Shearer et al. 2023, this volume). This is supported by the fact that the vertical extent of a region containing inter-connected partial melt produced by pressure-release melting is inversely proportional to acceleration due to gravity. Wilson and Head (2017a) translated the ~50 km vertical extent of melting in a rising mantle diapir on Earth to the Moon, implying that lunar mantle melting could have taken place over a vertical extent of $\lesssim$ 300 km. Therefore, they concluded that in the absence of convection, melting could have occurred throughout any region in which heat from radioisotope decay was accumulating, possibly even extending to most of the mantle.

(a)



(b)

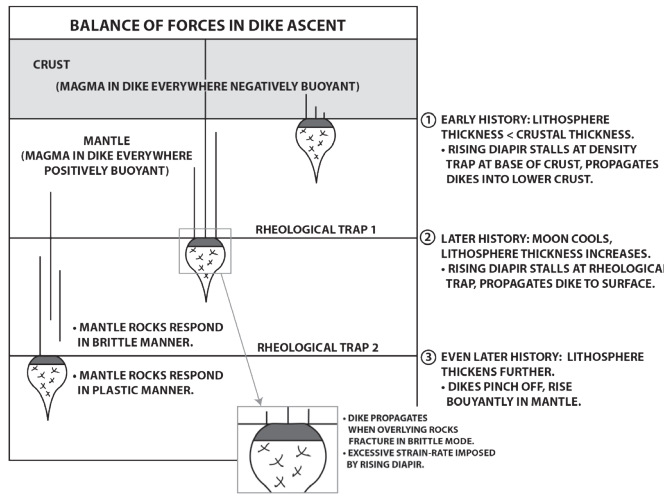


Figure 4. Basic principles of generation, ascent and eruption of mare basalt magma (From Head and Wilson 2017). **a)** Relationships of initial diapiric rise, melt accumulation, and factors leading to dike propagation, rise in the mantle and through the crust, to erupt. **b)** Conceptual cross-sectional interpretation of the balance of forces in diapir formation and rise, brittle fracturing and dike propagation; also shown is their relationship to changes in style related to lunar thermal evolution.

4.3. Magma body excess pressure

Magma body maximum excess pressure depends on its environment (Wilson and Head 2017a) (Fig. 4a). If melt percolates upward from a partial melt zone and accumulates as a magma reservoir (either at the density trap at the base of the crust or at the rheological trap at the base of the elastic lithosphere) (Fig. 4b), the excess pressure, located at the top of the magma body, will exert an elastic stress on the overlying rocks. Eventually, when the excess pressure rises to close to twice the tensile strength of the host rocks (perhaps up to ~10 MPa), this will cause failure

of these rocks in tension, and a magma-filled crack (dike) will propagate upward from this point (Fig. 4a). Partial melting occurring in a larger region deep in the mantle will be different, however. Connections between melt pockets and veins may not occur until a finite amount of melting has occurred (probably a few percent). When these interconnections do occur, the excess pressure at the top of the partial melt zone will rise abruptly to a high value and initiate a brittle magma-filled fracture, i.e., a dike. This excess pressure corresponds to the product of 1) the finite vertical extent of the melt zone, 2) the difference in density between the host rocks and the melt, and 3) the acceleration due to gravity. For example, if the vertical extent of the partial melt zone is 300 km, the excess pressure due to a typical 360 $kg \cdot m^{-3}$ difference in density between a magma and its host mantle would rise abruptly to ~174 MPa. This pressure is significantly greater than the value needed to initiate a dike. On the basis of these principles, Wilson and Head (2017a) explored excess source pressures over the range of 10 to at least 100 MPa.

4.4. Dikes, intrusions and eruptions: Magma bodies at/near the base of the crust

For the case where eruptions take place through dikes extending upward from the base of the crust (Fig. 4b), the mantle magma pressure at the dike initiation point must be greater than the pressure due to the weight of the liquid magma column. For the lunar nearside (Fig. 1b), therefore, the excess pressure must be at least ~19 ± 9 MPa for an eruption to occur. On the lunar farside the corresponding range of minimum excess pressures is ~29 ± 15 MPa for an eruption to occur. Slightly smaller excess pressures are needed if the top of the magma body feeding an erupting dike is somewhat below the base of the crust, due to the fact that the magma is positively buoyant in the part of the dike within the upper mantle. Wilson and Head (2017a) found that it is likely that even the smallest of these excess pressures is greater than the ~10 MPa maximum value in a magma reservoir at the base of the crust or elastic lithosphere. However, these values are easily met by excess pressures expected in extensive partial melt zones deeper within the mantle. In summary, magma accumulations at the base of the crust are predicted 1) to have been able to intrude dikes part-way through the crust, but 2) not able to feed eruptions to the lunar surface. In order for magma to have been erupted to the surface, magma must have been extracted from deeper mantle sources, consistent with the petrologic evidence (e.g., Shearer et al. 2023, this volume).

4.5. Dikes, intrusions and eruptions: Magma bodies deep in the mantle

Wilson and Head (2017a) showed that deep mantle sources could have provided excess pressures of up to 100 MPa. They used the pressure gradient driving magma flow and the mean dike width to determine the magma rise speed and found that magma motion is turbulent for any plausible lunar magma viscosity, and the rise speeds are of order 10 $m \cdot s^{-1}$. Buoyant dikes extending upward from deep mantle partial melt sources can actually disconnect from the source regions and travel upward through the mantle as isolated bodies of melt that can encounter and penetrate the crust–mantle density boundary (Fig. 4b). These disconnected dikes adjust their lengths and internal pressure excesses as they rise so that the stress intensity at the lower tip is always zero.

4.6. Implications for the vertical extent of magma source regions

The vertical extent of the source region from which a dike grows determines the potential total vertical extent of the resulting melt body. If the source extent is small, the upper tip of the resulting dike that crosses the crust–mantle boundary cannot reach the surface anywhere on the Moon, resulting in dike intrusion only. For intermediate source-region extents, the dike can reach the surface and erupt on the nearside but still cannot reach the surface on the farside. For larger source extents, eruptions could occur on both the lunar nearside and the farside (Fig. 1b, 4). Wilson and Head (2017a) used the observed paucity of farside eruptions to imply a restricted range of vertical extents of partial melt source region sizes, between ~16 and ~36 km.

4.7. Pressure gradient driving magma flow

Wilson and Head (2017a) found that when eruptions can occur, the available pressure in excess of what is needed to support a static magma column to the surface can be used to determine the pressure gradient driving magma flow. Typical turbulent magma rise speeds are ~10 to a few tens of $m \cdot s^{-1}$, dike widths are of order 100 m, and eruption rates from 1 to 10 km-long fissure vents are of order 10^5 to 10^6 $m^3 \cdot s^{-1}$.

4.8. Lava volume eruption rates

When dikes open to the surface, the lava volume eruption rates corresponding to the magma rise speeds involve the horizontal lengths of active fissures. Wilson and Head (2017a) found that observable lunar features interpreted as fissure vents (e.g., elongate sinuous rille source depressions) are rarely longer than ~10 km. Although longer fissures may have existed (and been covered by erupted lavas), they used 10 km as a conservative example. They calculated volume fluxes to be of order 10^5 to 10^6 $m^3 \cdot s^{-1}$. Lunar eruption volume fluxes derived from lava flow thicknesses and surface slopes, or rille lengths and depths, were found to be of order 10^5 to 10^6 $m^3 \cdot s^{-1}$ for volume-limited lava flows and $>10^4$ to 10^5 $m^3 \cdot s^{-1}$ for sinuous rilles, with dikes widths of ~50 m (Wilson and Head 2017a).

In summary, the Wilson and Head (2017a) analysis that incorporates a range of new and updated values underlines a series of important guidelines for the generation ascent and eruption of magma on the Moon, and provides a physical volcanological framework of predictions to be tested against new observations and data (Fig. 4): First, essentially all lunar magmas were negatively buoyant everywhere within the lunar crust. Secondly, at least 20–30 MPa positive excess pressures must have been present in mantle melts at or below the crust-mantle interface to drive magmas to the surface. Thirdly, such a range of pressures can easily be produced in zones of partial melting by at least two sources: 1) pressure-release melting during mantle convection, or 2) simple radioisotope heat accumulation. Fourthly, magma volume fluxes calculated to be available from melts accumulating at the top of partial melt zones are consistent with the volume fluxes implied by earlier analyses of surface flows (10^5 to 10^6 $m^3 \cdot s^{-1}$).

We now use these basic principles, guidelines and predictions (Fig. 4) to compare to the field volcanological documentation of the array of known lunar volcanic features, deposits and structures (Figs. 3, 5) in order to assess the physical volcanology of their eruption conditions.

5. LUNAR VOLCANIC LANDFORMS AND IMPLICATIONS FOR MAGMA ERUPTION CONDITIONS

The nature of lunar volcanic landforms can provide important insights into eruption conditions on the Moon, compositions and volatile contents of magma, the nature of magma source regions, and changes in these aspects with time. In the first five decades of the Space Age, individual lunar volcanic features were identified, catalogued and interpreted on a case-by-case basis, with the broad goal of comparing them to those on the Earth, establishing associations, and generally defining the nature of lunar volcanism. Subsequent to NVM (2006), the acquisition of high spatial/spectral resolution data, as well as high resolution topography, has considerably enhanced our understanding of the morphology, morphometry and mineralogy of these features (Fig. 5, EA-11-1-14). In parallel, improved models of magma generation, ascent and eruption (summarized in Section 3) provide a basic framework in which to relate dike emplacement events and eruptions to the array of volcanic landforms (e.g., Head and Wilson 2017) (Fig. 5). Finally, the discovery and improved understanding of the production and exsolution of volatiles in rising magma (Saal et al. 2008; Hauri et al. 2011, 2015; Rutherford et al. 2017) permitted the development of a predictive model of volatile-containing lava flow emplacement (e.g., Wilson and Head 2018a). Here we briefly summarize

the major lunar volcanic features (Fig. 5, EA-11-1-14), indicate what we do observe and do not observe relative to Earth, and discuss the relationships of landforms to dike emplacement events (Fig. 5). We then place these in the context of recent models for the generation, ascent and eruption of magma, and use these results to summarize our current knowledge of secondary crustal formation on the Moon. Finally, we outline a series of significant unanswered questions, and describe the types of missions and research that might help to address these (EA-11-17,18).

5.1. Dikes that propagate to the near-surface and stall

In some cases, dikes can stall in the lunar crust and not reach the surface to erupt (Fig. 5), generating a range of seemingly unrelated, but now predictable, outcomes. If dike ascent stalls in the lower to middle crust, heat will be conducted to surrounding crustal rocks and dike solidification will occur (decades-scale cooling times) (Wilson and Head 2017a). This scenario is particularly favored in the thicker highland crust of the lunar farside (Figs. 1b, 4) (e.g., Jozwiak et al. 2015a–their Figure 11; Head and Wilson 2017). Dikes propagating to somewhat shallower depths might be manifested at the surface by the venting of gas from the top of the dike to produce linear crater chains (either collapse or explosion craters) along the surface trace of the dike (Fig. 5b); the 190 km long Mendeleev crater chain is a candidate example (Head and Wilson 2017; their Figure 12). Depending on the dike width and depth of intrusion, shallow dike emplacement can set up near-surface extensional stress fields resulting in graben formation above the dike (e.g., Head and Wilson 1993). Linear and arcuate graben can also be produced by regional tectonic stresses (Solomon and Head 1980), and thus the distribution of graben on the Moon (Petrycki et al. 2004; French et al. 2015; Fig. 3c) is not simply a map of subsurface dikes. Klimczak (2014) described high-resolution topography techniques that can be used to identify graben related to dike emplacement. A further indication of dikes that have intruded to the shallow subsurface and stalled are graben that are populated by pit craters (Okubo and Martel 1998), caused by degassing and collapse (e.g., Hyginus; Wilson et al. 2011) (Fig. 5b–c; EA-11-1) and small pyroclastic cones located along the trace of the graben (Fig. 5c) (e.g., Rima Parry 5; Head and Wilson 1993, 2017–their Fig. 21). Other, isolated pit craters (e.g., Haruyama et al. 2009a; Robinson et al. 2012; Wagner and Robinson 2014) (EA-11-2) are more enigmatic, but are important targets of investigation (e.g., Nesnas et al. 2019) due to their exposure of mare stratigraphy, their link to the subsurface (sinuous rilles, magmatic void spaces), and their potential use for shelter in future human exploration. A major outstanding question is the abundance of these near-surface and deeper dikes (and void spaces) and how their quantity influences the density structure of the highlands crust.

5.2. Dikes that propagate to the near-surface and intrude sills

On Earth, small dike volumes and low propagation velocities favor shallow intrusions. On the Moon, dike propagation velocities are typically sufficiently high that shallow sill formation is not favored (Wilson and Head 2017a). However, local low-density breccia zones beneath impact crater floors may cause lateral migration to form laccoliths (e.g., Vitello Crater) and sills (e.g., Humboldt Crater) (EA-11-3-4) (Jozwiak et al. 2012, 2015a,b). The population of lunar floor-fractured craters (FFCs) (Fig. 3e) (Schultz 1976a,b; Jozwiak et al. 2012, 2015a,b) is interpreted to represent the surface manifestation of a class of magma-filled cracks (dikes) rising to the surface from great depth that encounter contrasts in host rock lithology where an increase in ductility (base of breccia lens) or rigidity (base of solidified melt sheet) occurs, causing the magma to spread laterally, forming a laccolith or sill, and uplifting and deforming the crater floor. Dynamical considerations strongly favor the subcrustal breccia lens as the location of the physical property contrast localizing lateral intrusion, at a depth of several kilometers; this leads to the conclusion that dike magma volumes are up to ~1100 km^3 (generally insufficient to form FFCs on the lunar farside) (Jozwiak et al. 2015a,b). Estimated magma volumes available for injection into lunar nearside sills (up to ~800 km^3)

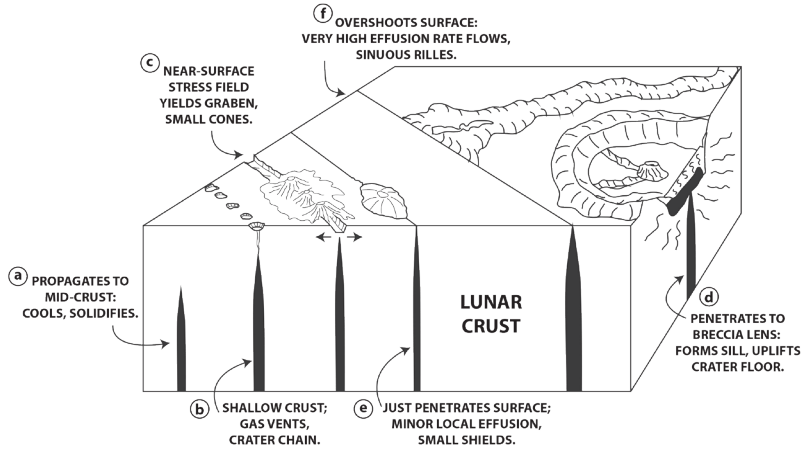


Figure 5. Block diagram showing a synthesis of the predicted variety of behaviors of mare basalt crustal dikes approaching, stalling, intruding and erupting. (From Head and Wilson 2017.)

are comparable to the observed floor uplift in many smaller FFCs, and thus consistent with a single dike emplacement event; larger FFCs may require more than one intrusion (e.g., Jozwiak et al. 2012, 2015a,b).

New knowledge about the presence and behavior of magmatic volatiles (e.g., Rutherford et al. 2017) has provided additional perspectives on shallow intrusion processes in FFCs (Wilson and Head 2018c). Increasingly lower overburden pressure encountered as the magma ascends enhances gas formation and brings the magma into the realm of the low-pressure release of H_2O and sulfur compounds. Wilson and Head (2018c) outlined a temporal sequence of events in FFC formation, including syn- and post-intrusion uplift, degassing, bubble rise, foam layer formation and collapse, and subsidence (Fig. 6). Subsidiary dikes can be emplaced in the fractures at the uplift margins and will rise to the isostatic level of the initial dike tip; if these contain sufficient volatiles to decrease magma density, eruptions can also occur, and many such manifestations are seen in FFCs as effusive and explosive eruption products (Jozwiak et al. 2012, 2015a,b) (EA-11-3-4).

Gravity data have been interpreted to provide evidence for a several km thick sill at shallow depths below the Marius Hills (Kiefer 2013) (EA-11-5) and the lack of comparable vertical topographic offset from this intrusion has been attributed to magmatic percolation and thermal annealing densifying the fractured highlands crust. However, the efficiency of such processes appears to be low (Head and Wilson 2019), and models for vertical dike propagation beneath the Marius Hills appear to satisfy the gravity data (Deutsch et al. 2019).

5.3. Dikes that propagate to the surface and produce regional pyroclastic deposits

Explosive, i.e., pyroclastic, eruptions and deposits are common on the Moon (e.g., Gaddis et al. 2003; Fig. 3f). The low-pressure environment in propagating dike crack-tips can cause gas formation at great depths and throughout dike ascent (e.g., Wilson and Head 2003a); at shallow crustal depths magmatic volatiles in mare basalt magmas contribute to significant shallow degassing and pyroclastic activity associated with the dike as it erupts at the surface (e.g., Chen et al. 2015; Rutherford et al. 2017). Dikes penetrating to the surface produce a wide range of explosive eruption types (Fig. 7) whose manifestations are modulated by patterns of gas release and lunar environmental conditions: 1) terrestrial strombolian-style eruptions map to cinder/spatter cone-like constructs (e.g., Isis and Osiris) (Fig. 7e); 2) hawaiian-style eruptions map to broad flat pyroclastic blankets (e.g., Taurus-Littrow Apollo 17 dark mantle

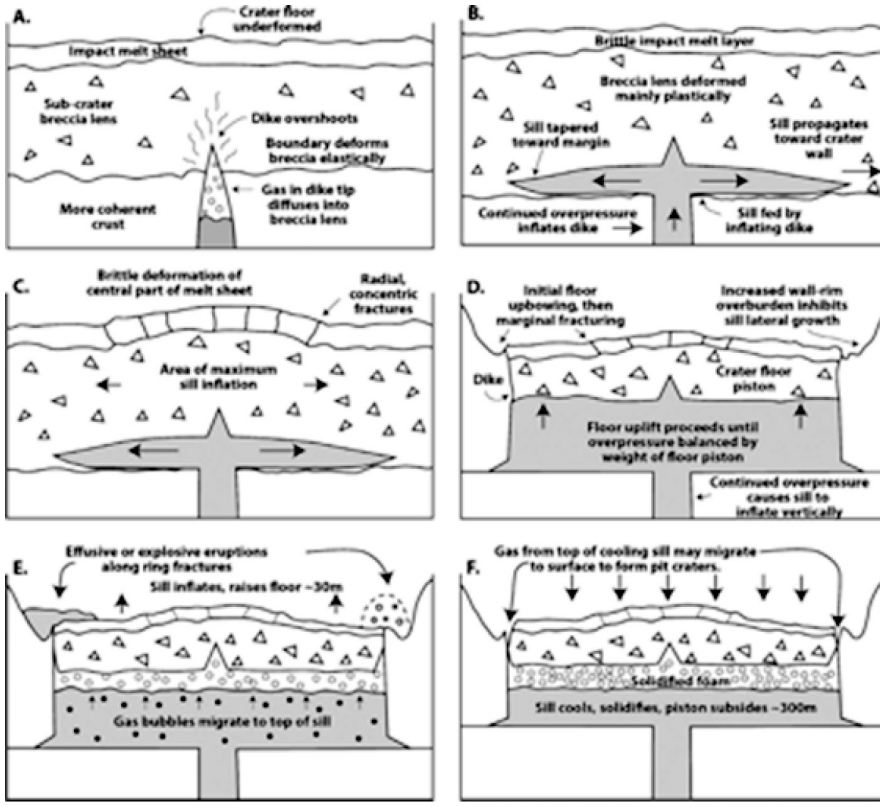


Figure 6. Emplacement and evolution of a sill below the floor of a large floor-fractured crater (FFC) (See Fig. 3e; EA-11–4). Dike emplacement and sill intrusion events are very rapid compared with the time necessary for: 1) sill volatile evolution, and 2) magma cooling until sill solidification. Sequence of predicted surface deformational and volcanic processes caused by a dike and sill intrusion beneath an impact crater. **a)** Dike intrudes, stalls below crater floor at a physical properties transition, typically overshooting by several hundred meters. **b/c)** Continued overpressure from buoyant magma causes dike to inflate and feed a sill that propagates laterally until it reaches 1) a supply limitation, 2) pressure equilibration, or 3) the base of the crater wall. **d)** Propagating sill reaches margins of crater floor in a few hours; increased rim/wall overburden inhibits lateral sill propagation, continued overpressure causes sill to inflate vertically, inducing initial floor upbowing, fracturing at sill margins (edge of crater floor) and piston-like uplift. Uplift of the crater floor proceeds until dike emplacement overpressures are balanced by the piston-like crater floor overlying weight. Magma can rise along peripheral piston fractures to form ring-dike-like intrusions. **e)** Following initial piston-like floor uplift, gas bubbles rise in the intruded sill, forming a foam layer over several months, raising height of floor ~30 m; magma will now be buoyant in the ring-fracture dikes and can erupt. **f)** In the final stage, the sill cools over decades to centuries, causing volume contraction and ~350 m of crater floor subsidence. (From Wilson and Head 2018c).

deposits) (Fig. 7d); 3) gas-rich ultraplinian-like venting can cause Moon-wide dispersal of gas and foam droplets (Fig. 7c) (e.g., many isolated glass beads in lunar soils; e.g., Delano 1986); 4) vulcanian-like eruptions caused by solidification of magma in the dike tip, buildup of gas pressure and explosive disruption, can form dark-halo craters with variable amounts of non-juvenile country rock (e.g., Alphonsus crater floor) (Head and Wilson 1979; Jawin et al. 2015) (Fig. 7b); 5) an Ionian-like eruption (Fig. 7a) can be caused by in situ secondary gas buildup in wide dikes, energetic explosive eruption, and formation of a dark pyroclastic ring (e.g., Orientale dark ring) (Head et al. 2002); 6) multiple eruptions from gas-rich fissures can form regional dark mantle deposits (e.g., Rima Bode, Sinus Aestuum); and 7) long duration,

relatively high effusion rate eruptions accompanied by continuing pyroclastic activity can cause a central thermally eroded lava pond and channel, a broader pyroclastic 'spatter' edifice, an even broader pyroclastic glass deposit and, if the eruption lasts sufficiently long, an associated inner thermally eroded vent and sinuous rille channel (e.g., Cobra Head and Aristarchus Plateau dark mantle; EA-11-9-10; Jawin et al. 2016).

In addition to these independent descriptive eruption types, physical volcanological analysis of the temporal production and loss of volatiles in single dike emplacement/eruption events shows that many of these types (Fig. 7) can occur in different phases of a single eruption (e.g., Wilson and Head 2018b) (see also Fig. 11b). Recent analysis of the formation and dispersal of pyroclasts on the Moon (Morgan et al. 2021) has shown that the bimodal formation of magmatic gas bubbles in rising dikes (CO bubbles generated at much greater pressures and depths than those of other volatile species) should result in a bimodal distribution of pyroclasts, with modes at ~120 and 650 microns. Furthermore, expansion to extremely low pressures on the Moon leads to interactions between the gas and pyroclasts that are more complex than when a significant atmosphere is present; as a result, the median grainsize in lunar pyroclastic deposits is expected to first increase and then decrease with increasing distance from the vent (instead of decreasing monotonically as is normal in explosive eruptions on Earth). Morgan et al. (2021) also found that if the volatile inventory from the Apollo 17 picritic magma that produced the orange glass beds is typical of lunar magmas, maximum ranges of the bulk of the pyroclasts would have been ~30 km. They show that the maximum range scales essentially linearly with the total mass fraction of volatiles released, and so predictions of the maximum radial range for other compositions can be readily made as data become available. Wilson and Head (2018b) and Morgan et al. (2021) show how the nature of volatile formation and behavior (Fig. 11a) for a single end-to-end eruption (Fig. 11b) can produce most of the diversity pyroclastic eruptions styles described above. Finally, the volatile content (and release patterns) of the full range of lunar mare basalt magma compositions is unknown (Shearer et al. 2023, this volume) and is essential to understanding the relationship of pyroclastic deposits to ascent and eruption conditions.

5.4. Dikes that propagate to the surface and produce effusive eruptions

Effusive eruptions (Figs. 5e–f, 8) are modulated by effusion rates, eruption durations, cooling and supply limitations to flow length, and pre-existing topography (Head and Wilson 2017). Relatively low effusion rate, cooling-limited flows (Figs. 5, 8) lead to small shield volcanoes (e.g., Tobias Mayer, Milicius) (Fig. 8c; EA-11-6-7); higher effusion rate, cooling-limited flows lead to compound flow fields (Fig. 8d; EA-11-8) (e.g., most mare basins). Even higher effusion rate (Fig. 5f), long-duration flows lead to thermal erosion of the vent, effusion rate enhancement, and thermal erosion of the substrate to produce sinuous rilles (Hurwitz et al. 2012) (e.g., Valles Schroeteri, Rimae Prinz) (EA-11-9-11). Extremely high effusion rate flows on slopes lead to volume-limited flow with lengths of many hundreds of kilometers (e.g., the young Imbrium basin flows) (EA-11-11-12). For example, new detrended topography data (Kreslavsky et al. 2017) provide a basis to subdivide an individual Imbrium lava flow into four ponded areas, revealing the dynamics of flow emplacement and the relationship of growing tectonic features (mare arches and wrinkle ridges) to lava emplacement (Chen et al. 2019a; Davis et al. 2022) (EA-11-12), and made it possible to calculate refined values for effusion rate, flow turbulence and channel behavior. These data also permitted a refined search for and the identification of candidate associated vent features in the young lava flow source region (Chen et al. 2019b).

In summary, detailed characterization and analysis of lunar mare volcanic landforms over the last several decades, together with improved models of the generation, ascent, intrusion and eruption of magma, have permitted a much better understanding of the mode of formation and physical volcanology of these individual features and their eruptive context.

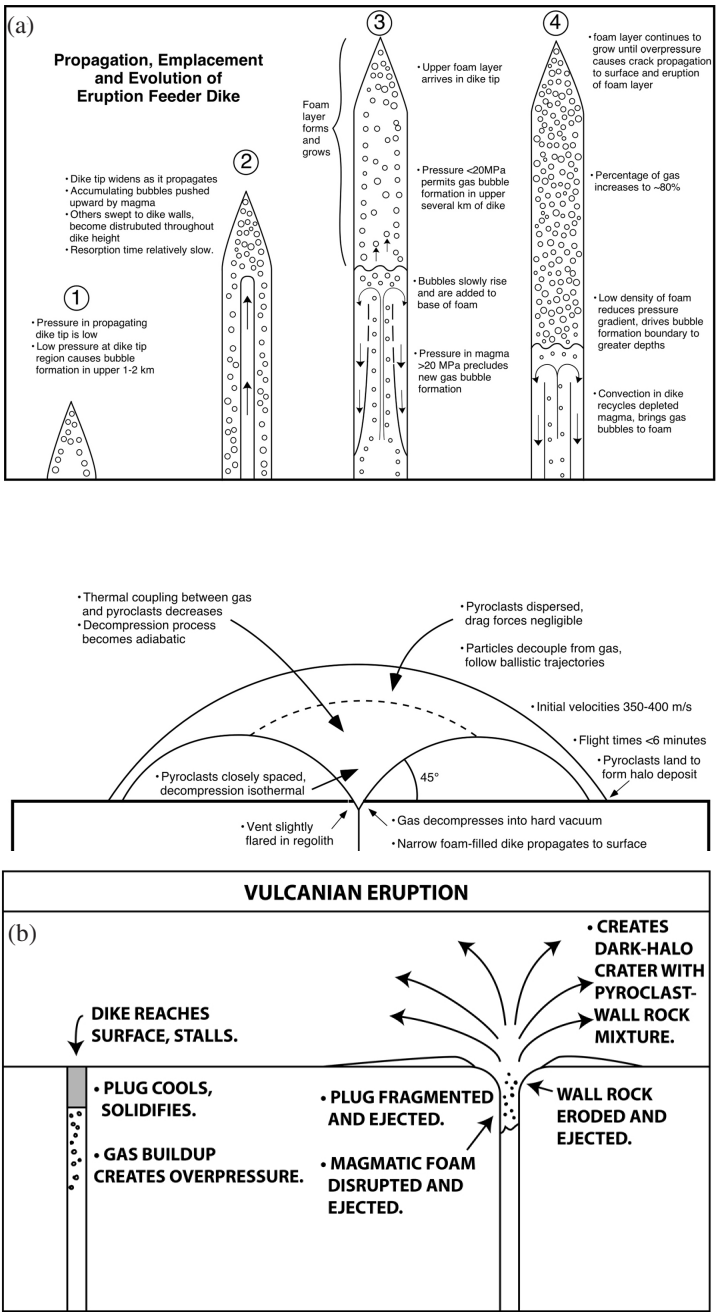


Figure 7. Lunar pyroclastic eruption types: Factors influencing the stalling, penetration to the surface and evolution of dikes emplaced in the crust and their effects on producing different types of pyroclastic eruptions at the surface. **a)** Ionian: Wide dike stalls a few kilometers deep in the crust; convection in the wide stalled dike builds up excess gas and pressure, gas vents to the surface, forms Ionian–type eruption. (From Head et al. 2002.) **b)** Vulcanian: Upper part of narrower dike solidifies, gas buildup causes explosive disruption of solidified cap and country rock, producing a lunar vulcanian-style eruption. Typical of dark-halo craters in floor-fractured craters (Head and Wilson 1979; Jozwiak et al. 2015b, 2017; Wilson and Head 2018d).

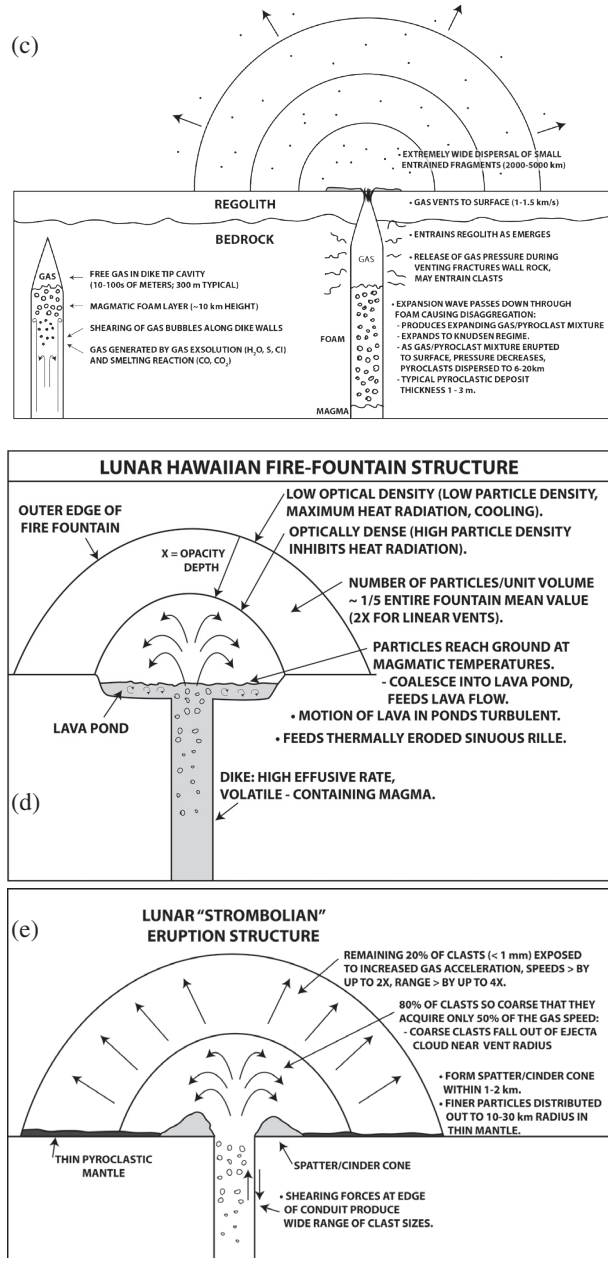


Figure 7 (cont'd). Lunar pyroclastic eruption types: Factors influencing the stalling, penetration to the surface and evolution of dikes emplaced in the crust and their effects on producing different types of pyroclastic eruptions at the surface. **c)** Ultraplinian: Dike vents gas and disrupted foam in upper part of dike as dike penetrates to the surface in first stage of the eruption (e.g., Wilson and Head 2018d). (From Head and Wilson 2017). **d)** Hawaiian: Volatile-containing magmas erupting into vacuum form lunar hawaiian-style fire-fountain eruption; details of fountain structure and consequences of deposit accumulation. (From Head and Wilson 2017.) **e)** Strombolian: Lower effusion rates (often in the later stages of an eruption event; Wilson and Head 2018d; Morgan et al. 2021), enhanced volatile production and accumulation produces lunar strombolian-style eruption structure and deposits. (From Head and Wilson 2017.)

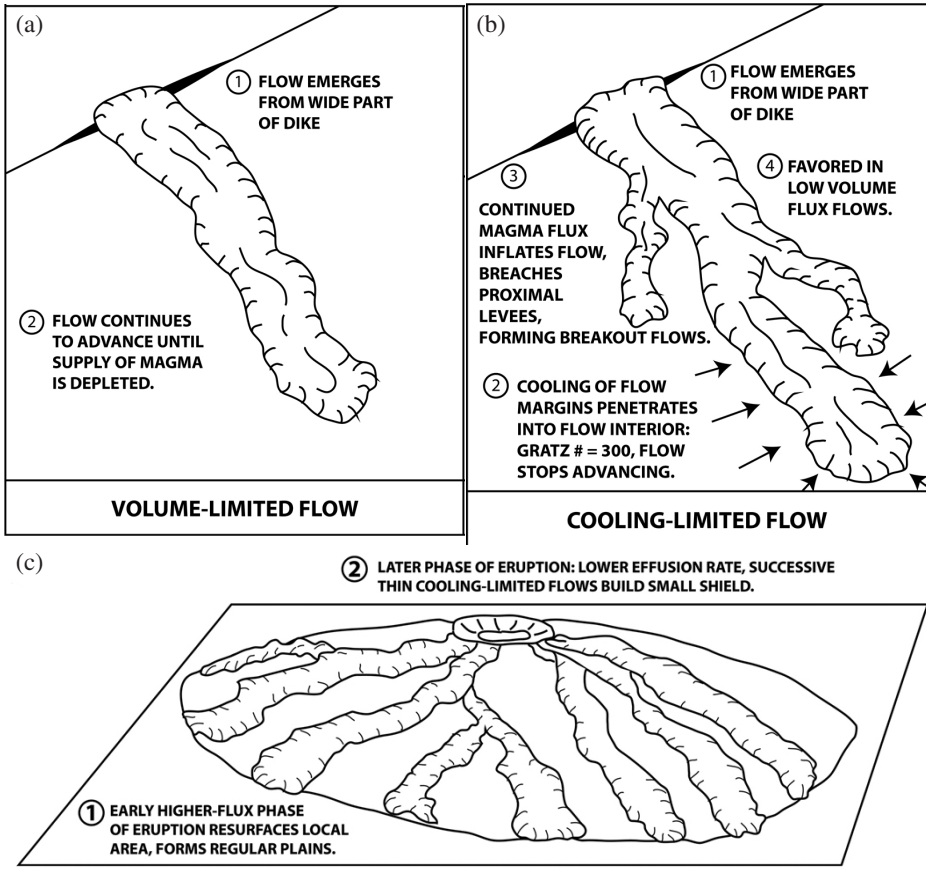


Figure 8. Relationships of variations in lava flow morphology to eruption conditions. Lava flow lengths and morphology can be influenced by magma supply and lava cooling. (From Head and Wilson 2017.) a) Volume-limited: flow advances until depletion of magma supply. b) Cooling-limited: flow forward advance ceases due to cooling, causing breakouts in proximal and medial regions. c) Sequence of events in the building of small lunar shield volcanoes (Head and Gifford 1980).

6. RECENT OBSERVATIONS OF LUNAR MARE FEATURES AND IMPLICATIONS FOR ERUPTION CONDITIONS

The high resolution image and topography data collected by LRO (LROC, Robinson et al. 2010; LOLA, Smith et al. 2010; Zuber et al. 2010) and Kaguya (Kato et al. 2008) have revolutionized our thinking about lunar mare volcanism, enabling new discoveries and enhancing our understanding of known features and deposits. Here we describe two such features and show how the increased knowledge has led to new insights into the mode of emplacement of lunar mare deposits and their time of formation.

6.1. Irregular Mare Patches (IMPs)

While examining orbital images obtained by Apollo 15 astronauts, Whitaker (1972) discovered a distinctive and enigmatic central nearside volcanic feature, Ina. The unusual meniscus-like morphology and morphological crispness of the mounds within Ina, combined with the roughness and optical immaturity of its floor (Fig. 9a,b), led many workers to interpret Ina as representing very young volcanic activity (Schultz et al. 2006, suggested as young as

~10 Ma). Braden et al. (2014) undertook a global analysis of LRO LROC data and documented a total of 70 small (0.1–5 km maximum dimension) topographic anomalies with irregular Ina-like morphologies and textures, calling these *Irregular Mare Patches* (IMPs). Detailed analysis of the two textures (rough floor and meniscus-like domes) and their stratigraphic relations characterizing Ina and other IMPs led Braden et al. (2014) to conclude that the mounds are generally superposed on the rough deposits (Fig. 9c), consistent with their formation as small basaltic eruptions. On the basis of the paucity of superposed impact craters >10 m in diameter, Braden et al. (2014) found that the three largest IMPs (Ina, Sosigenes and Cauchy 5) were younger than 100 Ma! Such extremely recent ages, occurring in the latest Copernican over

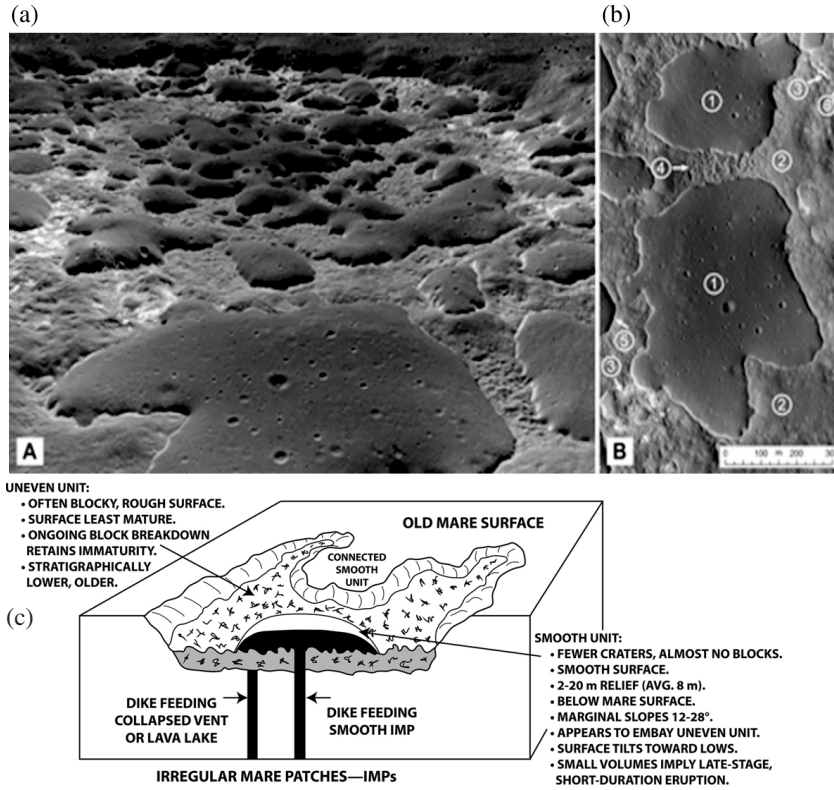


Figure 9. Perspective view of interior of the Ina Pit Crater atop an ~30 km shield volcano, an example of an Irregular Mare Patch (IMP) (Braden et al. 2014), and proposed interpretations for its origin. **a)** Perspective view of the Ina interior viewed from east to west across Ina. LROC NAC M119815703 overlain on LROC NAC digital terrain model. Vertical exaggeration is ~3. **b)** Ina interior morphological characteristics: Relatively flat basal terraces (6) at the edge of the Ina interior. (1) Irregularly shaped mounds are surrounded by hummocky (2) and pitted (4) textured floor terrain, and blocky materials (3). At the margin of the mounds, (5) topographically lower moats are often observed. Portion of LROC NAC M119815703. (From Qiao et al. 2017). **c)** The major characteristics of the irregular mare patches (IMP) illustrated in a block diagram highlighting the interpretation of Braden et al. (2014) that the floor and mounds represent very late-stage extrusions (< 100 Ma) compared with the surrounding ancient mare basalts (in the case of Ina and Sosigenes ~2–3.5 Ga). In the Braden et al. (2014) interpretation, the floor units and mounds are both extremely young, but the mounds postdate the floor units. In the interpretation of Garry et al. (2012), the mounds are inflated lava flows and the rough floor units extrude from the base of the inflated flow. In the interpretation of Schultz et al. (2006), the anomalously young ages (< 10 Ma in the case of Ina) are caused by deep-seated gas release that elutriates, blows out, and ejects the fines, causing the observed rough, immature, and blocky/hummocky floor units.

(d)

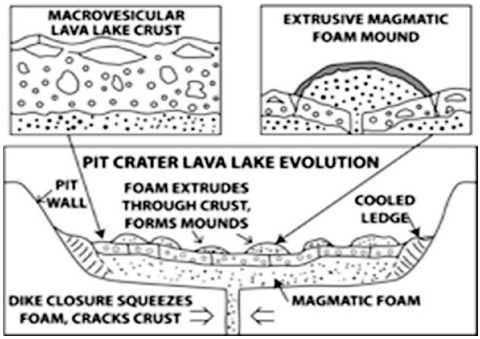


Figure 9 (cont'd). d) Cross section of the waning stage processes of lava lake solidification and magmatic foam emplacement in the Ina small shield volcano summit pit crater. In the Qiao et al. (2017, 2018a,b, 2019a) and Wilson and Head (2017b) interpretations, the rough floor units are the surface of a lava lake and the mounds are extrusion of late-stage magmatic foams. In these interpretations, the young ages are attributed to the unusual properties of the magmatic foam and the solidified micro/macrovesicular lava lake. (From Qiao et al. 2017).

a billion years after the most recent CSFD-dated mare lava flows (Figs. 2, 3b), raised the question of how IMPs, and their petrogenesis and eruption conditions, could be reconciled with current models for lunar thermal evolution (e.g., Ziethe et al. 2009).

An alternative interpretation for the age and origin of Ina and the larger IMPs was proposed by Qiao et al. (2017, 2018a, 2019a), who noted that they were often closely associated with small shield volcanoes and linear rilles, apparently contemporaneous with adjacent ancient mare deposits emplaced during the peak periods of volcanism between 3–4 Ga. They interpreted the three major IMPs as representing late-stage evolution of pit craters on volcanic edifices (Ina and Cauchy 5) (Fig. 9d) or late-stage graben formation atop dikes (Sosigenes): stalled volatile-rich magma cooled and solidified to form the macro-porous rough floor units, and underlying magmatic foams extruded to form the mounds (Fig. 9d). Drainage of regolith particles into the macro-porous floor inhibited regolith buildup on the rough unit, and the solidified foam nature of the mounds altered the morphology and size of superposed craters; both effects were interpreted to lead to the anomalously young ages reported by Braden et al. (2014).

Support for this latter interpretation was provided by Wilson and Head (2017b), who modeled late stages of eruptions in summit pit craters on lunar small-shield volcanoes. They found that the negligible atmospheric pressure and low gravity on the Moon formed lunar versions of late-stage summit eruption activity, and unusual eruption products, neither predicted nor observed on Earth. For example, as the lava lake floor developed a very vesicular thermal boundary layer, and the ascending magma rise rate slowed to zero, volatile exsolution in the dike and lava lake formed a very vesicular foam (Fig. 9d); as the dike began to close, stresses in the lava lake crust formed fractures through which the foam extruded to form the convex mound shape due to its non-Newtonian rheology (Fig. 9d). Wilson and Head (2017b) pointed out that the very porous physical properties of the floor, and the aerogel-like properties of the foam, could inhibit formation of typical impact craters and regolith development (e.g., Fassett and Thomson 2014, 2015), and potentially create artificially young crater retention ages.

Current debate about the origin and evolution of IMPs centers on these two alternative models: 1) Late Copernican volcanic activity (Braden et al. 2014), and 2) Ancient (Imbrian) volcanic activity producing unusual morphologies and anomalously young ages due to late-stage gas exsolution and production of macro-vesicular and foamy substrates (e.g., Qiao et al. 2017, 2018a, 2019a; Wilson and Head 2017b). Critical unresolved issues include: 1) determining the actual effects of impacts into model-predicted porous substrates and how these map out into CSFD ages (Basilevsky and Michael 2021), 2) the relationship between the three large IMPs and the dozens of smaller versions (see the hybrid example at Cauchy 5; Qiao et al. 2020), and 3) the manner in which topographic and morphologic crispness and sharp boundaries can be retained for >3 Ga if the IMPs are indeed ancient.

6.2. Ring Moat Dome Structures (RMDS)

In a comprehensive analysis of Lunar Orbiter images, Schultz (1976a,b), Schultz and Greeley (1976) and Schultz et al. (1976) reported the presence of small features in the lunar maria that they designated ring-moat structures, and interpreted them as kipukas from earlier flows, pseudo-vents, or squeeze-ups in the associated flow. On the basis of new high-resolution LROC images obtained under a wider variety of Sun illumination geometries, Zhang et al. (2017) documented many thousands of similar features that they named Ring-Moat Dome Structures (RMDS) (Fig. 10). These low domes (a few meters to ~20 m height with slopes <5 degrees) are typically surrounded by narrow annular depressions or moats (Fig. 10; EA-11-14). RMDS diameters range from tens to hundreds of meters and their albedo is essentially the same as that of immediately adjacent ancient mare plains. Furthermore, the spatial distribution of the TiO_2 and FeO contents of the host maria are not influenced by their presence or absence.

Zhang et al. (2017) considered four candidate hypotheses for RMDS origin. Two hypotheses are associated with the emplacement of the associated lava flows: 1) small squeeze-ups/hornito-like features; 2) magmatic foam development below a cooling lava flow surface; extrusion of foams to form the mounds and subsidence to form the moats. Two other hypotheses, based on the viscous-appearing mound morphology and apparent mound embayment relationships with degraded impact craters (e.g., Basilevsky et al. 2019) call on later extrusion unassociated with the lava flows on which they occur: 1) Domes of a more viscous composition unassociated with mare basalt emplacement; 2) Small eruptions occurring tens to many hundreds of millions of years following the emplacement of the mare lava flows. The close association of the RMDS with the lunar maria and their albedo and compositional similarities (Fig. 10; EA-11-14) led Zhang et al. (2017) to favor the interpretation of RMDS as a product of contemporaneous, but late stage emplacement of the lava flows on which they occurred, due to modification of the initial lava flows through inflated flow squeeze-ups and/or extrusion of magmatic foams below a cooling lava flow surface. In more detailed analyses, Zhang et al. (2018a, 2020) extended the initial survey to include more than 8,000 RMDSs in most nearside maria, and an in-depth characterization of over 500 RMDS occurrences; this revealed that mounds occur in clusters with a maximum density of ~5/km^2, and are typically a few hundred meters wide (average ~200 m), have a mean height of ~3.5 m, and are surrounded by moats ranging in width from tens to >100 meters, and depths up to several meters. Zhang et

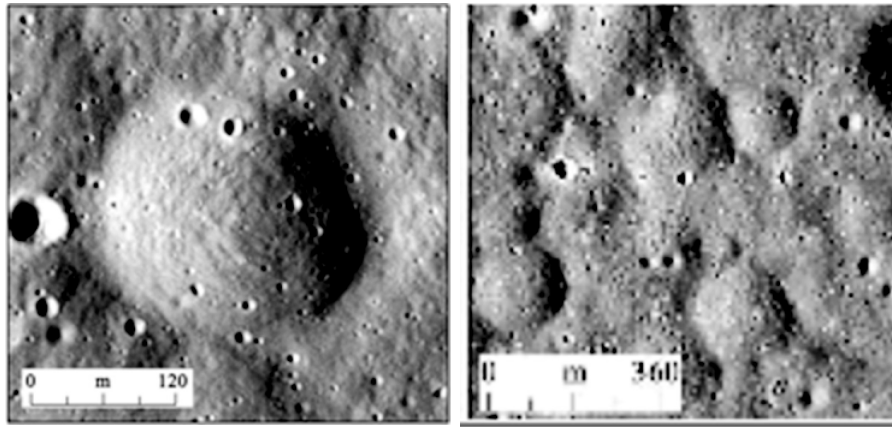


Figure 10. Ring Moat Dome Structures (RMDS) (Zhang et al. (2017). Individual RMDS (left), and clustered RMDSs (right) in Mare Tranquillitatis in LROC NAC mosaic (frames M1096293859LE and RE). Sun illumination direction is from left to right. North is up in all images. See EA-11–14,15 for RMDS topographic profiles.

al. (2018a, 2020) documented numerous RMDSs that occur on or around fractures, graben and small volcanic shield edifices, and found a spatial association between RMDSs and irregular mare patches (IMPs).

In a theoretical analysis of late stage lunar lava emplacement, Wilson et al. (2019a) noted the close association of RMDSs with the maria on which they occurred and explored mechanisms for late stage lava flow emplacement and cooling that might explain the distribution and characteristics of RMDSs (EA-11-15). They found that the molten cores of cooling flows can be inflated during the late stages of eruptions by injection of additional magma still containing dissolved volatiles. Upon crystallization, this newly injected lava undergoes second boiling (e.g., an increase in vapor pressure to the point of supersaturation due to crystallization of the melt), and that this generates abundant quantities of bubbles and magmatic foam layers at the top and bottom of the central core of the flow. Due to flow inflation of many meters accompanying the formation of the foam layers, the cooled upper crustal layer flexes, forming fractures that permit extrusions of the magmatic foams onto the surface. Wilson et al. (2019a) interpret these processes to have formed the domes, with subsidence of the subjacent and surrounding surface forming the moats (EA-11-15). In this interpretation, the RMDS domes and moats, as well as the adjacent lava plains, were formed more than 3 Ga ago, and the very young apparent ages of the domes and plains deduced from the small-crater counts (~25–36 Ma; Zhang et al. 2017) are the result of the small sampling area that underrepresents large craters coupled with the unusual nature of impacts into foamy materials that cause smaller and deeper craters (Wilson and Head 2017b).

Unresolved are examples of contradictory RMDS ages (Zhang et al. 2021) including: 1) RMDS embayment relationships into depressions interpreted as impact craters with different degradation states (suggesting that the emplacement of some RMDSs occurred many hundreds of millions of years after emplacement of the underlying mare unit) (e.g., Basilevsky et al. 2019), and 2) preservation of fine-scale morphologic and morphometric features on RMDSs despite several billion years of regolith development (Fassett and Thomson 2014, 2015).

7. ESTABLISHING THE RELATIONSHIPS BETWEEN MARE BASALT MAGMA GAS RELEASE PATTERNS AND THE NATURE OF INDIVIDUAL DIKE EMPLACEMENT EVENTS AND ERUPTIONS: A FRAMEWORK OF PREDICTIONS FOR TESTING IN THE FUTURE EXPLORATION OF THE LUNAR MARIA

There has been great progress in the Space Age in initially understanding the volcanic origin and ancient age of the lunar maria, establishing the mineralogic and chemical diversity and chronology of mare basalts and their deep mantle petrogenesis (e.g., Taylor 1975; Shearer 2006), documenting the nature and thickness of the crust and the outlines of lunar thermal evolution (e.g., Wieczorek et al. 2006, 2013), identifying the basic principles of generation, ascent and eruption of basaltic magma and understanding the influence of surface vacuum conditions and low gravity on volcanic landforms and deposit configuration (e.g., Wilson and Head 1981, 2017a; Head and Wilson 1992, 2017; Morgan et al. 2021), and discovering the very significant role of water and other volatiles in the eruption of lunar magmas, previously thought to have been highly volatile depleted (e.g., Saal et al. 2008; Hauri et al. 2015). This sequence of discoveries and insights has set the stage in the last several years for combining predicted magma gas production patterns during mare basalt magma ascent from mantle source regions (e.g., Rutherford et al. 2017) (Fig. 11a with the nature and physical volcanology of typical dike emplacement events and eruptions (e.g., Wilson and Head 2017a, 2018a–d; Morgan et al. 2021) (Fig. 11b). Such predictions can provide the basis and a framework for further unifying the seemingly disparate relationships of individual mare basalt samples, field

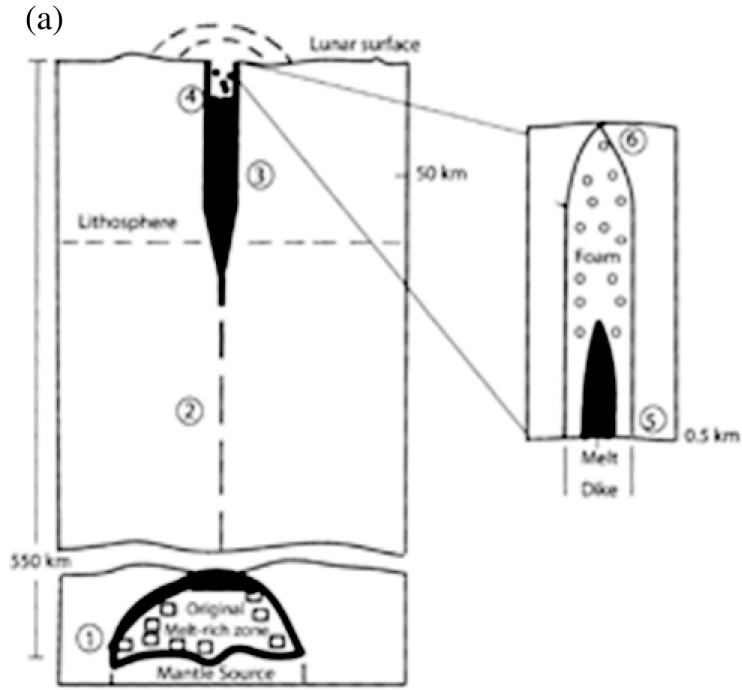


Figure 11. Gas production during dike ascent and four stages in the ensuing eruption. **a.** Model of lunar orange picritic glass magma gas production during dike emplacement): (1) Partial melt last equilibrates with residual mantle diapir at ~550 km; dike propagation begins at melt-rich zone contact of with overlying mantle; (2) dike reaches ~78 km vertical extent (for a 25 km vertical melt zone), then separates and begins to move rapidly upward; (3) depth of CO-rich gas formation is 7 km minimum, 50 km maximum, followed by continuous degassing of CO-rich gas during ascent; gas and foam collect at propagating dike tip; (4) ~7–15 vol% bubbles in magma at 0.5 km for closed system degassing (initial C contents of 4–50 ppm; (5) Stage 3 degassing begins with fragmentation (bead formation) at 0.5 km depth (H_2O and SO_2, S_2, and H_2S); (6) dike tip breaches surface; melt beads released into hot suspension of >92 vol% gas. (From Rutherford et al. 2017).

observations by Apollo astronauts, the wide array of volcanic landforms and deposits, and the stratigraphy and modes of emplacement of lunar secondary crust. This proposed paradigm also makes very specific predictions which can be tested with future exploration and analysis (e.g., Jawin et al. 2019). In this section, we describe the relationships of gas production and release patterns as a function of time in basaltic magma ascending in a dike, its eruption at the surface, and the subsequent behavior as the ascending magma flux decreases and the dike trends toward closure and solidification. Described in parallel are the sequence of deposits predicted by this physical volcanology paradigm (Fig. 11a,b).

Rutherford et al. (2017) used data from analyses of the Apollo 17 orange glass (74220) and petrological constraints from gas solubility experiments to construct a model for the magma origin, ascent, and explosive eruption. They identified three stages in the eruption (Fig. 11a): Stage 1 extends from the A17 orange glass magma source region, at ~550 km, to ~50 km depth. On the basis of melt inclusion analyses and measurements, they identified Stage 2, which extends from ~50 km to 500 m; here a C-O-H-S gas phase formed and grew in volume. Using the minimum and maximum estimates of CO, H_2O, and S loss from the melt, they calculated the volume of the gas phase at 500 m depth below the surface to be ~7 to 15 vol% of the magma. At depths shallower than ~450 m (Stage 3), the rising magma exsolved an additional 800–900 ppm H_2O and 300 ppm S; this increased the gas mole fraction by a factor of 3–4. At

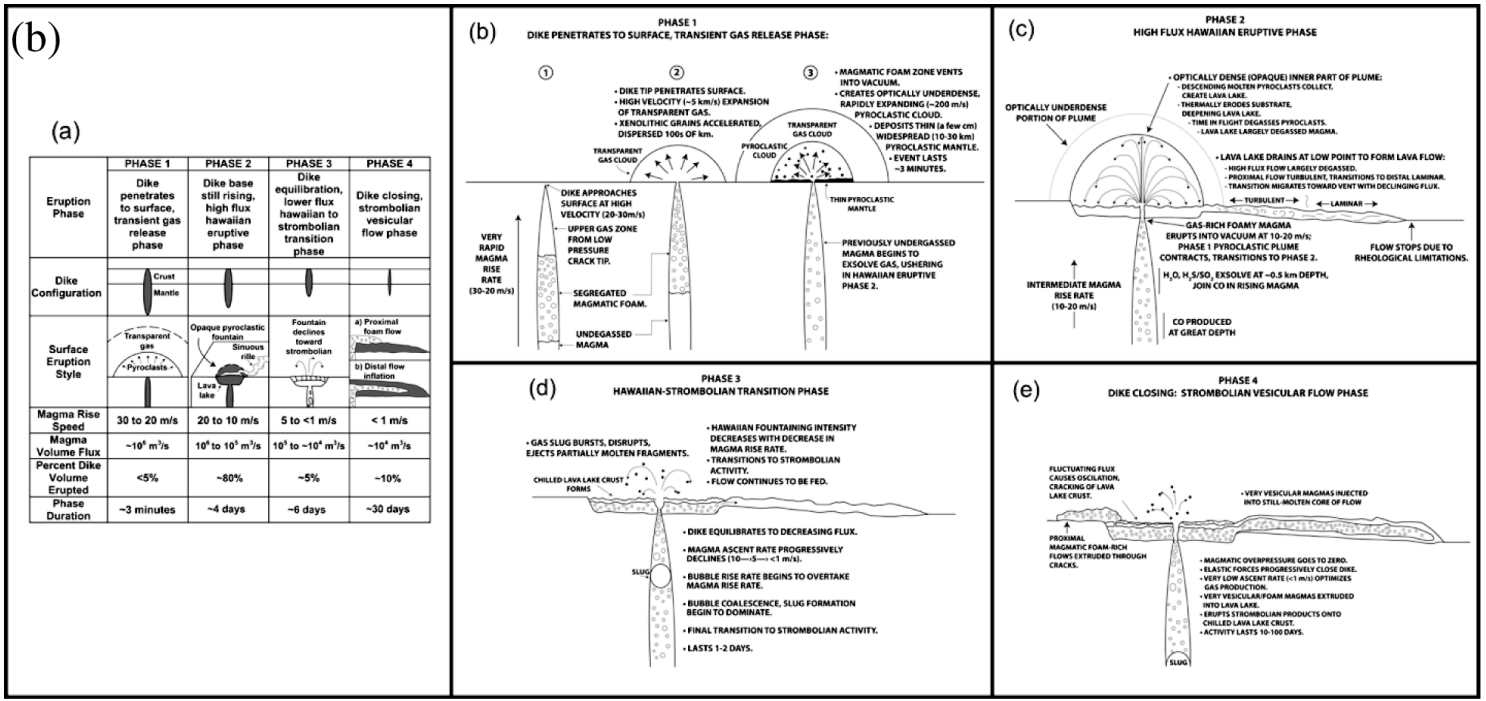


Figure 11. (cont'd) b) Characteristics of the four eruption phases during a typical lunar eruption (Wilson and Head 2018d). Phase 1: transient gas release phase; Phase 2: high-flux hawaiian eruptive phase; Phase 3: hawaiian to strombolian transition phase; Phase 4: strombolian, vesicular flow phase. Listed parameters represent average values and the total dike volume and vertical extent dictate the relative duration of individual phases. (From Morgan et al. 2021).

~130 m depth, the closed-system gas phase is calculated to reach ~70 vol%, sufficiently high to fragment the magma, forming pyroclastic droplets. On the basis of the pressure necessary to explain the C content of the orange glass beads, however, fragmentation and bead formation is interpreted to have occurred at depths ranging from 600 to 300 m. At this depth, the 70% gas volume required for magma fragmentation is a factor of ~5 greater than that for closed-system degassing at 500 m; this strongly implies that the gas was produced by open-system degassing as the magma ascends from greater depths. Rapid dike propagation from the ~550 km deep source facilitates gas collection in the upper part of the dike by open-system degassing during crack propagation (Wilson and Head 2003a, 2017a). Rutherford et al. (2017) concluded that this gas-assisted eruption scenario (Fig. 11a) was supported by the explosive nature of the orange glass eruption, bead composition homogeneity, and evidence in the ascending magma for a Fe-metal forming reduction event during Stage 2, followed by a Stage 3 oxidation event.

Wilson and Head (2018d) and Morgan et al. (2021) used the Rutherford et al. (2017) analysis of mare basalt gas release patterns during individual eruptions (Fig. 11b) to provide a basis for predicting the effect of vesiculation processes on the structure and morphology of associated features formed during a typical mare basalt eruption, subdividing eruptions into four phases, and linking these phases to predicted mare basalt deposits and landforms (Fig. 11b).

As the magma-filled crack (dike) rapidly ascends through the mantle and through the crust from the source region at great depth, the propagating dike tip contains a mixture of gas and foam above the rapidly rising magma (e.g., Wilson and Head 2003a, 2018d; Head and Wilson 2017; Rutherford et al. 2017). When the dike tip penetrates to the surface at ~20–30 m/s, the *Eruption Phase 1–Surface Transient Gas Release Phase* (Fig. 11b) is initiated with the onset of a very explosive venting phase, lasting only minutes, and producing a very widespread, thin pyroclastic deposit. Initial explosive venting of the pure gas zone in the upper 100–200 m tip of the dike is immediately followed by the arrival to the surface of the upper (~10 km) extremely vesicular magmatic foam part of the dike. Due to the very high rise speeds and venting of magmatic foam into a vacuum, Phase 1 lasts as little as 3 minutes and produces an extremely thin, but very widespread deposit (Head and Wilson 2017) that may explain many of the isolated glass beads found in mare and highland soils (Delano 1986; Head and Wilson 2020).

As the dike continues to rise very rapidly (20–10 m/s) toward a neutral buoyancy configuration, the very highest magma volume flux part of the eruption begins (*Eruption Phase 2–High-Flux Hawaiian Eruptive Phase*) (Fig. 11b). During Phase 2, magma volume fluxes of 10^6–10^5 m^3/s result in near-steady explosive eruption of magma (with variations dictated by the representative volatile content of the bulk of the magma). During this Phase 2, the efficient release of uniformly distributed volatiles produces a relatively steady, predominantly optically dense hawaiian fire fountain consisting of sub-mm pyroclastic droplets; these fall back into a vesicle-deficient lava lake that surrounds the vent. Initially, lava flows turbulently away from the lava lake, forming soon-to-be distal parts of long flows or extensive flow fields and sinuous rilles. A significant part of the total dike magma volume would have been erupted during Phase 2 (~80%); Phase 2 would have lasted of the order 4 days for a typical range of dike volumes (Wilson and Head 2017a) and the erupted magma volume flux would have decreased from ~10^6 to ~10^5 m^3/s over the course of this phase.

As the rapidly rising dike slows and reaches equilibrium, the vertical extent becomes fixed, and the magma rise rate is now driven by lower internal dike pressure and dike closure and thus decreases radically. This initiates the onset of *Eruption Phase 3—Dike Equilibration and Lower Flux Hawaiian to Strombolian Transition Phase* (Fig. 11b). The onset of low magma rise speeds (~5–<1 m/s) means that gas bubbles can now rise faster than the magma rise speed and thus can coalesce, grow, and disrupt the surface of the vent and lava lake. This represents a distinctive transition from hawaiian to strombolian eruptive activity which continues for several days until most deep-sourced gas is exhausted and explosive activity

is minimal. During Phase 3, vigorous hawaiian lava fountaining declines toward strombolian activity, magma flux decreases from ~10^5 to ~10^4 m^3/s, and over the course of several days ~5% of the total dike volume is erupted and exits the vent area at ≲ 0.1 m/s, with initially low vesicularity increasing as a function of time during this phase.

As the dike emplacement event reaches its final stage, relaxation of magmatic stresses holding the dike open continue to cause horizontal dike closure and to force magma extrusion at a low rise speed (≲1 m/s) and volume flux (~10^4 m^3/s). This ushers in *Eruption Phase 4—Dike Closure and Strombolian–Vesicular Flow Phase* (Fig. 11b). During Phase 4, magma from the lower part of the dike is still being forced toward the surface, producing some CO at all depths and causing minor continued strombolian activity as the gas bubbles and slugs reach the surface, occasionally disrupting the stable crust that forms on the magma that is still emerging from the vent and flowing away as lava. In *small total volume eruptions*, Phase 4 activity will be characterized by the formation of a stable crust on still-emerging lava flowing away from the vent at a low flux. This lava consists of magma with vesicles derived from magmatic H_2O and S species released in the dike upper ~500 m. Exposure of this highly vesicular magma to the vacuum is predicted to cause immediate formation of a bubble-wall fragment shard layer (Head and Wilson 2020); this will overlie a vesicle-rich layer, atop a molten lava layer still containing dissolved volatiles. The magnitude and state of global stresses closing the dike and the cooling of the dike magma dictate the duration of this phase, at most 1–2 years.

In Phase 4 activity associated with *large total volume eruptions* (vertically extensive dikes), a large fraction of the total magma remaining in the dike remains available for extrusion as vesicular lava. Due to the formation of a stable crust on the low flux, still-emerging lava flowing away from vent, such volatile and vesicle-rich rising magma is likely to intrude into the still-hot interiors of previously-emplaced non-vesicular flows. This will cause these earlier flows to inflate (similar to flood-basalt lava fields on Earth). Subsequent to magmatic injection and flow inflation, the lava cores will also undergo volatile release through second boiling upon cooling; this will result in a new population of gas bubbles, causing an additional, possibly very extensive, inflation episode (e.g., Wilson et al. 2019a; their Fig. 5).

This basic paradigm (Wilson and Head 2017a) (Fig. 11b) for the ascent, intrusion, volatile production and release (Rutherford et al. 2017)(Fig. 11a), and eruption of specific individual dike emplacement events can now be used to revisit the array of individual features (and their interpretive mode of formation; Head and Wilson 2017, Morgan et al. 2021), and place them in the context of characteristics and variations in single eruptive events (Fig. 11b). This approach helps address the question: Do individual mare basalt features, landforms and deposits represent different and unique eruption conditions, or are many of the observed variations linked to specific stages in single dike emplacement and eruptive events? Many dike emplacement events intrude into the shallow crust without leading to an initial eruption and produce a range of manifestations: e.g., crater chains, graben, graben with small cones, Ionian-like eruptions, floor-fractured craters (Fig. 5a–d). We focus here on features formed in association with dikes that have erupted to the surface (Fig. 5e–f).

7.1. Long lava flows

The young, extensive Imbrium lava flows (e.g., Schaber 1973; Bugiolacchi and Guest 2008; Zhang et al. 2016, 2018b; Chen et al. 2019a–b) (Fig. 5f; EA-11-12) are among the most readily distinguished and well-known mare volcanic landforms. On the basis of the dike-eruption paradigm (Fig. 11b), such flows would represent eruption Phase 2, linked to large-volume dikes that feed fissure vents ~10–15 km long. The distal parts of the flow field emplaced during the early stages of the eruption are little influenced by the magma volatile content, because the associated Phase 2 near-vent optically dense fire fountains that produce a lava lake feeds the hot, turbulent volatile-free lava flows. Magma volatile content for such flows may become much important later in Phases 3–4, if proximal flow injection and inflation

occur (predicted for such high-volume eruptions). The flow phase model (Fig. 11b) thus clearly predicts that such long lava flows should differ in their character along their strike due to the several phases (Phases 2–4) involved in their emplacement (e.g., Wilson and Head 2018d).

Generally unaccounted for in these models (e.g., Wilson and Head 2017a, 2019) is the influence of pre-existing topography on lava flow emplacement. Complications introduced by complex topography, particularly that related to tectonic features such as mare arches and wrinkle ridges (e.g., Watters and Johnson 2010; Nahm et al. 2023, this volume) can affect: 1) the dynamic flow behavior, 2) flow thicknesses and lengths, and 3) final outcrop patterns of a deposit from an individual lava flow. For example, Chen et al. (2019a) (EA-11-12) combined altimetry and detrended topography data, and high-resolution images, to document the role of topography in modifying lava flow morphology and morphometry in one of the long, initially ~10 km wide, lobate, high-Ti, Eratosthenian-aged lava flows in Mare Imbrium. The substrate topography (generally orthogonal to lava flow direction) was related to the initiation and growth of mare ridges and arches (Schaber 1973; Schaber et al. 1976) formed by loading, flexure and deformation caused by earlier-emplaced lava flows (e.g., Solomon and Head 1979, 1980; Byrne et al. 2015). Chen et al. (2019a) analyzed an individual lava flow, about 250 km in length and ~10–25 m in thickness, that crosses a series of five wrinkle ridges and documented the topography/morphology in both along-flow and across-flow directions (EA-11-12). Current topography of the along-flow direction shows a stair-step pattern away from the vent region, caused by the presence of wrinkle ridges and arches. Some of these predated the emplacement of the flow, blocking the forward, generally downslope motion of the flow, changing the structure and morphology of the central channel, and causing widening, ponding and deepening of the flow (EA-11-12). In some places, increased deepening of the pond caused lateral diversions, and in others breaching of the mare arch, and change in flow behavior as the flow incresased velocity in the narrow spillway. The lava flow showed no change in behavior at one mare arch (EA-11-12), suggesting that this arch formed subsequent to the lava flow emplacement. The final surface pattern of the solidified lava flow is thus very informative from the perspective of flow dynamics and presence/absence of tectonic features at the time of eruption, but also illustrates the complexity of flow emplacement and interpretation of average flow unit thicknesses and volumes in obtaining flux estimates (see Davis et al. 2022).

7.2. Sinuous rilles and their source depressions

Sinuous rilles typically emerge from circular to elongate source depressions and often extend for several hundred kilometers (Hurwitz et al. 2012, 2013; Williams et al. 2000) (Figs. 11b, EA-11–9-11). These are initiated during Phase 2 of eruptions from dikes that contain a large volume of magma that erupts through a fissure $\lesssim 5$ km long, thus ensuring a moderate volume flux. This Phase 2 setting tends to create a near-circular lava pond containing lava at magmatic temperature, but having relatively low volatile content due to having lost most of its volatiles in the optically dense hawaiian lava fountain (Morgan et al. 2021). A turbulent lava flow is then fed from the lava draining from the pond; over the ensuing course of the eruption (during Phases 3 and 4), the lava may efficiently erode its substrate to form a sinuous channel (Wilson and Head 2022).

7.3. Compound flow fields

Relatively small-volume dikes with low eruption fluxes encourage the formation of compound flow fields (Figs. 8b, EA-11-8) (e.g., Greeley 1976; Kreslavsky et al. 2016, 2017; Qiao et al. 2016). The formation of compound flow fields is favored by Phase 2 (Fig. 11b) of fissure eruptions on appreciable slopes (in contrast to small shield volcanoes; Wöhler et al. 2007); the presence of cooling-limited flows then induces multiple marginal breakouts in the flow upslope toward the vent. This produces the typical compound flow field digitate map outline (Figs. 8b, EA-11–8).

7.4. Small shield volcanoes

Relatively small-volume dikes with low eruption fluxes (Fig. 11b) also encourage the formation of small shield volcanoes (Fig. 8c, EA-11-5,7,13). In contrast to compound flow fields, Phase 2 of eruptions producing small shields have small volumes and erupt from a central (not linear) vent. Lava lake overflows are fed by a low eruption volume flux and the resulting lava flows do not travel far (~5–15 km) before cooling causes them to stop. Successive overflows exit from evolving low points in the summit crater rim, causing flow accumulation in all radial directions and the progressive accumulation into a low shield volcano. Qiao et al. (2021b) recently described over 280 small shield volcanoes in Mare Tranquillitatis concentrated on a broad, ~450 km circular topographic rise. The small shields have a median diameter of 5.6 km, median height of 68 m and 74% contain summit pits. Later-stage (Phase 3/4) activity (Fig. 11b) can also build small shields and additional features at shield summits (strombolian spatter, foam layers) and late-stage dike closure can even result in extrusion and eruption of magmatic foams out onto the surrounding shield volcano (e.g., Cauchy 5; Qiao et al. 2018b).

7.5. Summit pit craters

These can initially form from Phase 2 pyroclastic activity in low effusion rate, small-shield building eruptions, with hawaiian pyroclast ranges out to ~0.5–1.5 km radius. They may also be the result of Phase 4a activity (Fig. 11b) from small-volume dikes erupting volatile-poor magma from small shield summit vents, coupled with volume adjustments during late-stage magma cooling (Figs. 7f, 11b). They also appear to commonly involve only short fissure vents, so that although the low volatile content causes short pyroclast ranges, nevertheless, a small and roughly circular lava pond forms around the vent. In one case (Hyginus) (EA-11–1), escape of gas that has accumulated in lateral dikes linked to the summit vent created an unusually large pit crater (Wilson et al. 2011).

7.6. Pyroclastic deposits and mantles

These can form during at least two phases of the emplacement of a lava flow. During Phase 1 (Fig. 11b), virtually all lunar eruptions should be accompanied by short, intense explosive eruptive events as the gas-rich tip of a dike initially breaches the surface; deposits are predicted to be very thin and easily masked or covered. During Phase 2 (Fig. 11b) hawaiian eruptions, pyroclasts can be dispersed around the vent (depending on total and eruption-variable magmatic volatile content) out to radii of hundreds of meters to several tens of kilometers, producing pyroclastic mantle thicknesses depending largely on eruption volume and duration (Morgan et al. 2021). The recent detection of enhanced water contents associated with regional pyroclastic deposits (Milliken and Li 2017; Li and Milliken 2017) may reveal one end-member of this volatile abundance spectrum. Small spatter deposits and rootless flows could also form during the strombolian Phases 3/4 parts of the eruption (Fig. 11b).

7.7. Pyroclastic cones

In Phases 3 and 4 of intermediate volatile content eruptions, during the transition from steady to pulsating hawaiian activity (Fig. 11b), as the eruption progresses toward the strombolian stage, the outer parts of the fire fountain become sufficiently transparent such that pyroclasts can partially cool and reach the ground to form spatter or cinder cones (Fig. 11b). The amount of cooling that pyroclasts undergo in this optically under-dense part of the fountain will determine the temperature at which the clasts will reach the surface, and thus the degree of welding (e.g., Head and Wilson 1989; Morgan et al. 2021).

7.8. Irregular Mare Patches (IMPs)

Controversy surrounds the age and mode of emplacement of IMPs (Braden et al. 2014; Qiao et al. 2017). If they are formed at the same time as their associated mare deposits, they

are most likely to be related to Phase 4a activity from small-volume dikes (Fig. 11b). Toward the end of the eruption, explosive activity becomes minimal, and magma in the dike rises very slowly. This optimizes the production of very vesicular magma in the dike and its emplacement under a cooling lava lake crust above the vent (Fig. 11b): 1) the magmatic foam could break through the crust to form bulbous mounds (one class of IMP, in the Ina small shield summit crater; Qiao et al. 2019a) (Fig. 9d); 2) it can also raise the lava lake crust, causing overflow onto the upper flanks (Fig. 11b), where partial collapse of the foam could produce another type of IMP (e.g., flanks of Cauchy 5; Qiao et al. 2018b).

7.9. Ring Moat Dome Structures (RMDS)

RMDSs occur in concentrations in many maria, and consist of clusters of small dome-like features each surrounded by a moat (Zhang et al. 2017) (Figs. 10; EA-11-14). These are interpreted to be the consequence of late-stage Phase 4b activity associated with a large-volume dike (Fig. 11b). Long, volatile-poor lava flows emplaced earlier in the sequence (Phases 1–3) are followed by Phase 4b activity during which partly vesiculated lava can be injected into the hot cores of the earlier flows, resulting in flow inflation (EA-11-15). Cooling and crystallization subsequent to inflation drive exsolution of the remaining volatiles (second boiling). This causes even more inflation and produces large amounts of magmatic foam. Foam venting through cracks in the cooled lava flow crust could form RMDSs with the surrounding moat caused by local loading and subsidence over the void (Wilson et al. 2019a) (EA-11-15).

In summary, we have used the basic principles of magma generation, ascent, and eruption to examine the range of dike volumes, effusion rates, volatile species, and release patterns as a function of time and eruption duration (e.g., Wilson and Head 2018d). Eruptions can be subdivided into four sequential phases (Fig. 11b), each with specific individual characteristics and predictions. The resulting unifying quantitative conceptual model illustrates the relationships among a wide and diverse range of related observed volcanic landforms and structures and provides the basis for clues to the nature of magma source regions. These predictions and correlations can be further tested by future human and robotic lunar exploration to specific destinations (EA-11-17,18).

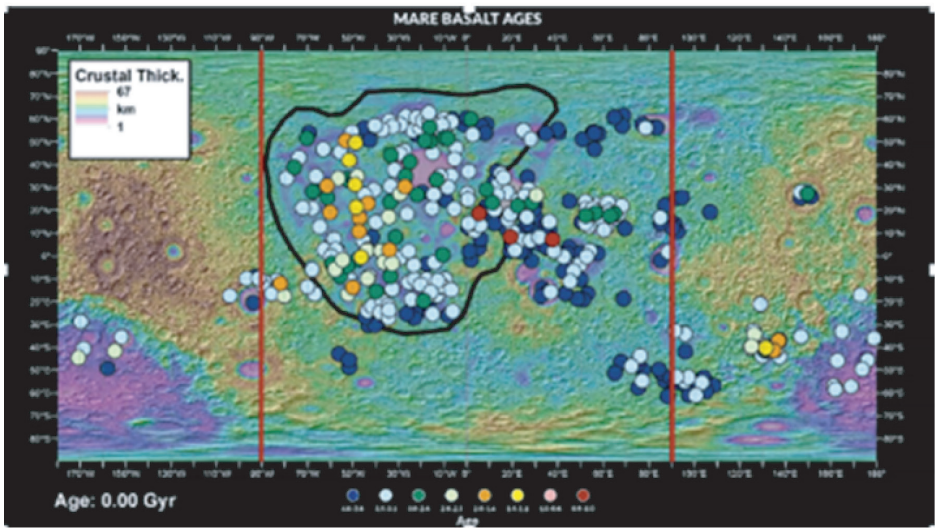
8. LUNAR SECONDARY CRUST: SUMMARY, SYNTHESIS AND OUTSTANDING QUESTIONS

We now outline a summary and synthesis of the nature and modes of formation of lunar secondary crust (Figs. 1b, 11–12), including a listing of many outstanding questions and how future lunar investigations and missions can address them (EA-11-17,18).

8.1. Duration of mare basalt volcanism and recent activity

It is clear that extrusive mare basalt volcanism occurred from the late major basin formation cryptomare period throughout the Imbrium period and into the Eratosthenian, and perhaps into the Copernican (Fig. 12a–b). Less clear is its beginning and end. Evidence for very early onset is found in the basaltic fragments in regolith breccias (Fig. 2a), but the provenance of these samples is unknown; geophysical and mineralogical evidence suggests more abundant cryptomaria of uncertain age (Whitten et al. 2015a,b; Sori et al. 2016), but distinguishing these anomalies from Mg-suite plutons and deposits is uncertain. The end of mare volcanism is no less clear. Ring Moat Dome Structures are hypothesized to form in association with the emplacement of ancient mare deposits, but apparent embayment relationships with degraded impact craters suggest that RMDSs may have formed over many hundreds of millions of years, well into the Copernican (Zhang et al. 2021). Further, the enigmatic morphologies, optical immaturity, and CSFD ages of both large and small Irregular Mare Patches have been interpreted to mean that IMPs formed or were volcanically active in the last few tens

(a)



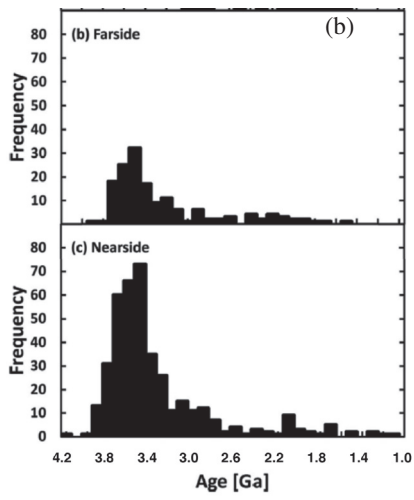


Figure 12. Updated temporal and spatial distribution of lunar mare basalt units addressing the major questions: Where is the earliest and latest mare basalt volcanism? How do eruption patterns change in time and space? Is there a NS/FS asymmetry in age distribution? What is the role of crustal thickness and the PKT (Procellarum-KREEP Terrain)? **a)** Final frame from movie (EA-11-16) illustrating the location of mare basalt units as a function of time. Map color scale is in GRAIL-derived crustal thickness, **black line** is PKT outline, **red lines** indicate NS/FS boundaries. In the EA-11-16, every two seconds = 100 Ma, a beep means that one or more units were emplaced at that time, the **colored dots** show the unit location, and the dots are color-coded according to the age scale (**bottom**). Data based on absolute model ages (AMA) of all investigated mare basalts on the Moon; data from Haruyama et al. (2009b), Morota et al. (2009, 2011a,b, 2015), Pasckert et al. (2015, 2018), and Hiesinger et al. (2011, 2023, this volume). Three youngest dots (<100 Ma) represent the three youngest eruptions of large IMPs from AMA of Braden et al. (2014). **b)** Histogram of nearside and farside mapped and dated mare basalt units with time.

of millions of years of lunar history (Braden et al. 2014; Schultz et al. 2006; Fassett and Thomson 2014, 2015). Improving our knowledge of the onset and termination (?) of lunar mare volcanism is one of the greatest challenges for exploration and research in the coming decades (EA-11-17,18).

8.2. Lunar mare basalt chronology, flux, and nearside–farside distribution

Critical to the understanding of mare basalt volcanism and secondary crust formation is the relationship of observed surface processes and deposits to lunar mantle composition and structure, and the thermal evolution of the Moon (Fig. 12). Necessary to answer this question is a first order knowledge of the *volcanic flux*, the volume of mare basalt magma delivered to the surface as a function of *time*, and its location on the lunar surface (a proxy for the location and level of mantle activity in *space*). Identification of geologic and mineralogic mare basalt

(c)

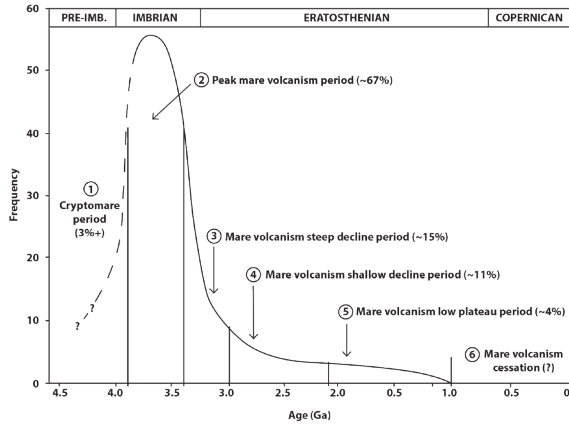


Figure 12 (cont'd). c) Updated synthesis of generalized mare basalt flux curve, phases, nomenclature and the lunar geologic time scale (Wilhelms 1987; Stöffler et al. 2006). Generalized curve is derived from data from Fig. 11–12a.

units exposed at the lunar surface, and determination of their stratigraphy and CSFD ages (calibrated to returned Apollo, Luna and Chang'e samples), offers the most comprehensive data to address these problems (e.g., Hiesinger et al. 2023, this volume). In order to begin to address these questions, we have compiled a video of the global distribution and sequence of dated lunar mare basalt units as a function of time and location, crustal thickness, Procellarum-KREEP Terrane (PKT) boundaries, and nearside-farside location (Fig. 15a; EA-11-16). This display enables us to address the following series of questions:

8.3. What is the general trend of lunar mare basalt extrusive volcanic flux?

A plot of the number of dated mare basalt units (n = 319) as a function of time in 100 million year increments (Fig. 12; EA-11-16) shows that the mode is at 3.7 Ga and the average unit age is 3.3 Ga. The shape of the flux distribution is leptokurtic and skewed toward younger ages. Uncertain is the shape back into the basin-forming period, but it cannot be symmetrical and is unlikely to be skewed in that direction because of the paucity of abundant ancient mare basalts in lunar breccia samples and remote sensing data. On the basis of these unit statistics, we can divide the period of mare volcanism and secondary crust formation into the following periods: 1) 4.0–3.9 Ga: *Cryptomaria period* (~3% of the units, but probably more occurs but is unaccounted for); activity is focused on the eastern limb (~50–130 E) in areas of ancient impact basins, with other occurrences in the southwestern nearside Schiller-Schickard region, and in the SPA basin (Fig. 3a, 12c; EA-11-16). 2) 3.8–3.4 Ga: *Peak mare volcanism period* (~67%); extrusive activity begins on the eastern nearside (Tranquillitatis and Fecunditatis) and western farside in the same area as the most abundant Phase 1 cryptomaria occurrences (Fig. 3a), then spreads to the central nearside and Sinus Roris areas. 3) 3.3–3.0 Ga: *Mare volcanism steep decline period* (~15%); volcanism becomes more evenly distributed throughout the lunar nearside, with many fewer occurrences throughout the farside (Fig. 12b). 4) 2.9–2.1 Ga: *Mare volcanism shallow decline period* (~11%); number of units emplaced is decreasing, emplacement is relatively evenly distributed throughout the nearside maria, and broadly distributed but in smaller numbers on the farside. 5) 2.0–1.0 Ga: *Mare volcanism low plateau per*iod (~4%); primarily Oceanus Procellarum, Farside NE Australe, local units in Orientale and SW Imbrium. 6) 1.0–0 Ga: *Mare volcanism cessation period (?)* (~0%, or with 3 IMP occurrences, <1%); no known major units emplaced; possibly IMPs and RMDSs.

Caveats to the application of this flux curve are: 1) Only the number of units, not their volumes, are taken into consideration. 2) Later volcanic units tend to cover up earlier ones, obscuring their abundance, total area and volumes. 3) Enhanced topography, such as crater and basin interiors (Head 1982; Whitten and Head 2013), are potential receptacles for large volumes of early mare volcanism, the volumetric importance of which may be obscured by later deposit veneers. The sign of each of these factors is likely to be positive, adding both units and volumes to the older part of the flux curve and increasing its kurtosis (Fig. 12c).

8.4. What is the total duration of lunar secondary crustal formation and what is the influence of thermal and tectonic evolution?

Secondary crust formation extended from at least as early as 4.0 Ga to at least as young as 2.0 Ga (Che et al. 2021; Li et al. 2021), about 62% of lunar history and perhaps much longer. These limits need refining. Also important are further analyses of the relationship of extrusive volcanism and tectonism and the general thermal evolution of the Moon. The combination of the evolving global state of stress in the lithosphere (increasingly contractional) and the increased deposition of mare basalts in impact basins and their loading, flexure and deformation of the crust and lithosphere introduces complexities to the interpretation of the ascent and eruption of mare basalts (Solomon and Head 1979, 1980; Byrne et al. 2015). For example, wrinkle ridges are known to grow over time, and their presence and evolution to influence patterns of mare basalt emplacement (e.g., Schaber 1973; Schaber et al. 1976; Chen et al. 2019a–b). Chen et al. (2019a; EA-11-12) showed that wrinkle ridges and arches both predated and postdated a specific Imbrium basin lava flow. The along-flow width and morphology of the narrow (typically ~10 km before encountering obstacles), lava flow extending downslope in an area currently characterized by five across-strike topographic ridges of various heights showed that: 1) Lack of flow modification at R1 suggests that the ridge postdates the flow. 2) Blocking of the flow at R2 caused ponding, but that the current topography of the ridge (~200 m) is much more prominent than it was at the time the flow was emplaced (~20 m height). 3) Ponding and diversion of lava behind R3·suggests that it was present but not prominent. 4) The lava flow width appears unmodified by R4, suggesting it was not present at the time of flow emplacement. 5. The blunt shape of the flow termination at R5 suggests that R5 served as a final barrier to flow advancement. Documentation and exploration of additional examples such as this (e.g., Palumbo et al. 2019) will help to provide insight into the critical interplay of volcanism and tectonism in the thermal evolution of the Moon.

8.5. Lunar secondary crust: Synthesis

In the context of planetary evolution (Taylor 1983, 1989), secondary crusts are derived from partial melting of the mantle, and follow in time the primary crust, formed as a result of melting and differentiation related to planetary accretionary energy (Taylor 1989). The secondary crust of the Moon (Fig. 1b), was derived from partial melting of the lunar mantle following the formation of the magma ocean-derived primary anorthositic flotation crust (LMO), its underlying KREEP and Ti-rich cumulate layers and residual mantle products, and the aftermath of density instabilities and overturn. Details of the transition from the LMO phase to the initiation of mare basalt volcanism and secondary crust formation are the subject of current research (see summaries in Elardo et al. 2023; Shearer et al. 2023, both this volume), but a plausible paradigm is that of Hess and Parmentier (1995), who postulated that the density-driven overturn of the LMO residual layer (Fe-Ti-rich KREEP layer) resulted in mantle mixing, deep mantle heating, and the rise of diapirs that were the source of melting for the mare basalts magmas (Fig. 4). Maliik et al. (2019) have then explored the buoyancy of partial melts formed near the base of the mantle and whether those that are positively buoyant match the characteristics of the Apollo lunar basalt collections. Most agree that mare basalts are derived from deep mantle melting and that they ascended to the surface and erupted on top of the primary anorthositic crust (Fig. 1b), whose thickness had been shaped by broad nearside-farside differences, and by regional thicknesses and surface

topography associated with impact basins. Thus, the lunar secondary crust can be characterized as being a *vertical accretionary secondary crust*, in contrast to the laterally accreting oceanic secondary crust of the Earth (Fig. 1a-b).

The stark contrast between the solidified LMO anorthositic crust and the basaltic secondary crust permits assessment of their relationships, and the nature of the vertically accreting mare basaltic crust (Fig. 11–12). The total volume of the lunar secondary crust is less than 1% of its primary crust (the total volume of Earth's secondary oceanic crust produced over 4 Ga is estimated to be ~2% of Earth's volume; Taylor 1989). There is no evidence that the lunar secondary crust was ever laterally or vertically recycled into the mantle and remelted. In contrast to our terrestrial view of constant volcanic activity somewhere on Earth (dominantly at divergent and convergent plate boundaries), the Moon was characterized by very low mean and peak time-averaged mare basalt eruption rates. Assuming a total secondary crustal volume of $1–2\times10^7$ km^3, and a mare basalt time span period of ~3 Ga (~4 Ga to 1 Ga) (Fig. 2, 12), the mean flux for mare basalts is ~ $3–6\times10^{-3}$ km^3/a, to be compared with the Earth's annual rate of crustal accretion of ~20 km^3/a from crustal spreading alone and of ~0.1 km^3/a for a typical volcano such as those observed in Hawaii or Etna. The peak flux during mare basalt emplacement occurred in the Imbrium Period, between 3.4 and 3.8 Ga (Fig. 12c). If we assume that 67% of the mare basalt magma was emplaced during this time, the peak flux was characterized by rates of ~0.017 km^3/a. The maximum flux during mare basalt volcanism has also been estimated by Needham and Kring (2017) to be ~ 0.01 km^3/a at about 3.7 Ga. All of these fluxes are well below the peak eruption rates of mare basalts inferred for individual units and eruptions, and predicted from theory (~10^6 m^3/s, corresponding to 3×10^4 km^3/a). Predicted and erupted volumes generally lie in the range 100–300 km^3 and predicted durations of individual eruptions are less than a few years. Dividing the typical erupted volume by the 10^7 km^3 total volume of secondary crust indicates that there were of the order of 30,000 to 100,000 mare basalt eruptive events during the emplacement of the lunar secondary crust, with an average repose interval of 4,000 to 13,000 years. Thus, a single short eruptive event could exceed the mean flux value by a factor of up to ~2×10^6!

This behavior is unusual by terrestrial standards but is readily understood in the context of the generation, ascent and eruption of mare basalts (Figs. 1b, 4, 11). Density contrasts between regions with an elevated abundance of heat sources and the bulk mantle will cause larger heated regions to rise as buoyant melt-rich diapirs; these generate partial melts that can undergo collection into magma source regions. Diapirs will rise to the base of the anorthositic crustal density trap (when the crust is thicker than the elastic lithosphere) (Fig. 4b) or, later in history, to the base of the lithospheric rheological trap (when the thickening lithosphere exceeds the thickness of the crust). In order for magma generated deeper in the mantle by radioactive heating and/or diapiric rise to reach the surface, 1) a sufficient volume of melt must be produced and collected in the source region at depth, 2) sufficient source region overpressure must be generated to propagate a dike toward the surface, 3) the magma must have sufficient positive buoyancy to rise in the mantle, 4) the low density anorthositic crust must be thin enough to permit penetration by positive magma buoyancy, 5) the lithosphere must be thin enough such that magma does not stall at a deeper rheological boundary, 6) the global lithospheric state of stress must be overcome (increasingly contractional after ~3.6 Ga), and 7) the dike width must be large enough that conductive cooling along the dike walls does not cause magma solidification during transit from the source to the surface.

How then, is it envisioned that magma is generated and that magma-filled cracks (dikes) are propagated toward the surface? Residual diapiric buoyancy, combined with continued production and arrival of diapiric material, increases melt volume and overpressurizes the source regions (Fig. 4a). This produces sufficient stress to cause brittle deformation of the elastic part of the overlying lithosphere and a magma-filled crack initiates and propagates toward the surface

as a convex upward, blade-shaped dike (Fig. 4b). Calculations of the volume of magma released in a single event shows that it is likely to lie in the range 10^2 km^3 to at most 10^3 km^3 (Wilson and Head 2017a). This corresponds to dikes with widths of 40–100 m and both vertical and horizontal extents of 60–100 km, favoring eruption on the lunar nearside (Figs. 1b, 4b, 12). Although shallower magma sources will produce continuous dikes from the source region to the surface, dikes propagated from deeper sources will detach from the source region and rise as discrete penny-shaped structures (Fig. 4b). As lunar thermal evolution progresses and the Moon cools with time: 1) the lithosphere thickens, 2) source regions become less abundant and rheological traps become increasingly deep, and 3) the state of stress in the lithosphere becomes increasingly contractional, inhibiting dike emplacement and surface eruptions.

These factors readily account for many of the characteristics of lunar mare volcanism and secondary crust formation (Figs. 2, 3, 11, 12). Large dike widths and eruption volumes are favored simply to enable magma to successfully travel from the deeper mantle sources to the surface. The combined low frequency of eruptions and large eruption volumes can account for the lack of large shield volcanoes and calderas on the Moon. On Earth and Mars, large shield volcanoes are related to the formation of shallow neutral buoyancy zones and magma reservoirs and copious magma supply, creating many sequential small-volume flows to build up the edifice, and evolution of the shallow magma reservoir to form the caldera. On the Moon, individual intrusive episodes are too infrequent to build up shallow magma reservoirs or to form large edifices from multiple small-volume flows. Instead, large dikes propagate to the surface infrequently, at high speeds, and with large volumes, disfavoring shallow reservoir formation. This scenario is supported by the presence of floor-fractured craters (FFCs) (Figs. 3e, EA-11-3-4), the only shallow intrusive reservoirs confidently known on the Moon. In these cases, large-volume dikes encounter host rock discontinuities in the terminal stages of their ascent to the surface, forming sills below the floor of the crater that result in uplift and deformation of the crater floor. The volume required for such sills and the magnitude of floor uplift are both consistent with the emplacement of large-volume, low-frequency dike events. Indeed, such shallow "reservoirs" can undergo evolution (Wilson and Head 2018c; Fig. 6) and they represent the only known, but imperfect, analog to terrestrial shallow magma reservoirs.

Also absent on the Moon are broad topographic swells and associated gravity anomalies attributed to mantle plume development (Beta Regio on Venus; Tharsis and Elysium on Mars; Hawai'i on Earth). Factors that might account for this absence are the small mantle convective scale length, the rapid cooling of the lunar mantle and thickening lithosphere, and the high lunar mantle viscosity. The only surface features that might be attributed to the surface manifestation of "hot spots" might be the three Oceanus Procellarum volcanic complexes, Mons Rumker, Aristarchus Plateau and Marius Hills (EA-11-5,9,13), Rumker and Marius being located in areas of regionally thin crust. Recent analysis of the Marius Hills suggests that the gravity, topography and geologic data may be consistent with multiple dikes propagated from the top of a small diaper at depth (Deutsch et al. 2019).

If lunar mare basalt eruptions are dominated by infrequent, large volume, dike emplacement events and eruptions, what accounts for the diversity and abundance of small shields, cones, domes, pyroclastic deposits, sinuous rilles, compound flow fields, etc., all apparently reflecting an Earth-like diversity of eruption environments? Why don't mare basalt eruptions simply manifest themselves as high-volume, high-effusion rate flood basalt eruptions? Two factors appear to account for this. The first is that, despite the great depths of origin and transit distance to the surface, the population (frequency distribution) of dike emplacement events appears to be centered on a mean that ensures magma eruption to the surface at high volumes and fluxes (similar to flood basalts), but also results in dike penetration into the shallow subsurface and stalling, or just penetrating to the surface to produce low-volume, low effusion rate eruptions (Fig. 5). This conclusion is supported by: 1) the wide array of landforms related to shallow dike

intrusion and stalling (Figs. 3, EA-11-5–7,13), 2) the nature, origin, and circum-mare location of FFC shallow intrusions (Fig. 3e) (Jozwiak et al. 2012; their Fig. 15), 3) the presence of very large-volume flood-basalt like extrusions, and 4) the relationship between presence/absence and style of eruptions, and crustal thickness, most prominently in the pronounced nearside-farside mare basalt deposit asymmetry in abundance, but not necessarily in timing (Figs. 3, 12b). These factors all point to a family of dike emplacement conditions that favor emplacement of mare basalt dikes to mid-crustal levels, with extrusion favored in regions of thinner crust. If this scenario is correct, then a map of individual eruption locations may be more indicative of "crustal thickness filtering" then the actual presence of mantle source regions at depth.

The second factor accounting for the diversity of landforms is related to the surface eruption environment of the Moon. The low gravity and lack of an atmosphere at the surface means that magmatic gas exsolution is significantly favored relative to the Earth (Fig. 1a–b), and that eruption into the vacuum at the surface will cause massive magma disruption, fragmentation and dispersal. This environment clearly contributes to the diversity of resulting lunar pyroclastic landforms (e.g., cones, vents, pyroclastic mantles, etc.). Indeed, modeling of a typical lunar basaltic eruption sequence, regardless of its flux and volume, predicts a wide range of ultra-plinian, hawaiian and strombolian activity (Wilson and Head 2018d; Morgan et al. 2021) during the course of a single eruption (Fig. 11).

In summary, secondary crustal formation on the Moon (Fig. 1b) was dominated by emplacement of lavas derived from melting in deeper mantle sources, delivered to the surface by large, infrequent diking events whose emplacement characteristics (ascent and eruption) favored eruption in relatively thinner crust, with a range of shallow intrusive to extrusive consequences (Fig. 5). Associated landforms and deposits are significantly influenced by lower lunar gravity, enhanced near-surface gas exsolution, and eruption into the lunar vacuum. Lunar secondary crustal formation and accretion is *vertical* in nature (in contrast to the Earth), but the thin veneer of vertically accreting secondary crust (low total volume and thickness) on the primary anorthositic crust, while sufficient to cause local loading and flexure, is insufficient to generate any significant interaction with the lunar interior.

The rapidly declining mare basalt flux (Fig. 12) is readily understood in the context of the thermal evolution of the Moon. Efficient conductive cooling associated with the general thermal evolution of the Moon increased the depth of the melting geotherm required for magma generation, and thickened the lithosphere as a function of time, deepening magma source regions and the depth of rheological traps for magma ascent. The increasingly contractional state of stress in the lithosphere after ~3.6 Ga (Figs. 2, 4b) inhibited dike propagation and increasingly cooler crust and mantle favored ascending dike heat loss in transit, all leading to the deepening of mantle magma source regions and decline in the ability to drive melt to the surface.

8.6. Secondary crust: Major outstanding questions

We now outline some of the major outstanding questions concerning the origin and evolution of lunar mare basaltic secondary crust and link these to modes of future investigation (EA-11-17,18).

8.6.1. Distribution. Despite very significant progress, major unknowns remain concerning the three-dimensional (areal and vertical) distribution of mare basalts. When during lunar thermal evolution do impact basins cease significant thermal relaxation and start to provide major topographic receptacles for mare basalt accumulation? How much extrusive mare basalt is hidden below the current surface deposits deep in impact basins? What is the total census of cryptomaria and when in the past does the increased impact flux destroy their coherence as deposits? Additional major questions include: *Nearside-farside (NS/FS) mare basalt asymmetry*. There is a pronounced nearside-farside (NS/FS) asymmetry in abundance of mare volcanic units and deposits (Figs. 3, 12a–b; EA-11-16). Is there a NS/FS asymmetry in age distribution? The current data (Fig. 12a–b) support the idea that over most of the

course of mare basalt volcanism (~4.0 to ~2.1 Ga), eruptions occurred on both the nearside and farside, but that the number of eruptions and the total deposit volume were significantly less on the farside. After about 1.5 Ga, no mare deposits have been found on the farside, and the remaining nearside mare units are concentrated in Oceanus Procellarum, within the PKT (Fig. 12). *What is the role of crustal thickness in mare basalt distribution?* There is a significant anti-correlation between the occurrence of mare volcanism and crustal thickness (Fig. 12a); the vast majority of volcanic deposits occur in crustal areas of thin or intermediate thickness, and this is reflected in the first-order nearside-farside asymmetry in mare basalt deposit distribution. Clearly, the farside mantle is producing mare basalt melts and delivering them to the surface throughout the majority of the mare basalt era. Thus, future analyses need to distinguish between crustal thickness effects on basaltic magma ascent and eruption (e.g., Wilson and Head 2017a), fundamental differences in nearside-farside mantle composition and source regions, and the role of the PKT in magma generation and secondary crust duration (e.g., Jolliff et al. 2000; Wieczorek and Phillips 2000; Laneuville et al. 2013).

These questions concerning nearside-farside differences can be addressed (EA-11-17,18) through additional sample return, dating, and petrogenetic studies, particularly from the lunar farside. Local and regional geophysical networks and studies are required to make progress on the three dimensional distribution of mare basalts, particularly in basin centers.

8.6.2. Duration. The increased impact flux earlier in lunar history obscures the onset and distribution of early mare volcanism, as evidenced by the cryptomaria. *Where is the earliest exposed mare basalt volcanism?* On the basis of the assessment of cryptomaria distribution and the earliest mare volcanism (Figs. 3a, 12a), the onset of mare volcanism appears focused on the eastern limb of the Moon (eastern nearside, western farside). Sample return from these areas and regional geophysical studies would improve our knowledge. Of critical importance is a better understanding of the geodynamical processes involved in the transition from primary crust formation to the onset of secondary crust. *Where is the most recent mare basalt volcanism?* It has long been known that the most recent mare basalt units (younger than 1.5 Ga) occur in southern, central and northern Oceanus Procellarum and this is confirmed by our most recent synthesis (Fig. 12a; EA-11-16). The Chang'e 5 mission, which returned samples from these young lava flows (Qian et al. 2021a–b) helped to calibrate the ages and petrogenesis of these latest stages of mare volcanism, and more such missions are needed. If the CSFD ages of the three major IMPs (< 100 Ma) are shown to be correct by future sample return, this would shift the locus of most recent volcanism from Oceanus Procellarum eastward to the Tranquillitatis-North of Mare Vaporum region (Fig. 15a). Remaining unknown are the implications of potentially young RMDSs (e.g., Basilevsky et al. 2019).

8.6.3. Flux. The broad outlines of the flux curve are known (Fig. 12c), but the onset and early flux are obscured by the impact record, and the termination of mare volcanism is not well established in terms of samples of youngest CSFD-dated basalts. Chang'e 5 sample return) significantly improved this situation (Che et al. 2021; Li et al. 2021; Qian et al. 2021a,b). Improvements are also needed in determining total mare basalt volume and chronology (amount and ages of buried lava, particularly in the deep mare basins). Shallow geophysical surveys (ground penetrating radar pioneered by the Chang'e program: Chang'e 3–5) are providing new insights into mare stratigraphy (Xiao et al. 2015; Wu et al. 2019), but better models of regolith development, and distinguishing impact regolith from volcanically-generated auto-regolith (Head and Wilson 2019) are needed to help refine future interpretations. Critical too, are detailed *in situ* vertical analyses of mare stratigraphy exposed in the walls of pit craters (Haruyama et al. 2009a; Nesnas et al. 2019) (EA-11-2) and impact craters. Large-scale regional geophysical surveys and seismic networks are essential for deeper basin mare basalt documentation. Also uncertain is the global extrusion to intrusion ratio; local and regional seismic and magnetic surveys could improve our understanding.

8.6.4. Volatiles. Understanding the abundance of lunar basalt magmatic volatiles and their release patterns is essential to assess the provenance of current polar ice deposits (external or internal) (e.g., Lawrence 2017; Needham and Kring 2017; Qiao et al. 2019b; Deutsch et al. 2020; Head et al. 2020). *What is the nature, rate and fate of volatile exsolution and does it permit a lunar transient atmosphere?* Necessary to address this question is the detailed peak and mean volcanic flux, and the volatile exsolution efficiency. The minimal volatile flux for producing a transient atmosphere is estimated to be about 10^5 kg/s. On the basis of the lunar volcanic flux, the only time in the lunar mare basalt era that this flux is even approached is in the *Peak Mare Flux Period* (3.8–3.4 Ga) (Fig. 12a). Needham and Kring (2017) have estimated that a peak at 3.5 Ga was sufficient to produce an atmosphere for a period estimated to be ~70 Ma. Head et al. (2020) found that only under extreme circumstances could a short transient atmosphere have been produced. More detailed modeling of volatile release from the full range of basaltic magma compositions are needed (e.g., Morgan et al. 2021), and the release patterns during lava flow emplacement and in the latest stages of eruptions (Phases 2–4; Fig. 11b) need to be better determined. Geophysical analyses of basin interior structure is an essential step forward to assess the presence and timing of peak mare basalt volatile output and the provenance of polar ice.

8.6.5. Mantle properties: What do these data tell us about mantle source regions in space and time? To a first order, the distribution of mare basalt deposits suggests that 1) mare volcanism began on the eastern limb, and mantle source regions were common throughout secondary crust formation on both the nearside and farside (Fig. 12) during the span of lunar history. High titanium basalts were common early in lunar mare history (primarily in Mare Tranquillitatis and Serenitatis) and much later in mare history (Oceanus Procellarum). Uncertain is whether titanium content is a proxy for mantle depth of melting, or whether the variable titanium content as a function of time represents mantle heterogeneity (e.g., Mallik et al. 2019). Analysis of mare basalts returned by Chang'e 5 from the young Procellarum high titanium maria (Che et al. 2021; Li et al. 2021) suggest that the source regions were not KREEP-rich (Tian et al. 2021).

8.6.6. Thermal structure and evolution: How do these fluxes and trends relate to global thermal evolution trends? The thermal evolution of the Moon is characterized by early accretional heat and mantle heating by radioactive decay, followed by progressive conductive cooling and less significant heat loss by mare basalt advection, a trend leading from a net extensional global lithospheric state of stress to a net contractional state of stress, with a transition thought to have occurred at ~ 3.6 Ga toward the end of the peak of mare volcanic flux (Fig. 2a, 12) (Lucchitta and Watkins 1978; Solomon and Head 1979, 1980). Parallel trends in lithospheric thickening drive mare basalt melt zones to greater depths and result in an increasingly contractional lithospheric stress state, making dike propagation to the surface progressively more difficult. Required for improved understanding are better estimates of current heat flow from the Moon and improved estimates of thermal gradients as a function of lunar history and how they are likely to have influenced mantle convection patterns. What are the links between major linear gravity anomalies (e.g., Andrews-Hanna et al. 2018) and magma ascent and eruption pathways? How can surface tectonic patterns and their interaction with lava flow emplacement provide a better record of thermal and tectonic evolution (e.g., Byrne et al. 2015; Chen et al. 2019a)? Important too, are assessments of local and global thermal heterogeneity (nearside/farside?) and how this was maintained or homogenized with time (e.g., Wieczorek and Phillips 2000; Wieczorek et al. 2006; Laneuville et al. 2013), specifically in relation to the South Pole-Aitken basin (Evans et al. 2019; Moriarty et al. 2021; Chen et al. 2020; Jones et al. 2022).

8.6.7. Origin and evolution of the lunar magnetic field. The Moon possessed a magnetic field throughout a significant part of its history, thought to have been generated by advection in a liquid core (Weiss and Tikoo 2014), a phenomenon clearly linked to its thermal evolution and the generation, ascent and eruption of mare basalts. Significant gaps in paleomagnetic data exist between about 3 Ga and 1 Ga, precluding an understanding of the rate of decline

between an earlier high-field epoch and a later low-field epoch (Tikoo et al. 2014, 2017). Detailed analyses of this rate of decline could help distinguish between models for the origin of the magnetic field; additional mare basalt and related samples in this time interval would help to resolve this problem, and provide new insights into mare basalt origin and evolution. Furthermore, oriented *in situ* basalt returned samples could significantly enhance our knowledge of magnetic field polarity and the possibility of true polar wander.

8.6.8. The role of impact basins in the generation, ascent, eruption, and collection of mare basalts. Some have hypothesized that mantle uplift processes might immediately induce pressure release melting, or induce convective upwelling that might lead to volcanism soon thereafter (e.g., Elkins-Tanton and Hager 2005). Whitten et al. (2011) showed that the mare basalts that erupted into the Orientale basin interior were delayed many tens of millions of years from the time of the basin event and their emplacement was subsequently spread over several billion years, thus apparently unrelated to either of these factors but see Feng et al. 2018b). Less certain is the link, in ancient impact basins when heat flux was higher (e.g., Miljković et al. 2013, 2015, 2016, 2021), between immediately generated mare volcanism, basin relaxation and the thickness of mare basalt fill. Also uncertain is the nature and influence of very early impact basins and their relation to large-scale crustal provinces such as the PKT (e.g., Zhu et al. 2019).

8.6.9. Lunar tertiary crust and its relation to secondary crust. Tertiary crusts were originally defined by Taylor (1989) in the context of an assessment of the growth of planetary crusts. The original definition envisioned that tertiary crusts would "arise through further melting and differentiation of the extruded material comprising the secondary crusts". Abundant evidence exists for candidate lunar tertiary crust (e.g., Gruithuisen domes, Hansteen Alpha, Compton-Belkovich) (see detailed descriptions and candidate petrogenetic interpretations in Head et al. 2022), and many aspects of these non-mare features are treated in this volume (e.g., Shearer et al. 2023; Elardo et al. 2023, both this volume).

8.6.10. Petrogenesis. Major questions remain in understanding lunar mare basalt petrogenesis (see Mallik et al. 2019; Elardo et al. 2023; Shearer et al. 2023, both this volume). What events were responsible for initiation and continuation of mare basalt emplacement? How to account for the compositional differences and temporal spread of the range of basalt compositions? Why are there apparently no extrusive basalt equivalents of the picritic glasses? What is role of Procellarum-KREEP Terrane in mare basalt generation? The PKT is hypothesized to have formed prior to the onset of mare volcanism (Joliff et al. 2000), and to have been influential in mare basalt genesis and duration (Wieczorek and Phillips 2000). Our analyses (Figs. 3, 12, EA-11-16) show that early onset of mare volcanism occurs outside the PKT, that it is subsequently widespread both within the PKT and elsewhere, including the farside, and that the final units emplaced lie primarily within the PKT. These late stage mare units are also located in some of the thinnest crust on the Moon. Models for the origin of the PKT (e.g., Laneuville et al. 2013; Zhu et al. 2019; Jones et al. 2022; Zhang et al. 2022), and the influence of PKT on mare volcanism generation, ascent and eruption, should account for this distribution in space and time. Results from the Chang'e 5 PKT mare basalt sample return mission (Tian et al. 2021) suggest that KREEP was not present in the magma souce region.

8.7. How applicable to other terrestrial planetary bodies is the lunar model of secondary crust formation?

Lunar vertical secondary crustal formation and accretion differs from that of the Earth, which is dominated by lateral oceanic crustal spreading and recycling (Fig. 1). Mars, with no evidence of plate tectonics and crustal recycling throughout its observed geologic history (Carr and Head 2010), also appears to have been dominated by vertical secondary crustal accretion, with abundant evidence of early regional volcanic plains resurfacing at least 30% of the surface. In addition, the generation, ascent and eruption of secondary crust on Mars

has involved both major hot spot mantle plume volcanism and shallow magma reservoirs producing giant shield volcanoes and calderas, perhaps related to the increased convection scale length. The lack of evidence for anorthositic primary flotation crust on Mars means that primary crust compositions may mimic secondary crust partial melts of the mantle, and obscure the distinction between the two crustal types. Mercury shows evidence for the vertical accretion of an extensive secondary crust of a generally basaltic nature, but no evidence of an anorthositic primary crust (Nittler et al. 2018) or plate tectonics (Phillips et al. 2018). In a manner similar to the Moon, large expanses of volcanic plains, dating to the first third of Solar System history, fill impact basins and form intercrater plains (Denevi et al. 2013; Whitten et al. 2013). Little evidence is seen for broad volcanic complexes, major shield volcanoes or large calderas, perhaps due to the very small scale-length of mantle convection (Head et al. 2011; Byrne et al. 2018). The lack of an anorthositic crust complicates the distinction between primary and secondary crustal materials. The geologic record of the last 0.5–1 Ga of Venus is dominated by vertical secondary crustal growth with ~80% of the surface composed of volcanic units generally interpreted to be of basaltic origin (e.g., Ivanov and Head 2011, 2013). It is unclear whether Venus ever experienced global plate tectonic-driven secondary crustal growth and recycling. Some have argued that Venus underwent "runaway" vertical crustal accretion, leading to compositional and thermal instabilities and global overturn and recycling (Parmentier and Hess 1992; Head et al. 1994), and that Venus may have experienced multiple such events in its past. A smaller planetary body such as the Moon would have escaped such a fate due to its very limited vertical crustal accretion related to its smaller mantle volume, and more rapid net heat loss. The nature of the primary crust of Venus is unknown.

In summary, the distinctive and possibly unique anorthositic primary crust of the Moon (Fig. 1b) makes the application of lessons from the Moon to other terrestrial planetary bodies tentative in terms of the nature of primary and secondary crust distinctions and transitions. This same unique distinction does, however, provide an important baseline for the characterization of a paradigm for the nature and formation of vertically accreting secondary crust, particularly in its earliest stages. Due to its accessibility and our depth of knowledge, the Moon provides a fundamental cornerstone and keystone in the current understanding and future exploration (e.g., Jawin et al. 2019; Planetary Science Decadal Survey https://www.nationalacademies.org/our-work/planetary-science-and-astrobiology-decadal-survey-2023-2032) of the planets and satellites in the Solar System.

ACKNOWLEDGMENTS

We very gratefully acknowledge the many years of intense efforts on the part of dedicated engineers, scientists and managers from a multitude of national and international space agencies and organizations, who conceived, designed, planned and implemented the many hundreds of experiments, missions and data analysis programs that made this research possible. Special thanks to the experiment PIs who shared their data through the NASA Planetary Data System and China's Lunar Exploration Engineering Ground Application System (GRAS) at http://moon.bao.ac.cn. We would specifically like to acknowledge the NASA Lunar Reconnaissance Orbiter (LRO) Mission personnel for their longstanding dedication to data acquisition and analysis for science, exploration and outreach. Special thanks to Mark Robinson, LRO Camera PI, for bringing the beauty of the Moon, and volcanic morphology and morphometry, to the scientific community and public on a daily basis, and unselfishly making hundreds of extremely useful data products available to the international scientific community at https://www.lroc.asu.edu/. Outside reviews by numerous colleagues, particularly David Williams, are gratefully acknowledged. Special thanks are extended to Anne Cote for assistance in preparation of the manuscript at all stages.

REFERENCES

Andrews-Hanna JC, Head III JW, Johnson BC, Keane JT, Kiefer WS, McGovern PJ, Neumann GA, Wieczorek MA, Zuber MT (2018) Ring faults and ring dikes around the Orientale basin on the Moon. Icarus 310:1–20

Andrews-Hanna JC, Weber RC, Garrick-Bethell I, Evans AJ, Kiefer WS, Grimm RE, Keane JT, Laneuville M, Ishihara Y, Kamata S, Matsuyama I (2023) The structure and evolution of the lunar interior. Rev Mineral Geochem 89:243–292

Arndt N (2003) Komatiites, kimberlites, and boninites. J Geophys Res 108(B6):2293

Basilevsky AT, Zhang F, Wöhler C, Bugiolacchi R, Head III JW, Wilson L (2019) Lunar ring-moat dome structures and their relationships with small impact craters. Lunar Planet Sci Conf 50:1507

Besse S, Sunshine JM, Staid MI, Petro NE, Boardman JW, Green RO, Head III JW, Isaacson PJ, Mustard JF, Pieters CM (2011) Compositional variability of the Marius Hills volcanic complex from the Moon Mineralogy Mapper (M3). J Geophys Res 116:E00G13

Borg LE, Shearer CK, Asmerom Y, Papipke JJ (2004) Prolonged KREEP magmatism on the Moon indicated by the youngest dated lunar igneous rock. Nature 432:209–211

Braden SE, Stopar JD, Robinson MS, Lawrence SJ, van der Bogert CH, Hiesinger H (2014) Evidence for basaltic volcanism on the Moon within the past 100 million years. Nat Geosci 7:787–791

Bugiolacchi R, Guest JE (2008) Compositional and temporal investigation of exposed lunar basalts in the Mare Imbrium region. Icarus 197:1–18

BVSP (Basaltic Volcanism Study Project) (1981) Basaltic Volcanism on the Terrestrial Planets. Pergamon, New York

Byrne PK, Klimczak C, McGovern PJ, Mazarico E, James PB, Neumann GA, Zuber MT, Solomon SC (2015) Deep-seated thrust faults bound the Mare Crisium lunar mascon. Earth Planet Sci Lett 427:183–190

Byrne PK, Whitten JL, Klimczak C, McCubbin FM, Ostrach LR (2018) The volcanic character of Mercury. *In*: Solomon SC, Nittler LR, Anderson BJ (eds). Mercury: The View After MESSENGER. Cambridge University Press, New York, p 287–323

Campbell BA, Hawke BR, Campbell DB (2009) Surface morphology of domes in the Marius Hills and Mons Rumker regions of the Moon from Earth-based radar data. J Geophys Res 114:E01001

Carr MH (1974) The role of lava erosion in the formation of lunar rilles and martian channels. Icarus 22:1–23

Carr M, Head III JW (2010) Geologic history of Mars. Earth Planet Sci Lett 294:185–203

Carter LM, Campbell BA, Hawke BR, Campbell DB, Nolan MC (2009) Radar remote sensing of pyroclastic deposits in the southern Mare Serenitatis and Mare Vaporum regions of the Moon. J Geophys Res 114:E11004

Che X, Nemchin A, Liu D, Long T, Wang C, Norman MD, Joy KH, Tartèse R, Head J, Jolliff B, Snape JF (2021) Age and composition of young basalts on the Moon, measured from samples returned by Chang'e-5. Science 374: 887–890

Chen Y, Zhang YX, Liu Y, Guan YB, Eiler J, Stolper EM (2015) Water, fluorine, and sulfur concentrations in the lunar mantle. Earth Planet Sci Lett 427:37–46

Chen Y, Head III JW, Li CL, Kreslavsky M, Wilson L, Liu JJ, Ren X (2019a) The role of pre-existing topography in modulating lunar lava flow widths, depths and channel structure: An example of an Eratosthenian lava flow in Mare Imbrium (part 1-observations). Lunar Planet Sci Conf 50:2182

Chen Y, Head III JW, Li CL, Liu JJ, Ren X (2019b) Source regions of young lava flows in southwest Mare Imbrium: Characterization of the Euler and Lambert regions. Lunar Planet Sci Conf 50:2942

Compton WD (1989) Where no man has gone before: A history of Apollo lunar exploration missions. NASA, Washington, D.C

Curran NM, Joy KH, Snape JF, Pernet-Fisher JF, Gilmour JD, Nemchin AA, Whitehouse MJ, Burgess R (2019) The early geological history of the Moon inferred from ancient lunar meteorite Miller Range 13317. Meteorit Planet Sci 54:1401–1430

Davis E, Wilson L, Chen Y, Head JW (2022) Rheology and flow dynamics of lunar lava flows. Lunar Planet Sci Conf 53:1352

DeHon RA (1976) Geologic structure of the eastern mare basins. Proc Lunar Sci Conf 7:2729–2746

DeHon RA (1979) Thickness of the western mare basalts. Proc Lunar Planet Sci Conf 10:2935–2955

Delano J (1986) Pristine lunar glasses: Criteria, data, and implications. Proc Lunar Planet Sci Conf 16:D201–D213

Denevi BW, Ernst CM, Meyer HM, Robinson MS, Murchie SL, Whitten JL, Head JW, Watters TR, Solomon SC, Ostrach LR, Chapman CR (2013) The distribution and origin of smooth plains on Mercury. J Geophys Res 118:1–17

Deutsch AN, Neumann GA, Head III JW, Wilson L (2019a) GRAIL-identified gravity anomalies in Oceanus Procellarum: Insight into subsurface impact and magmatic structures on the Moon. Icarus 331:192–208

Deutsch AN, Head III JW, Neumann GA (2020) Analyzing the ages of south polar craters on the Moon: Implications for the sources and evolution of surface water ice. Icarus 336:113455

Elardo SM, Pieters CM, Dhingra D, Donaldson Hanna KL, Glotch TD, Greenhagen BT, Gross J, Head JW, Jolliff BL, Klima RL, Magna T, McCubbin FM, Ohtake M (2023) The evolution of the lunar crust. Rev Mineral Geochem 89:293–338

Elkins-Tanton LT, Hager BH (2005) Giant meteoroid impacts can cause volcanism. Earth Planet Sci Lett 239:219–232

Elkins-Tanton LT, Burgess S, Yin QZ (2011) The lunar magma ocean: Reconciling the solidification process with lunar petrology and geochronology. Earth Planet Sci Lett 304:326–336

Ernst RE (2014) Large Igneous Provinces. Cambridge University Press, Cambridge
Evans AJ (2019) The lunar geochemical asymmetry: Implications for KREEP and magma ocean crystallization. Lunar Planet Sci Conf 52:2733
Evans AJ, Soderblom JM, Andrews-Hanna JC, Solomon SC, Zuber MT (2016) Identification of buried lunar impact craters from GRAIL data and implications for the nearside maria. Geophys Res Lett 43:2445–2455
Evans AJ, Andrews-Hanna JC, Head III JW, Soderblom JM, Solomon SC, Zuber MT (2018) Reexamination of early lunar chronology with GRAIL data: Terranes, basins, and impact fluxes. J Geophys Res 123:1596–1617
Fassett CI, Thomson BJ (2014) Crater degradation on the lunar maria: Topographic diffusion and the rate of erosion on the Moon. J Geophys Res 119:2255–2271
Fassett CI, Thomson BJ (2015) A landscape evolution perspective on how young is young on the lunar surface. Lunar Planet Sci Conf 46:1120
French RA, Bina CR, Robinson MS, Watters TR (2015) Small-scale lunar graben: Distribution, dimensions, and formation processes. Icarus 252:95–106
Gaddis L (2004) A new lunar geologic mapping program. Lunar Planet Sci Conf 37:1418
Gaddis LR, Staid MI, Tyburczy JA, Hawke BR, Petro NE (2003) Compositional analyses of lunar pyroclastic deposits. Icarus 161:262–280
Garry WB, Robinson MS, Zimbelman JR, Bleacher JE, Hawke BR, Crumpler LS, Braden SE, Sato H (2012) The origin of Ina: Evidence for inflated lava flows on the Moon. J Geophys Res 117:E00H31
Gong SX, Wieczorek MA, Nimmo F, Kiefer WS, Head III JW, Huang CL, Smith DE, Zuber MT (2016) Thicknesses of mare basalts on the Moon from gravity and topography. J Geophys Res 121:854–870
Greeley R (1976) Modes of emplacement of basalt terrains and an analysis of mare volcanism in the Orientale basin. Proc Lunar Sci Conf 7:2747–2759
Greeley R, Kadel SD, Williams DA, Gaddis LR, Head JW, McEwen AS, Murchie SL, Nagel E, Neukum G, Pieters CM, Sunshine JM (1993) Galileo imaging observations of lunar maria and related deposits. J Geophys Res 98:17,183–17,205
Guest JE (1971) Centres of igneous activity in the maria. *In*: Fielder G (ed). Geology and Physics of the Moon. Elsevier, New York, p 41–53
Han KY, Wang D (2019) The project of 1:2.5 M-scale lunar geological map-Compilation of China. Lunar Planet Sci Conf 49:1535
Haruyama J, Hioki K, Shirao M, Morota T, Hiesinger H, van der Bogert CH, Miyamoto H, Iwasaki A, Yokota Y, Ohtake M, Matsunaga T (2009a) Possible lunar lava tube skylight observed by SELENE cameras. Geophys Res Lett 36:L21206
Haruyama J, Ohtake M, Matsunaga T, Morota T, Honda C, Yokota Y, Abe M, Ogawa Y, Miyamoto H, Iwasaki A, Pieters CM (2009b) Long-lived volcanism on the lunar farside revealed by SELENE Terrain Camera. Science 323:905–908
Harvey B (2007a) Russian Planetary Exploration: History, Development, Legacy and Prospects. Spring, New York
Harvey B (2007b) Soviet and Russian Lunar Exploration. Springer, New York
Hauri EH, Weinreich T, Saal AE, Rutherford MC, Van Orman JA (2011) High pre-eruptive water contents preserved in lunar melt inclusions. Science 333:213–215
Hauri EH, Saal AE, Rutherford MJ, Van Orman JA (2015) Water in the Moon's interior: Truth and consequences. Earth Planet Sci Lett 409:252–264
Head III JW (1976) Lunar volcanism in space and time. Rev Geophys 14:265–300
Head III JW (1982) Lava flooding of ancient planetary crusts: Geometry, thickness, and volumes of flooded lunar impact basins. Moon Planets 26:61–88
Head III JW, Gifford A (1980) Lunar mare domes: Classification and modes of origin. Moon Planets 22:235–258
Head III JW, Wilson L (1979) Alphonsus-type dark-halo craters: Morphology, morphometry, and eruption conditions. *In*: Proc Lunar Sci Conf (Suppl 11, Geochim Cosmochim Acta). Vol 10. Pergamon Press, New York, p 2861–2897
Head III JW, Wilson L (1989) Basaltic pyroclastic eruptions: Influence of gas-release patterns and volume fluxes on fountain structure and the formation of cinder cones, spatter cones, rootless flows, lava ponds and lava flows. J Volcan Geotherm Res 37:261–271
Head III JW, Wilson L (1991) Absence of large shield volcanoes and calderas on the Moon: Consequence of magma transport phenomena? Geophys Res Lett 18:2121–2124
Head III JW, Wilson L (1992) Lunar mare volcanism: Stratigraphy, eruption conditions, and the evolution of secondary crusts. Geochim Cosmochim Acta 56:2155–2175
Head III JW, Wilson L (1993) Lunar graben formation due to near-surface deformation accompanying dike emplacement. Planet Space Sci 41:719–727
Head III JW, Wilson L (2017) Generation, ascent and eruption of magma on the Moon: New insights into source depths, magma supply, intrusions and effusive/explosive eruptions (part 2: observations). Icarus 283:176–223
Head III JW, Wilson L (2019) Rethinking lunar mare basalt regolith formation: New concepts of lava flow protolith and evolution of regolith thickness and internal structure. Lunar Planet Sci Conf 50:2532
Head JW, Wilson L (2022) Planetary volcanology: Progress, problems, and opportunities. Bull Volcanol 84:23

Head JW, Adams JB, McCord TB, Pieters CM, Zisk SH (1978) Regional stratigraphy and geologic history of Mare Crisium. *In*: Merrill RB, Papipke JJ (eds) Mare Crisium: The View from Luna 24. Pergamon Press, New York, NY, p 43–74
Head III JW, Parmentier EM, Hess PC (1994) Venus: Vertical accretion of crust and depleted mantle and implications for geological history and processes. Planet Space Sci 42:803–811
Head III JW, Wilson L, Weitz CM (2002) Dark ring in southwestern Orientale Basin: Origin as a single pyroclastic eruption. J Geophys Res 107(E1):5001
Head JW, Chapman CR, Strom RG, Fassett CI, Denevi BW, Blewett DT, Ernst CM, Watters TR, Solomon SC, Murchie SL, Prockter LM (2011) Flood volcanism in the northern high latitudes of Mercury revealed by MESSENGER. Science 333:1853–1856
Head JW, Wilson L, Deutsch AN, Rutherford MJ, Saal AE (2020) Volcanically induced transient atmospheres on the Moon: Assessment of duration, significance, and contributions to polar volatile traps. Geophys Res Lett 47:e2020GL089509
Heather DJ, Dunkin SK, Wilson L (2003) Volcanism on the Marius Hills plateau: Observational analyses using Clementine multispectral data. J Geophys Res 108(E3):5017
Heiken GH, Vaniman DT, French BM (eds) (1991) Lunar Sourcebook. Cambridge University Press, Cambridge, UK
Hess PC, Parmentier EM (1995) A model for the thermal and chemical evolution of the Moon's interior: Implications for the onset of mare volcanism. Earth Planet Sci Lett 134:501–514
Hiesinger H, Head III JW (2006) New views of lunar geoscience: An introduction and overview. Rev Mineral Geochem 60:1–81
Hiesinger H, Head III JW, Wolf U, Jaumann R, Neukum G (2002) Lunar mare basalt flow units: Thicknesses determined from crater size–frequency distributions. Geophys Res Lett 29:1248
Hiesinger H, Head III JW, Wolf U, Jaumann R, Neukum G (2003) Ages and stratigraphy of mare basalts in Oceanus Procellarum, Mare Nubium, Mare Cognitum, and Mare Insularum. J Geophys Res 108(E7):5065
Hiesinger H, Head III JW, Wolf U, Jaumann R, Neukum G (2011) Ages and stratigraphy of lunar mare basalts: A synthesis. *In*: Ambrose WA, Williams DA (eds) Recent Advances and Current Research Issues in Lunar Stratigraphy. Geol Soc Am Spec Paper 477, p 1–51
Hiesinger H, van der Bogert CH, Michael G, Schmedemann N, Iqbal W, Robbins SJ, Ivanov B, Williams J-P, Zanetti M, Plescia J, Ostrach LR, Head III JW (2023) The lunar cratering chronology. Rev Mineral Geochem 89:401–451
Hinners NW (1971) The new Moon: A view. Rev Geophys 9:447–522
Huntress Jr. WT, Marov MY (2011) Soviet Robots in the Solar System: Mission Technologies and Discoveries. Springer, New York
Hurwitz DM, Head III JW, Wilson L, Hiesinger H (2012) Origin of lunar sinuous rilles: Modeling effects of gravity, surface slope, and lava composition on erosion rates during the formation of Rima Prinz. J Geophys Res 117: E00H14
Hurwitz DM, Head III JW, Hiesinger H (2013) Lunar sinuous rilles: Distribution, characteristics, and implications for their origin. Planet Space Sci 79–80:1–38
Ivanov MA, Head III JW (2011) Global geological map of Venus. Planet Space Sci 59:1559–1600
Ivanov MA, Head III JW (2013) The history of volcanism on Venus. Planet Space Sci 84:66–92
Jawin ER, Head JW (2018) Assessing the volcanic history of the Prinz-Harbinger region using radar and spectroscopy. Lunar Planet Sci Conf 49:1237
Jawin ER, Besse S, Gaddis LR, Sunshine JM, Head JW, Mazrouei S (2015) Examining spectral variations in localized lunar dark mantle deposits. J Geophys Res Planets 120:1310–1331
Jawin ER, Head JW, Wilson L (2016) Huge pyroclastic cones surrounding Cobra Head, Aristarchus Plateau: Relation to Vallis Schroteri. Lunar Planet Sci Conf 47:1505
Jawin ER, Valencia S, Watkins R, Crowell J, Neal C, Schmidt G (2019) Lunar science for landed missions workshop findings report, Earth Space Sci 6:2–40
Jolliff BL, Gillis JJ, Haskin LA, Korotev RL, Wieczorek MA (2000) Major lunar crustal terranes: Surface expressions and crust-mantle origins. J Geophys Res 105:4197–4216
Jolliff BL, Wieczorek MA, Shearer CK, Neal CR (eds) (2006) New Views of the Moon, Reviews in Mineralogy & Geochemistry, Vol. 60, Min Soc Am, USA
Jolliff BL, Wiseman SA, Lawrence SJ, Tran TN, Robinson MS, Sato H, Hawke BR, Scholten F, Oberst J, Hiesinger H, Van Der Bogert CH (2011) Non-mare silicic volcanism on the lunar farside at Compton-Belkovich. Nat Geosci 4:566–571
Jones MJ, Evans AJ, Johnson BC, Weller MB, Andrews-Hanna JC, Tikoo SM, Keane JT (2022) A South Pole–Aitken impact origin of the lunar compositional asymmetry. Sci Adv 8:eabm8475
Jozwiak LM, Head III JW, Zuber MT, Smith DE, Neumann GA (2012) Lunar floor-fractured craters: Classification, distribution, origin and implications for magmatism and shallow crustal structure. J Geophys Res 117: E11005
Jozwiak LM, Head III JW, Neumann GA, Wilson L (2015a) The effect of evolving gas distribution on shallow lunar magmatic intrusion density: Implications for gravity anomalies. Lunar Planet Sci Conf 46:1580
Jozwiak LM, Head III JW, Wilson L (2015b) Lunar floor-fractured craters as magmatic intrusions: Geometry, modes of emplacement, associated tectonic and volcanic features, and implications for gravity anomalies. Icarus 248:424–447

Jozwiak LM, Head III JW, Neumann GA, Wilson L (2017) Observational constraints on the identification of shallow lunar magmatism: Insights from floor-fractured craters. Icarus 283:224–231
Kato M, Sasaki S, Tanaka K, Iijima Y, Takizawa Y (2008) The Japanese lunar mission SELENE: Science goals and present status. Adv Space Res 42:294–300
Kiefer WS (2013) Gravity constraints on the subsurface structure of the Marius Hills: The magmatic plumbing of the largest lunar volcanic dome complex. J Geophys Res 118:733–745
Kirk RL, Stevenson DJ (1989) The competition between thermal contraction and differentiation in the stress history of the Moon. J Geophys Res 95:12,133–112,144
Klimczak C (2014) Geomorphology of lunar grabens requires igneous dikes at depth. Geology 42:963–966
Kreslavsky MA, Head JW, Neumann GA, Zuber MT, Smith DE (2016) Mare-forming lava flows on the Moon revealed by detrended LOLA topography. Lunar Planet Sci Conf 47:1331
Kreslavsky MA, Head III JW, Neumann GA, Zuber MT, Smith DE (2017) Low-amplitude topographic features and textures on the Moon: Initial results from detrended Lunar Orbiter Laser Altimeter (LOLA) topography. Icarus 283:138–145
Laneuville M, Wieczorek MA, Breuer D, Tosi N (2013) Asymmetric thermal evolution of the Moon. J Geophys Res 118:1435–1452
Lawrence DJ (2017) A tale of two poles: Toward understanding the presence, distribution, and origin of volatiles at the polar regions of the Moon and Mercury. J Geophys Res 122:21–52
Lawrence SJ, Stopar JD, Hawke BR, Greenhagen BT, Cahill JT, Bandfield JL, Jolliff BL, Denevi BW, Robinson MS, Glotch TD, Bussey DB (2013) LRO observations of morphology and surface roughness of volcanic cones and lobate lava flows in the Marius Hills. J Geophys Res 118:615–634
Li B, Ling ZC, Zhang J, Wu ZC, Ni YH, Chen J (2014) The classification and filling process of underlying basaltic units in Chang'E-3's landing area. Earth Sci Front 21:155–164 (in Chinese)
Li QL, Zhou Q, Liu Y, Xiao Z, Lin Y, Li JH, Ma HX, Tang GQ, Guo S, Tang X, Yuan JY, Li J, Wu FY, Ouyang Z, Li C, Li XH (2021) Two-billion-year-old volcanism on the Moon from Chang'e-5 basalts. Nature 600:54–58
Li S, Milliken RE (2017) Water on the Moon as seen by the Moon Mineralogy Mapper: Distribution, abundance and origins. Sci Adv 3:e1701471
Lipsky YN (1965a) Zond-3 photographs of the Moon's far side. Sky Telescope 30:338
Lipsky YN (1965b) Major victory for Soviet science—new data on the invisible side of the Moon. *In:* Major Victory for Soviet Science—New Data on the Invisible Side of the Moon. Moscow
Liu JZ, Guo DJ (2016) Chinese 1:2.5 M geologic mapping of the global Moon. Lunar Planet Sci Conf 47:2039
Lockwood JP, Hazlett RW (2017) Volcanoes: Global Perspectives. Wiley-Blackwell, Oxford
Lu TQ, Chen SB, Zhu K (2019) Global identification and spatial distribution of lunar subsurface faults from GRAIL gravity data. Chin J Geophys 62:2835–2844 (in Chinese)
Lucchitta BK, Watkins JA (1978) Age of graben systems on the Moon. Proc Lunar Sci Conf 9:3459–3472
Mallik A, Ejaz T, Shcheka S, Garapic G (2019) A petrologic study on the effect of mantle overturn: Implications for evolution of the lunar interior. Geochim Cosmochim Acta 250:238–250
McCord TB, Charette MP, Johnson TV, Lebofsky LA, Pieters CM, Adams JB (1972a) Lunar spectral types. J Geophys Res 77:1349–1369
McCord TB, Charette MP, Johnson TV, Lebofsky LA, Pieters CM (1972b) Spectrophotometry (0.3 to 1.1 μm) of visited and proposed Apollo lunar landing sites. Moon 5:52–89
McCord TB, Pieters CM, Feierberg MA (1976) Multi-spectral mapping of the lunar surface using groundbased telescopes. Icarus 29:1–34
McCord TB, Grabow M, Feierberg MA, MacLaskey D, Pieters CM (1979) Lunar multispectral maps: Part II of the lunar nearside. Icarus 37:1–28
Miljković K, Wieczorek MA, Collins GS, Laneuville M, Neumann GA, Melosh HJ, Solomon SC, Phillips RJ, Smith DE, Zuber MT (2013) Asymmetric distribution of lunar impact basins caused by variations in target properties. Science 342:724–726
Miljković K, Wieczorek MA, Collins GS, Solomon SC, Smith DE, Zuber MT (2015) Excavation of the lunar mantle by basin-forming impact events on the Moon. Earth Planet Sci Lett 409:243–251
Miljković K, Collins GC, Wieczorek MA, Johnson BC, Soderblom JM, Neumann GA, Zuber MT (2016) Subsurface morphology and scaling of lunar impact basins. J Geophys Res 121:1695–1712
Miljković K, Wieczorek MA, Laneuville M, Nemchin A, Bland PA, Zuber MT (2021) Large impact cratering during lunar magma ocean solidification. Nat Commun 12:5433
Milliken RE, Li S (2017) Remote detection of widespread indigenous water in lunar pyroclastic deposits. Nat Geosci 10:561–565
Morgan C, Wilson L, Head JW (2021) Formation and dispersal of pyroclasts on the Moon: Indicators of lunar magma volatile contents. J Volc Geotherm Res 413:107217
Moriarty DP, Watkins RN, Valencia SN, Kendall JD, Evans AJ, Dygert N, Petro NE (2021) Evidence for a stratified upper mantle preserved within the south pole–Aitken Basin. J Geophys Res Planets 121:e2020JE006589
Morota T, Haruyama J, Honda C (2008) Lunar cratering chronology: Statistical fluctuation of crater production frequency and its effect on age determination. Earth Planets Space 60:265–270

Morota T, Haruyama J, Honda C, Ohtake M, Yokota Y, Kimura J, Matsunaga T, Ogawa Y, Hirata N, Demura H, Iwasaki A (2009) Mare volcanism in the lunar farside Moscoviense region: Implication for lateral variation in magma production of the Moon. Geophys Res Lett 36:L21202

Morota T, Haruyama J, Ohtake M, Matsunaga T, Honda C, Yokota Y, Kimura J, Ogawa Y, Hirata N, Demura H, Iwasaki A (2011a) Timing and characteristics of the latest mare eruption on the Moon. Earth Planet Sci Lett 302:255–266

Morota T, Haruyama J, Ohtake M, Matsunaga T, Kawamura T, Yokota Y, Honda C, Kimura J, Hirata N, Demura H, Iwasaki A (2011b) Timing and duration of mare volcanism in the central region of the northern farside of the Moon. Earth Planet Space 63:5–13

Morota T, Ishihara Y, Sasaki S, Goossens S, Matsumoto K, Noda H, Araki H, Hanada H, Tazawa S, Kikuchi F, Ishikawa T (2015) Lunar mare volcanism: lateral heterogeneities in volcanic activity and relationship with crustal structure. *In:* Platz T, Massironi M, Byrne PK, Hiesinger H (eds) Volcanism and Tectonism Across the Inner Solar System. Geol Soc London, Spec Publ 401:127–138

Muehlberger WR, Batson RM, Boudette EL, Duke CM, Eggleton RE, Elston DP, England AW, Freeman VL, Hait MH, Hall TA, Head JW (1972) Preliminary geologic investigation of the Apollo 16 landing site. *In*: Apollo 16 Preliminary Science Report. NASA SP-315, p 6-1–6-81

Nahm AL, Watters TR, Johnson CL, Banks ME, van der Bogert CH, Weber RC, Andrews-Hanna JC (2023) Tectonics of the Moon. Rev Mineral Geochem 89:691–727

Needham DH, Kring DA (2017) Lunar volcanism produced a transient atmosphere around the ancient Moon. Earth Planet Sci Lett 478:175–178

Nesnas IA, Kerber L, Parness A, Kornfeld R, Sellar G, McGarey P, Brown T, Paton M, Smith M, Johnson A (2019) Moon Diver: A Discovery mission concept for understanding the history of secondary crusts through the exploration of a lunar mare pit. 2019 IEEE Aerospace Conference, Big Sky, MT, USA, p 1–23

Neumann GA, Zuber MT, Wieczorek MA, Head JW, Baker DM, Solomon SC, Smith DE, Lemoine FG, Mazarico E, Sabaka TJ, Goossens SJ (2015) Lunar impact basins revealed by Gravity Recovery and Interior Laboratory measurements. Sci Adv 1:e1500852

Nittler LR, Chabot NL, Grove TL, Peplowski PN (2018) The chemical composition of Mercury. *In*: Mercury: The View After MESSENGER. Solomon SC, Nittler LR, Anderson BJ (eds) Cambridge University Press, New York, p 30–51

Nyquist LE, Shih CY (1992) The isotopic record of lunar volcanism. Geochim Cosmochim Acta 56:2213–2234

Nyquist LE, Shih C-Y, Wooden JL, Bansal BM, Wiesmann H (1979) The Sr and Nd isotopic record of Apollo 12 basalts: Implications for lunar geochemical evolution. Proc Lunar Planet Sci Conf 10:77–114

Oberbeck VR (1975) The role of ballistic erosion and sedimentation in lunar stratigraphy. Rev Geophys 13:377–362

Okubo CH, Martel SJ (1998) Pit crater formation on Kilauea volcano, Hawaii. J Volcan Geotherm Res 86:1–18

Ouyang Z, Liu JZ (2014) The origin and evolution of the Moon and its geological mapping. Earth Sci Front 21:001–006 (in Chinese)

Palumbo AM, Deutsch AN, Bramble MS, Tarnas JD, Boatwright BD, Lark LH, Nathan EM, Wilner JA, Chen Y, Anzures BA, Denton CA (2019) Scientific exploration of Mare Imbrium with OrbitBeyond Inc.: Characterizing the regional volcanic history of the Moon. New Space: J Space Entrepreneurship Innovation 7:137–150

Parmentier EM, Hess PC (1992) Chemical differentiation of a convecting planetary interior: Consequences for a one plate planet such as Venus. Geophys Res Lett 19:2015–2018

Parmentier EM, Zhong S, Zuber MT (2002) Gravitational differentiation due to initial chemical stratification: Origin of lunar asymmetry by the creep of dense KREEP? Earth Planet Sci Lett 201:473–480

Pasckert JH, Hiesinger H, van der Bogert CH (2015) Small-scale lunar farside volcanism. Icarus 257:336–354

Pasckert JH, Hiesinger H, van der Bogert CH (2018) Lunar farside volcanism in and around the South Pole-Aitken basin. Icarus 299:538–562

Petrycki JA, Wilson L (1999a) Photographic observations of lunar nearside graben. Lunar Planet Sci Conf 30:1333

Petrycki JA, Wilson L (1999b) Volcanic features and age relationships associated with lunar graben. Lunar Planet Sci Conf 30:1335

Petrycki JA, Wilson L, Head III JW (2004) The significance of the geometries of linear graben for the widths of shallow dike intrusions on the Moon. Lunar Planet Sci Conf 35:1123

Phillips RJ, Adams GF, Brown Jr WE, Eggleton RE, Jackson P, Jordan R, Peeples WJ, Porcello LJ, Ryu J, Schaber G, Sill WR (1973) Preliminary results of the Apollo Lunar Sounder Experiment. Lunar Sci Conf 4:1221

Phillips RJ, Byrne PK, James PB, Mazarico E, Neumann GA, Perry ME (2018) Mercury's crust and lithosphere: Structure and mechanics. *In*: Solomon SC, Nittler LR, Anderson BJ (eds) Mercury: The View After MESSENGER. Cambridge University Press, New York, p 52–84

Pieters CM (1978) Mare basalt types on the front side of the Moon: A summary of spectral reflectance data. Proc Lunar Planet Sci Conf 9:2825–2849

Prissel TC, Parman SW, Head III JW (2016) Formation of the lunar highlands Mg-suite as told by spinel. Am Mineral 101:1624–1635

Qian YQ, Xiao L, Zhao SY, Zhao JN, Huang J, Flahaut J, Martinot M, Head III JW, Hiesinger H, Wang GX (2018) Geology and scientific significane of the Rümker region in northern Oceanus Procellarum: China's Chang'E-5 landing region. J Geophys Res 123:1407–1430

Qian Y, Xiao L, Wang Q, Head JW, Yang R, Kang Y, van der Bogert CH, Hiesinger H, Lai X, Wang G, Pang Y, Zhang N, Yuan Y, He Q, Huang J, Zhao J, Wang J, Zhao S (2021a) China's Chang'e-5 landing site: Geology, stratigraphy, and provenance of materials. Earth Planet Sci Lett 561:116855

Qian Y, Xiao L, Head JW, Wilson L (2021b) The long sinuous rille system in northern Oceanus Procellarum and its relation to the Chang'e-5 returned samples. Geophys Res Lett 48:e2021GL092663

Qiao L, Head JW, Wilson L, Kreslavsky MA, Xiao L (2016) Compound flow fields in southwest Mare Imbrium: Geomorphology, source regions, and implications for lunar basin filling. Lunar Planet Sci Conf 47:2038

Qiao L, Head III JW, Wilson L, Xiao L, Dufek JD (2017) Ina pit crater on the Moon: Extrusion of waning-stage lava lake magmatic foam results in extremely young crater retention ages. Geology 45:455–458

Qiao L, Head III JW, Xiao L, Wilson L, Dufek JD (2018a) The role of substrate characteristics in producing anomalously young crater retention ages in volcanic deposits on the Moon: Morphology, topography, subresolution roughness, and mode of emplacement of the Sosigenes lunar irregular mare patch. Meteorit Planet Sci 53:778–812

Qiao L, Head JW, Wilson L, Ling Z (2018b) Lunar Irregular mare patch (IMP) sub-types: Linking their origin through hybrid relationships displayed at Cauchy 5 small shield volcano. Lunar Planet Sci Conf 49:1390

Qiao L, Head III JW, Ling Z, Wilson L, Xiao L, Dufek JD, Yan J (2019a) Geological characterization of the Ina shield volcano summit pit crater on the Moon: Evidence for extrusion of waning-stage lava lake magmatic foams and anomalously young crater retention ages. J Geophys Res 124:1100–1140

Qiao L, Ling Z, Head III JW, Ivanov MA, Liu B (2019b) Analyses of Lunar Orbiter Laser Altimeter 1,064-nm albedo in permanently shadowed regions of polar crater flat floors: Implications for surface water ice occurrence and future in situ exploration. Earth Planet Sci Lett 6:467–488

Qiao L, Head JW, Wilson L, Ling Z (2021) Ina lunar irregular mare patch mission concepts: Distinguishing between ancient and modern volcanism models. Planet Sci J 2:66

Qiao L, Head JW, Wilson L, Chen J, Ling Z (2021b) Mare domes in Mare Tranquillitatis: Identification, characterization, and implications for their origin. J Geophys Res Planets 126:e2021JE006888

Robinson MS, Brylow SM, Tschimmel M, Humm D, Lawrence SJ, Thomas PC, Denevi BW, Bowman-Cisneros E, Zerr J, Ravine MA, Caplinger MA (2010) Lunar Reconnaissance Orbiter Camera (LROC) instrument overview. Space Sci Rev 150:81–124

Robinson MS, Ashley JW, Boyd AK, Wagner RV, Speyerer EJ, Hawke BR, Hiesinger H, van der Bogert CH (2012) Confirmation of sublunarean voids and thin layering in mare deposits. Planet Space Sci 69:18–27

Rutherford MJ, Head III JW, Saal AE, Hauri EH, Wilson L (2017) Model for the origin, ascent and eruption of lunar picritic magmas. Am Mineral 102:2045–2053

Saal AE, Hauri EH, Lo Cascio M, Van Orman JA, Rutherford MC, Cooper RF (2008) Volatile content of lunar volcanic glasses and the presence of water in the Moon's interior. Nature 454:192–195

Schaber GG (1973) Lava flows in Mare Imbrium: Geologic evaluation from Apollo orbital photography. Proc Lunar Planet Sci Conf 4:73–92

Schaber GG, Boyce JM, Moore HJ (1976) The scarcity of mappable flow lobes on the lunar maria: Unique morphology of the Imbrium flows. Proc Lunar Sci Conf 7:2783–2800

Schultz PH (1976a) Moon Morphology. University of Texas Press, Austin, TX

Schultz PH (1976b) Floor-fractured lunar craters. Moon 15:241–273

Schultz PH, Greeley R (1976) Ring-moat structures: Preserved flow morphology on lunar maria. Lunar Planet Sci Conf 7:788–789

Schultz PH, Spudis PD (1979) Evidence for ancient mare volcanism. Proc Lunar Planet Sci Conf 10:2899–2918

Schultz PH, Spudis PD (1983) Beginning and end of lunar mare volcanism. Nature 302:233–236

Schultz PH, Greeley R, Gault DE (1976) Degradation of small surface features. Proc Lunar Sci Conf 7:985–1003

Schultz PH, Staid MI, Pieters CM (2006) Lunar activity from recent gas release. Nature 444:184–186

Shearer CK, Elardo SM, Petro NE, Borg LE, McCubbin FM (2015) Origin of the lunar highlands Mg-suite: An integrated petrology, geochemistry, chronology, and remote sensing perspective. Am Mineral 100:294–325

Shearer C, Neal CR, Glotch TD, Prissel TC, Bell AS, Assis Fernandes V, Gaddis LR, Jolliff BL, Laneuville M, Magna T, Simon J (2023) Magmatic evolution II: A new view of post-differentiation magmatism. Rev Mineral Geochem 89:147–205

Shearer CK, Hess PC, Wieczorek MA, Pritchard ME, Parmentier EM, Borg LE, Longhi J, Elkins-Tanton LT, Neal CR, Antonenko I, Canup RM (2006) Thermal and magmatic evolution of the Moon. Rev Mineral Geochem 60:365–518

Smith DE, Zuber MT, Jackson GB, Cavanaugh JF, Neumann GA, Riris H, Sun X, Zellar RS, Coltharp C, Connelly J, Katz RB (2010) The Lunar Orbiter laser altimeter investigation on the Lunar Reconnaissance Orbiter Mission. Space Sci Rev 150:209–241

Snape JF, Curran NM, Whitehouse MJ, Nemchin AA, Joy KH, Hopkinson T, Anand M, Bellucci JJ, Kenny GG (2018) Ancient volcanism on the Moon: Insights from Pb isotopes in the MIL 13317 and Kalahari 009 lunar meteorites. Earth Planet Sci Lett 502:84–95

Snape JF, Nemchin AA, Whitehouse MJ, Merle RE, Hopkins T, Anand M (2019) The timing of basaltic volcanism at the Apollo landing sites. Geochim Cosmochim Acta: in press
Soderblom JM, Evans AJ, Johnson BC, Melosh HJ, Miljković K, Phillips RJ, Andrews-Hanna JC, Bierson CJ, Head III JW, Milbury C, Neumann GA (2015) The fractured Moon: Production and saturation of porosity in the lunar highlands from impact cratering. Geophys Res Lett 42:6939–6944
Sokol AK, Fernandes VA, Schulz T, Bischoff A, Burgess R, Clayton RN, Münker C, Nishiizumi K, Palme H, Schultz L, Weckwerth G (2008) Geochemistry, petrology and ages of the lunar meteorites Kalahari 008 and 009: New constraints on early lunar evolution. Geochim Cosmochim Acta 72:4845–4873
Solomon SC, Head III JW (1979) Vertical movement in mare basins: Relation to mare emplacement, basin tectonics and lunar thermal history. J Geophys Res 84:1667–1682
Solomon SC, Head III JW (1980) Lunar mascon basins: Lava filling, tectonics and evolution of the lithosphere. Rev Geophys 18:107–141
Sori MM, Zuber MT, Head III JW, Kiefer WS (2016) Gravitational search for cryptovolcanism on the Moon: Constraints on early igneous activity. Icarus 273:284–295
Spudis PD, McGovern PJ, Kiefer WS (2013) Large shield volcanoes on the Moon. J Geophys Res 118:1063–1081
Stadermann AC, Zanetti MR, Jolliff BL, Hiesinger H, van der Bogert CH, Hamilton CW (2018) The age of lunar mare basalts south of the Aristarchus Plateau and effects of secondary craters formed by the Aristarchus event. Icarus 309:45–60
Staid MI, Pieters CM, Head JW (1996) Mare Tranquillitatis: Basalt emplacement history and relation to lunar samples. J Geophys Res 101:23,213–223,228
Staid MI, Pieters CM, Besse S, Boardman J, Dhingra D, Green R, Head JW, Isaacson P, Klima R, Kramer G, Mustard JM (2011) The mineralogy of late-stage lunar volcanism as observed by the Moon Mineralogy Mapper on Chandrayaan-1. J Geophys Res 116:E00G10
Stöffler D, Ryder G, Ivanov BA, Artemieva NA, Cintala MJ, Grieve RA (2006) Cratering history and lunar chronology. Rev Mineral Geochem 60:519–596
Stopar JD, Hawke BR, Lawrence SJ, Robinson MS, Giguere TA (2014) Basaltic cones: A relatively common and distinct style of lunar volcansim. Lunar Planet Sci Conf 45:1425
Taylor SR (1975) Lunar Science: A Post Apollo View. Pergamon, Elmsford, N.Y
Taylor SR (1983) Planetary Science: A Lunar Perspective. Lunar and Planetary Institute, Houston
Taylor SR (1989) Growth of planetary crusts. Tectonophysics 161:147–156
Terada K, Anand M, Sokol AK, Bischoff A, Sano Y (2007) Cryptomare magmatism 4.35 Gyr ago recorded in lunar meteorite Kalahari 009. Nature 450:849-U814
Thomson BJ, Grosfils EB, Bussey DBJ, Spudis PD (2009) A new technique for estimating the thickness of mare basalts in Imbrium Basin. Geophys Res Lett 36:L12201
Tikoo SM, Weiss BR, Cassata WS, Shuster DL, Gattacceca J, Lima EA, Suavet C, Nimmo F, Fuller MD (2014) Decline of the lunar core dynamo. Earth Planet Sci Lett 404:89–97
Tikoo SM, Weiss BP, Shuster DL, Suavet C, Wang HP, Grove TL (2017) A two-billion-year history for the lunar dynamo. Sci Adv 3:e1700207
Trang D, Gillis-Davis JJ, Lemelin M, Cahill JTS, Hawke BR, Giguere TA (2017) The compositional and physical properties of localized lunar pyroclastic deposits. Icarus 283:232–253
Trask NJ, McCauley JF (1972) Differentiation and volcanism in the lunar highlands: Photogeologic evidence and Apollo 16 implications. Earth Planet Sci Lett 14:201–206
Vaughan WM, Head III JW (2014) Impact melt differentiation in the South Pole-Aitken basin: Some observations and speculations. Planet Space Sci 91:101–106
Vaughan WM, Head III JW, Wilson L, Hess PC (2013) Geology and petrology of enormous volumes of impact melt on the Moon: A case study of the Orientale basin impact melt sea. Icarus 223:749–765
Wagner RV, Robinson MS (2014) Distribution, formation mechanisms, and significance of lunar pits. Icarus 237:52–60
Wagner RJ, Head III JW, Wolf U, Neukum G (2002) Stratigraphic sequence and ages of volcanic units in the Gruithuisen region of the Moon. J Geophys Res 107
Wagner R, Head III JW, Wolf U, Neukum G (2010) Lunar red spots: Stratigraphic sequence and ages of domes and plains in the Hansteen and Helmet regions on the lunar nearside. J Geophys Res 115
Wang QL, Liu JZ, Ji JZ, Guo DJ, Liu JW (2016) Redefinition and geological significance of periods of basaltic magma filling in lunar Mare Imbrium. Acta Petrologica Sinica 32:29–42 (in Chinese)
Watters TR, Johnson C (2010) Lunar tectonics. *In*: Planetary Tectonics. Watters TR, Schultz RA (eds) Cambridge University Press, Cambridge, p 121–182
Weber RC, Lawrence SJ, Cohen BA, Bleacher JE, Boyce JW, Collier MR, Draper D, Fagan AL, Fassett CI, Gaddis L, Gross J, Gruener JE, Heldmann JL, McCubbin FM, Mitchell JL, Nahm AL, Needham DH, Noble S, Pieters CM, Petro N, Sato KY, Spann J, Young KE (2021) The Artemis III Science Definition Team Report. Lunar Planet Sci Conf 52:1261
Weider SZ, Crawford IA, Joy KH (2010) Individual lava flow thicknesses in Oceanus Procellarum and Mare Serenitatis determined from Clementine multispectral data. Icarus 209:323–336

Weiss BP, Tikoo SM (2014) The lunar dynamo. Science 346:1246753
Weitz CM, Head III JW (1999) Spectral properties of the Marius Hills volcanic complex and implications for the formation of lunar domes and cones. J Geophys Res 104:18,933–18,956
Weitz CM, Head III JW, Pieters CM (1998) Lunar regional dark mantle deposits: Geologic, multispectral, and modeling studies. J Geophys Res 103:22,725–22,759
Weitz CM, Staid MI, Gaddis LR, Besse S, Sunshine JM (2017) Investigation of lunar spinels at Sinus Aestuum. J Geophys Res: Planets 122:2013–2033
Whitaker EA (1972) An unusual mare feature. *In*: Apollo 15 Preliminary Science Report. NASA SP-289, US Govt Printing Office, Washington, DC, p 25-84–25-95
Whitford-Stark JL, Head III JW (1977) The Procellarum volcanic complexes: Contrasting styles of volcanism. *In*: Proc Lunar Sci Conf. Vol 8. Pergamon Press, New York, p 2705–2724
Whitten JL, Head III JW (2013) Detecting volcanic resurfacing of heavily cratered terrain: Flooding simulations on the Moon using Lunar Orbiter Laser Altimeter (LOLA) data. Planet Space Sci 85:24–37
Whitten JL, Head III JW (2015a) Lunar cryptomaria: Physical characteristics, distribution, and implications for ancient volcanism. Icarus 247:150–171
Whitten JL, Head III JW (2015b) Lunar cryptomaria: Mineralogy and composition of ancient volcanic deposits. Planet Space Sci 106:67–81
Whitten J, Head III JW, Staid MI, Pieters CM, Mustard JF, Clark R, Nettles JW, Klima RL, Taylor LA (2011) Lunar mare deposits associated with the Orientale impact basin: New insights into mineralogy, history, mode of emplacement, and relation to Orientale Basin evolution from Moon Mineralogy Mapper (M3) data from Chandrayaan-1. J Geophys Res 116:E00G09
Wieczorek MA, Phillips RJ (2000) The "Procellarum KREEP Terrane": Implications for mare volcanism and lunar evolution. J Geophys Res 105:20417–20430
Wieczorek MA, Zuber MT, Phillips RJ (2001) The role of magma buoyancy on the eruption of lunar basalts. Earth Planet Sci Lett 185:71–83
Wieczorek MA, Jolliff BL, Khan A, Pritchard ME, Weiss BP, Williams JG, Hood LL, Righter K, Neal CR, Shearer CK, McCallum IS (2006) The constitution and structure of the lunar interior. Rev Mineral Geochem 60:221–364
Wieczorek MA, Neumann GA, Nimmo F, Kiefer WS, Taylor GJ, Melosh HJ, Phillips RJ, Solomon SC, Andrews-Hanna JC, Asmar SW, Konopliv AS (2013) The crust of the Moon as seen by GRAIL. Science 339:671–675
Wilhelms DE (1987) The Geologic History of the Moon. USGS Prof Paper 1348, US Govt Printing Office, Washington, DC
Wilhelms DE, McCauley JF (1971) Geologic map of the nearside of the Moon. US Geol Surv Misc Geol Map I-703
Williams KK, Zuber MT (1998) Measurement and analysis of lunar basin depths from Clementine altimetry. Icarus 131:107–122
Williams DA, Fagents SA, Greeley R (2000) A reevaluation of the emplacement and erosional potential of turbulent, low-viscosity lavas on the Moon. J Geophys Res 105:20,189–20,206
Wilson L, Head III JW (1981) Ascent and eruption of basaltic magma on the Earth and Moon. J Geophys Res 86:2971–3001
Wilson L, Head III JW (2003a) Deep generation of magmatic gas on the Moon and implications for pyroclastic eruptions. Geophys Res Lett 30:1605
Wilson L, Head III JW (2003b) Lunar Gruithuisen and Mairan domes: Rheology and mode of emplacement. J Geophys Res 108(E2):5012
Wilson L, Head III JW (2017a) Generation, ascent and eruption of magma on the Moon: New insights into source depths, magma supply, intrusions and effusive/explosive eruptions (Part 1: Theory). Icarus 283:146–175
Wilson L, Head III JW (2017b) Eruption of magmatic foams on the Moon: Formation in the waning stages of dike emplacement events as an explanation of "irregular mare patches". J Volcan Geotherm Res 335:113–127
Wilson L, Head III JW (2018a) Lunar basaltic volcanic eruptions: Gas release patterns and variations in lava vesicularity: 1. Lava ponds, shield volcanoes, foams, and irregular mare patch (IMP) morphology. Lunar Planet Sci Conf 49:1325
Wilson L, Head III JW (2018b) Lunar basaltic volcanic eruptions: Gas release patterns and variations in lava vesicularity: 2. Fissures, mare flows, and ring moat dome structure (RMDS) morphology. Lunar Planet Sci Conf 49:1326
Wilson L, Head III JW (2018c) Lunar floor-fractured craters: Modes of dike and sill emplacement and implications of gas production and intrusion cooling on surface morphology and structure. Icarus 305:105–122
Wilson L, Head III JW (2018d) Controls on lunar basaltic volcanic erupton structure and morphology: Gas release patterns in sequential eruption phases. Geophys Res Lett 45:5852–5859
Wilson L, Head JW (2022) An integrated model fo the formation of large-scale lava flows and sinuous rilles on the Moon, Lunar Planet Sci Conf 53:1356
Wilson L, Hawke BR, Giguere TA, Petrycki ER (2011) An igneous origin for Rima Hyginus and Hyginus crater on the Moon. Icarus 215:584–595
Wilson L, Head III JW, Zhang F (2019a) A theoretical model for the formation of Ring Moat Dome Structures: Products of second boiling in lunar basaltic lava flows. J Volcan Geotherm Res 374:160–180

Wöhler C, Lena R, Phillips J (2007) Formation of lunar mare domes along crustal fractures: Rheologic conditions, dimensions of feeder dikes, and the role of magma evolution. Icarus 189:279–307
Wu W, Li C, Zuo W, Zhang H, Liu J, Wen W, Su Y, Ren X, Yan J, Yu D, Dong G (2019) Lunar farside to be explored by Chang'e-4. Nat Geosci 12:222–223
Xiao L, Zhu P, Fang G, Xiao Z, Zou Y, Zhao J, Zhao N, Yuan Y, Qiao L, Zhang X, Zhang H (2015) A young multilayered terrane of the northern Mare Imbrium revealed by Chang'E-3 mission. Science 347:1226–1229
Young JW, Mattingly TK, Duke CM (1972) Crew observations. *In*: Apollo 16 Preliminary Science Report. NASA SP-315, p 5-1–5-6
Zhang F, Zhu MH, Zou YL (2016) Late stage Imbrian volcanism on the Moon: Evidence for two source regions and implications for the thermal history of Mare Imbrium. Earth Planet Sci Lett 445:13–27
Zhang F, Head III JW, Basilevsky AT, Bugiolacchi R, Komatsu G, Wilson L, Fa W, Zhu M-H (2017) Newly discovered ring-moat dome structures in the lunar maria: Possible origins and implications. Geophys Res Lett 44:9216–9224
Zhang F, Wöhler C, Head JW, Bugiolacchi R, Wilson L, Grumpe A (2018a) Ring-Moat Dome Structures (RMDSs) in the lunar maria: Further statistical and morphological characterization. Lunar Planet Sci Conf 49:1374
Zhang F, Zhu MH, Bugiolacchi R, Huang Q, Osinski GR, Xiao L, Zou YL (2018b) Diversity of basaltic lunar volcanism associated with buried impact structures: Implications for intrusive and extrusive events. Icarus 307:216–234
Zhang F, Head JW, Wöhler C, Bugiolacchi R, Wilson L, Basilevsky A, Grumpe A, Zou YL (2020) A Ring-Moat Dome Structures (RMDSs) in the lunar maria: Statistical, compositional, and morphological characterization and assessment of theories of origin. J Geophys Res 125:e2019JE005967
Zhang J, Head JW, Liu J, Potter RWK (2020) Origin of the Lunar Procellarum KREEP Terrane (PKT): Stratigraphic Evidence and Implications for Lunar Geological and Thermal Evolution. Moscow Solar System Symposium 11
Zhang F, Head JW, Wöhler C, Basilevsky AT, Wilson L, Xie M, Bugiolacchi R, Wilhelm T, Althoff S, Zou YL (2021) The lunar mare ring-moat dome structure (RMDS) age conundrum: Contemporaneous with Imbrian-aged host lava flows or emplaced in the Copernican? J Geophys Res: Planets 126:e2021JE006880
Zhao J, Xiao L, Qiao L, Glotch TD, Huang Q (2017) The Mons Rümker volcanic complex of the Moon: a candidate landing site for the Chang'E-5 mission. J Geophys Res, Planets 122:1419–1442
Zhu M-H, Wünnemann K, Potter RWK, Kleine T, Morbidelli A (2019) Are the Moon's nearside–farside asymmetries the result of a giant impact? J Geophys Res 124:2117–2140
Ziethe R, Seiferlin K, Hiesinger H (2009) Duration and extent of lunar volcanism: Comparison of 3D convection models to mare basalt ages. Planet Space Sci 57:784–796
Zuber MT, Smith DE, Zellar RS, Neumann GA, Sun X, Katz RB, Kleyner I, Matuszeski A, McGarry JF, Ott MN, Ramos-Izquierdo LA (2010) The Lunar Reconnaissance Orbiter Laser ranging investigation. Space Sci Rev 150:63–80
Zuber MT, Smith DE, Watkins MM, Asmar SW, Konopliv AS, Lemoine FG, Melosh HJ, Neumann GA, Phillips RJ, Solomon SC, Wieczorek MA (2013) Gravity field of the Moon from the Gravity Recovery and Interior Laboratory (GRAIL) Mission. Science 339:668–671

APPENDIX—RECENT DEVELOPMENTS

The most significant recent developments in lunar volcanism have been three-fold: 1) the nature of young volcanism, 2) the origin of sinuous rilles, and 3) question of the duration of lunar volcanism and the implications for lunar thermal evolution. The Chang'e 5 sample return mission, targeted to the mare in the Procellarum-KREEP Terrane (PKT) (Jolliff et al. 2000) in northern Oceanus Procellarum, provided samples of a well-defined and homogeneous geologic unit (Em4) with an AMA in the range of 1.6–1.7 Ga (Qian et al. 2021a), and associated with a sinuous rille thought to be the longest on the Moon (Hurwitz et al. 2013). Chang'e 5 mission results showed that the mare basalts were emplaced at ~2 Ga (Che et al. 2021; Li et al. 2021), permitting improved calibration of the lunar impact flux and chronology, and found that the basalts were generated in mantle source regions that did not have the radioactive element abundances expected from the high levels associated with the PKT crust. Detailed analysis of the geologic context of the sampled unit (Qian et al. 2021a) showed that the longest sinuous rille on the Moon was actually two rilles from two distinct sources that met in the middle of the Em4 unit (Qian et al. 2021b), prompting re-examination of models of mare basalt unit emplacement and contemporaneous sinuous rille formation (Wilson et al. 2022). Parallel recent research resulted in further conundra concerning the time of cessation of lunar volcanism and whether it has continued up to the last few hundred million years, as suggested by AMAs of Irregular Mare Patches (IMPs) (Braden et al. 2014). Further characterization of IMPs (Qiao et al. 2020a,b) has clarified the competing arguments concerning whether these features are

contemporaneous with mare basalt emplacement or formed in recent history, and proposed future mission scenarios to test these two hypotheses (Qiao et al. 2021). Documentation of Ring-Moat Dome Structures (RMDS) and their stratigraphic relationships in the lunar maria has also raised the question of their emplacement ages (up to the last few hundred million years?) (Zhang et al. 2021). Together, IMPs and RMDS are prime targets for future exploration to resolve this major issue in lunar thermal evolution.

REFERENCES

Braden SE, Stopar JD, Robinson MS, Lawrence SJ, van der Bogert CH, Hiesinger H (2014) Evidence for basaltic volcanism on the Moon within the past 100 million years. Nat Geosci 7:787–791

Che X, Nemchin A, Liu D, Long T, Wang C, Norman MD, Joy KH, Tartèse R, Head J, Jolliff B, Snape JF (2021) Age and composition of young basalts on the Moon, measured from samples returned by Chang'e-5. Science 374:887–890

Hurwitz DM, Head JW, Hiesinger H (2013) Lunar sinuous rilles: distribution, characteristics, and implications for their origin. Planet.Space Sci 79–80:1–38

Jolliff BL, Gillis JJ, Haskin LA, Korotev RL, Wieczorek MA (2000) Major lunar crustal terranes: surface expressions and crust-mantle origins. J Geophys Res: Planets 105:4197–4216

Li QL, Zhou Q, Liu Y, Xiao Z, Lin Y, Li JH, Ma HX, Tang GQ, Guo S, Tang X, Yuan JY (2021) Two-billion-year-old volcanism on the Moon from Chang'e-5 basalts. Nature 600:54–58

Qian Y, Xiao L, Wang Q, Head JW III, Yang R, Kang Y, van der Bogert CH, Hiesinger H, Lai X, Wang G, Pang Y, Zhang N, Yuan Y, He Q, Huang, J, Zhao J, Wang J, Zhao S (2021a) China's Chang'e-5 landing site: Geology, stratigraphy, and provenance of materials, Earth Planet Sci Lett 561:116855

Qian Y, Xiao L, Head JW, Wilson L (2021b) The long sinuous rille system in Northern Oceanus Procellarum and its relation to the Chang'e-5 returned samples. Geophys Res Lett 48:e2021GL09266

Qiao L, Head JW, Ling Z, Wilson L (2020a) Lunar irregular mare patches: Classification, characteristics, geologic settings, updated catalog, origin, and outstanding questions. J Geophys Res 125:e2019JE006362

Qiao L, Head JW, Wilson L, Ling Z (2020b) The Cauchy 5 small, low-volume lunar shield volcano: Evidence for volatile exsolution-eruption patterns and Type 1/Type 2 hybrid irregular mare patch formation. J Geophys Res 125:e2019JE006171

Qiao L, Head JW, Wilson L, Ling Z (2021) Ina Lunar Irregular Mare Patch mission concepts: Distinguishing between ancient and modern volcanism models. Planet Sci J 2:66

Wilson L, Head JW, Qian Y, Xiao L (2022) Modeling the eruption of the lavas sampled by the Chang'e 5 mission, 53rd Lunar Planet Sci Conf, Abstract #1624

Zhang F, Head JW, Wöhler C, Basilevsky AT, Xie M, Bugiolacchi, R, Wilson L, Wilhelm T, Althoff S, Zou YL (2021) The Lunar Mare Ring-Moat Dome Structure (RMDS) age conundrum: Contemporaneous with Imbrian-aged host lava flows or emplaced in the Copernican? J Geophys Res: Planets 126: e2021JE006880

ELECTRONIC ANNEX

Figures and tables referred to by the prefix "EA" are in an electronic annex available at https://apenninus.u-aizu.ac.jp/NVM2-EA.html